Chapter 5
Sediment Modeling for Rivers and Reservoirs

Chapter 5
Sedimentation Modeling for Rivers and Reservoirs

by

Francisco J.M. Simões and Chih Ted Yang

5.1 Introduction

The study of natural river changes and the interference of man in natural water bodies is a difficult but important activity, as increasing and shifting populations place more demands on the natural sources of fresh water. Although the basic mechanical principles for these studies are well established, a complete analytical solution is not known but for the most basic cases. The complexity of the flow movement and its interaction with its boundaries, which are themselves deformable, have precluded the development of closed form solutions to the governing equations that describe the mechanical behavior of fluid and solid-fluid mixtures. As a result, alternative techniques have been developed to provide quantitative predictions of these phenomena as an aid to engineering projects and river restoration efforts. Modeling is one such technique.

There are two types of models: mathematical models and physical models (sometimes also called scale models). This chapter provides an overview of mathematical and numerical modeling, which is based on computation techniques, as opposed to physical modeling, which is based on traditional laboratory techniques and measurement.

Numerical modeling has become very popular in the past few decades, mainly due to the increasing availability of more powerful and affordable computing platforms. Much progress has been made, particularly in the fields of sediment transport, water quality, and multidimensional fluid flow and turbulence. Many computer models are now available for users to purchase. Some of the models are in public domain and can be obtained free of charge. Graphical user interfaces, automatic grid generators, geographic information systems, and improved data collection techniques (such as LiDAR, Light Distancing and Ranging) promise to further expedite the use of numerical models as a popular tool for solving river engineering problems.

5.1.1 The Numerical Modeling Cycle

In general, numerical models are used for the same reasons as physical models; i.e., the problem at hand cannot be solved directly for the prototype. The process from prototype data to the modeling and to final interpretation of the results (i.e., the modeling cycle) is complex and prone to many errors. Careful engineering judgment must be exercised at every step. The modeling cycle is schematically represented in Figure 5.1.

The prototype is the reality to be studied. It is defined by data and by knowledge. The data represents boundary conditions, such as bathymetry, water discharges, sediment particle size distributions, vegetation types, etc. The knowledge contains the physical processes that are known to determine the system's behavior, such as flow turbulence, sediment transport mechanisms, mixing processes, etc. Understanding the prototype and data collection constitute the first step of the cycle.
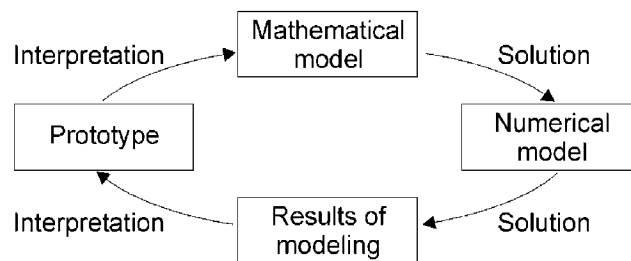
Figure 5.1. Computer modeling cycle from prototype to the modeling results. The cycle starts with the prototype being studied and ends with the interpretation of model results to withdraw conclusions about it.

In the first interpretation step, all the relevant physical processes that were identified in the prototype are translated into governing equations that are compiled into the mathematical model. A mathematical model, therefore, constitutes the first approximation to the problem. It is the prerequisite for a numerical model. At this time, many simplifying approximations are made, such as steady versus unsteady and one- versus two- versus three-dimensional formulations, simplifying descriptions of turbulence, etc. In water resources, one usually (but not always) arrives to the set-up of a boundary value problem whose governing equations contain partial differential equations and non-linear terms.

Next, a solution step is required to solve the mathematical model. The numerical model embodies the numerical techniques used to solve the set of governing equations that forms the mathematical model. In this step, one chooses, for example, finite difference versus finite element versus finite volume discretization techniques; selects the approach to deal with the non-linear terms; etc. Note that this is a further approximating step because the partial differential equations are transformed into algebraic equations, which are approximate but not equivalent to the former.

Another solution step involves the solution of the numerical model in a computer and provides the results of modeling. This step embodies further approximations and simplifications, such as those associated with unknown boundary conditions, imprecise bathymetry, unknown water and/or sediment discharges, friction factors, etc.

Finally, the data needs to be interpreted and placed in the appropriate prototype context. This last step closes the modeling cycle and ultimately provides the answer to the problem that drives the modeling efforts.

The choice of model for each specific problem should take into account the requirements of the problem, the knowledge about the system, and the data available. On one hand, the model must take into account all the significant phenomena that are known to occur in the system and that will influence the aspects that are being studied. On the other hand, model complexity is limited by the available data. At this time, there is no universal model that can be applied to every problem, and it may not even be desirable to have such a model. The specific requirements of each problem should be analyzed and the model chosen should reflect this analysis in its features and complexity. There is no lack of computer models for engineers to choose from. The success

of a study depends, to a large degree, on the engineer's understanding of fluvial processes, associated theories, and the capabilities and limitations of computer models. In many cases, the selection of a modeler is more important than the selection of the computer model.

5.2 Mathematical Models

5.2.1 Three-Dimensional Models

The flow phenomena in natural rivers are three dimensional, especially those at or near a meander bend, local expansion and contraction, or a hydraulic structure. Turbulence is an essentially three-dimensional phenomenon, and three-dimensional models are particularly useful for the simulation of turbulent heat and mass transport. These models are usually based on the Reynolds-averaged form of the Navier-Stokes equations, using additional equations of varied degree of complexity for the turbulence closure.

The derivation of the governing equations can be found in many basic textbooks on fluid dynamics; therefore, they will only be presented here without further consideration. Interested readers are directed to textbooks such as the ones by White (1991) and by Warsi (1993). The Navier-Stokes equations represent the statement of Newton's second law for fluids (i.e., the conservation of momentum), and in the Cartesian coordinate system and for incompressible fluids, they can be written as

$$\frac{\partial u_i}{\partial t} + \frac{\partial u_i u_j}{\partial x_j} = \frac{F_i}{\rho} - \frac{1}{\rho}\frac{\partial p}{\partial x_i} + \frac{\partial}{\partial x_j}\left(v\frac{\partial u_i}{\partial x_j} - \overline{u_i'u_j'}\right) \tag{5.1}$$

where

i,j	=	Cartesian directions (= 1 for x, = 2 for y, and = 3 for z),
j	=	Cartesian directions perpendicular to i
u_i	=	Cartesian component of the velocity along the x_i direction (i = 1,2,3),
ρ	=	fluid density,
p	=	pressure,
F_i	=	component of the body forces per unit volume in the i-direction,
v	=	kinematic molecular viscosity,
$-\rho\overline{u_i'u_j'}$	=	turbulent stresses,

and the indexed summation convention is used (see Figure 5.2 for convention used). Equations (5.1) constitute a system of equations, one for each coordinate direction (i.e., for i = 1, 2, and 3).

The body forces include gravitational, buoyancy, and Coriolis forces, or any other body forces that may be present (such as magnetic forces in magnetohydrodynamic fluids). Additionally, in turbulent flows, the molecular viscosity term may be safely neglected in comparison with the turbulent stresses.

Conservation of mass is expressed by the continuity equation for incompressible fluids:

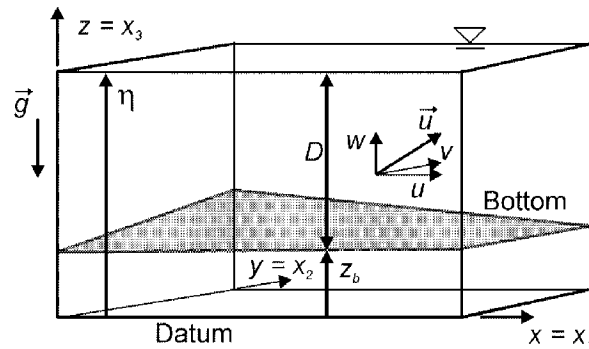$$\frac{\partial u_i}{\partial x_i} = 0 \tag{5.2}$$

Figure 5.2. Sketch showing the coordinate system used and the definition of some of the variables. Note that $u = u_1$, $v = u_2$, and $w = u_3$.

The transport of constituents, such as dissolved and suspended solids, requires one equation per substance transported. This is a convection-diffusion type of equation that can be written in general as

$$\frac{\partial c}{\partial t} + u_i \frac{\partial c}{\partial x_i} = \frac{\partial}{\partial x_i}\left(\Gamma \frac{\partial c}{\partial x_i} - \overline{u_i'c'} \right) + S_c \tag{5.3}$$

where c =   scalar quantity per unit of mass,
           Γ =   molecular diffusivity coefficient,
           $-\overline{u_i'c'}$ =   turbulent diffusion of c, and
           S_c =   source/sink (i.e., creation/destruction) of c.

The turbulence terms ($-\rho\overline{u_i'u_j'}$ and $-\overline{u_i'c'}$) result from averaging the original Navier-Stokes equations using the Reynolds decomposition (Tennekes and Lumley, 1972) for a more detailed explanation about the technique) and require additional closure equations. One of the commonly used closure techniques is given by the k-ε model (Rastogi and Rodi, 1978), but there are many other alternative choices. The reader is directed to the turbulence modeling monograph by Rodi (1993) for further details about this subject.

In free surface flows, an additional equation is required to solve for the position of the free surface. A common technique is to use a rigid lid approximation in which the flow is solved in the same manner as pressurized flow by assuming a rigid frictionless boundary at the approximate position where the free surface is located. This eliminates the need to use an additional

5-4

differential equation to compute the free surface position: the free surface location can be computed from the flow pressure by extrapolating (or interpolating) to the location where $p = p_a$, where p_a is the atmospheric pressure. Accuracy is lost when the free surface location differs significantly from the rigid lid location (say, by 10% or more of the flow depth), which may occur in bends and around obstacles.

The free surface elevation may also be computed by solving either the kinematic condition at the free surface,

$$\frac{\partial \eta}{\partial t} + u_s \frac{\partial \eta}{\partial x} + v_s \frac{\partial \eta}{\partial y} - w_s = 0 \tag{5.4}$$

or by using the depth-integrated continuity equation,

$$\frac{\partial D}{\partial t} + \frac{\partial (DU)}{\partial x} + \frac{\partial (DV)}{\partial y} = 0 \tag{5.5}$$

where η =   free surface elevation,
          u_s, v_s, w_s =   components of the velocity vector at the free surface,
          D =   water depth, and
          U, V =   components of the depth-averaged velocity vector (to be defined in the next section).

The depth-averaged continuity equation offers the advantage of using the principle of mass conservation, therefore helping to enforce the incompressibility constraint. Note that the kinematic condition, Equation (5.4), is used in the derivation of Equation (5.5) (for details about the derivation of Equation (5.5) see Pinder and Gray, 1977). Furthermore, the use of a depth-averaged velocity in Equation (5.5), does not mean that the depth-averaged momentum equations (as described in the next section) need to be used, because U and V can be computed directly from the three-dimensional velocity field, as done by Simões (1995).

An important simplification to the system of Equations (5.1) is accomplished when the vertical acceleration terms can be neglected with respect to the pressure and body forces. In this case, the third momentum equation (z-momentum) reduces to

$$0 = -\frac{1}{\rho} \frac{\partial p}{\partial z} - g \tag{5.6}$$

where g =   acceleration due to gravity (with a single component along the negative z- direction).

Equation (5.6) is the hydrostatic pressure approximation. This is a frequently used approximation in free surface flows, which is valid when the streamlines are only weakly curved in the vertical

plane (i.e., they are nearly parallel to the bottom of the channel). Using the hydrostatic pressure approximation, the pressure gradient can be replaced by the free surface slope in neutrally stratified flows:

$$\frac{1}{\rho}\frac{\partial p}{\partial x} = g\frac{\partial \eta}{\partial x}, \quad \frac{1}{\rho}\frac{\partial p}{\partial y} = g\frac{\partial \eta}{\partial y} \tag{5.7}$$

This allows the elimination of one unknown (the pressure p). The third momentum equation is not solved. Instead, the vertical component of the velocity at any vertical level z, w_z, is calculated directly from integrating Equation (5.2) along the vertical direction:

$$w_z = -\int_{z_b}^{z}\left(\frac{\partial u}{\partial x} + \frac{\partial v}{\partial y}\right)dz \tag{5.8}$$

Three-dimensional modeling is a very powerful tool in river engineering, but it also has high computational demands (i.e., faster computers with large memory space are needed). It also requires vast amounts of data for proper model setup, which takes time and is expensive to obtain. These requirements have, until recently, limited their use, but newer, faster, and more affordable computers, together with new data collection instrumentation, may overcome these limitations in the near future.

5.2.2 Two-Dimensional Models

Two-dimensional models for flow and sediment transport are becoming widely used due to the advent of fast personal computers and to the existence of a significant number of commercially available models.

Two-dimensional models can be classified into two-dimensional vertically averaged and two-dimensional horizontally averaged models. The former scheme is used where depth-averaged velocity or other hydraulic parameters can adequately describe the variation of hydraulic conditions across a channel. The latter scheme is used where width-averaged hydraulic parameters can adequately describe the variation of hydraulic conditions in the vertical direction. Most two-dimensional sediment transport models are depth-averaged models; hence, we focus on those in this section.

Two-dimensional, depth-averaged models result from vertically averaging the governing equations, Equations (5.1) and (5.2), after a few simplifying assumptions. First, integrating the continuity equation, making use of the kinematic condition at the free surface—Equation (5.4)—and the fact that the normal component of the velocity must vanish at the solid bed, one obtains

$$\frac{\partial D}{\partial t} + \frac{\partial (DU)}{\partial x} + \frac{\partial (DV)}{\partial y} = 0 \tag{5.9}$$

where U and V =   depth-averaged velocities defined as

$$U = \frac{1}{D} \int_{z_b}^{\eta} u\,dz \quad \text{and} \quad V = \frac{1}{D} \int_{z_b}^{\eta} v\,dz \tag{5.10}$$

where z_b =   bed elevation (see Figure 5.2).

The momentum equation, Equation (5.1), can be averaged in the same way, but this time non-linear terms appear, such as

$$\int_{z_b}^{\eta} uv\,dz = DUV + \int_{z_b}^{\eta} (u-U)(v-V)\,dz \tag{5.11}$$

Including the Coriolis and pressure terms, whose integration is trivial, the depth-averaged momentum equations become

$$\frac{\partial(DU)}{\partial t} + \frac{\partial(DU^2)}{\partial x} + \frac{\partial(DUV)}{\partial y} = F_x + fDV - gD\frac{\partial\eta}{\partial x} - \frac{gD^2}{2\rho_0}\frac{\partial\rho}{\partial x} - \frac{\tau_{bx}}{\rho_0} + \frac{\partial(D\tau_{xx})}{\partial x} + \frac{\partial(D\tau_{xy})}{\partial y} \tag{5.12}$$

$$\frac{\partial(DV)}{\partial t} + \frac{\partial(DUV)}{\partial x} + \frac{\partial(DV^2)}{\partial y} = F_y - fDU - gD\frac{\partial\eta}{\partial y} - \frac{gD^2}{2\rho_0}\frac{\partial\rho}{\partial y} - \frac{\tau_{by}}{\rho_0} + \frac{\partial(D\tau_{xy})}{\partial x} + \frac{\partial(D\tau_{yy})}{\partial y} \tag{5.13}$$

where f =   Coriolis parameter ($= 2\Omega \sin\phi$),
   Ω =   angular rate of earth's revolution,
   ϕ =   geographic latitude,
   F_i =   driving forces ($i = x,y$),
   ρ_0 =   density of a reference state, and
   τ_{bi} =   bottom stresses ($i = x,y$).

The above equations are sometimes called the shallow-water equations or the depth-averaged Navier-Stokes equations. The cross-stresses τ_{ij} include viscous friction, turbulent friction, and the non-linear terms resulting from the vertical averaging process (e.g., Equation (5.11)), which are usually called the radiation stresses:

$$\tau_{ij} = \frac{1}{D} \int_{z_b}^{\eta} \left[\nu\left(\frac{\partial u_i}{\partial x_j} + \frac{\partial u_j}{\partial x_i}\right) - \overline{u_i'u_j'} + (u_i - U_i)(u_j - U_j) \right] dz \tag{5.14}$$

In most natural bodies of water, the molecular viscosity terms can be safely neglected in comparison with the turbulence terms. The radiation stresses are often neglected, but they

represent important physical phenomena. For example, in bends they are at least partly responsible for shifting the high velocity part of the flow profile from the inner bank at the upstream region to the outer bank at the downstream region of the bend (Shimizu et al., 1991). In general, however, the terms of Equation (5.14) are collapsed in the form of diffusion coefficients and written as

$$\tau_{ij} = D_i \left(\frac{\partial U_i}{\partial x_j} + \frac{\partial U_j}{\partial x_i} - \frac{1}{2} \delta_{ij} \frac{\partial U_k}{\partial x_k} \right) \tag{5.15}$$

where δ_{ij} = Kronecker delta (= 1 if $i = k$, 0 otherwise), and
        D_i = diffusion coefficient in the ith direction (in general, $D_1 = D_2 = D_H$).

In turbulent flow, the diffusion coefficients can be prescribed or computed from any of the many existing turbulence models (see Rodi (1993) for more details), and the bottom shear stresses are assumed to have the same direction of the depth-mean velocity and be proportional to the square of its magnitude:

$$\frac{\tau_{bx}}{\rho} = C_f u \sqrt{u^2 + v^2} \quad \text{and} \quad \frac{\tau_{by}}{\rho} = C_f v \sqrt{u^2 + v^2} \tag{5.16}$$

where C_f = standard friction coefficient $\left(C_f \approx 0.003 \right)$.

Note that Equation (5.16) can also be written in terms of the Manning's roughness coefficient, n, or in terms of Chézy's roughness coefficient, C:

$$\frac{\tau_{bx}}{\rho} = \frac{gn^2}{D^{1/3}} u \sqrt{u^2 + v^2} = \frac{g}{C^2} u \sqrt{u^2 + v^2} \quad \text{and} \quad \frac{\tau_{by}}{\rho} = \frac{gn^2}{D^{1/3}} v \sqrt{u^2 + v^2} = \frac{g}{C^2} v \sqrt{u^2 + v^2} \tag{5.17}$$

The driving forces remaining in Equations (5.12) and (5.13) include such effects as atmospheric pressure gradients, wind stresses, density gradients, and tidal stresses.

Finally, the vertically-averaged form for the transport of a dissolved or suspended (very fine particles) constituent is

$$\frac{\partial (Dc)}{\partial t} + \frac{\partial (DUc)}{\partial x} + \frac{\partial (DVc)}{\partial y} = \frac{\partial}{\partial x} \left(DK_x \frac{\partial c}{\partial x} \right) + \frac{\partial}{\partial y} \left(DK_y \frac{\partial c}{\partial y} \right) + S_c \tag{5.18}$$

where K_x, K_y = diffusion coefficients in the x- and y-directions, respectively, and
        c = depth-averaged concentration.

In general, $K_x = K_y = K_H$, and K_H is directly related to D_H.

The shallow-water equations can be written in many possible forms. Those forms may include different terms than the ones considered above (corresponding to other physical effects), or they may be written in terms of curvilinear coordinates, for example. Many other aspects that are of interest, but that are outside the scope of this chapter, are described with much greater detail by Vreugdenhil (1994).

5.2.3 One-Dimensional Models

Most of the sediment transport models used in river engineering are one dimensional, especially those used for long-term simulation of a long river reach. One-dimensional models generally require the least amount of field data for calibration and testing. The numerical solutions are more stable and require the least amount of computer time and capacity. One-dimensional models are not suitable, however, for simulating truly two- or three-dimensional local phenomena.

One-dimensional models are usually based on the same conservation principles as the multi-dimensional models described in the previous two sections; i.e., the conservation of mass and momentum. Conservation of mass (continuity equation) can be expressed as

$$\frac{\partial A}{\partial t} + \frac{\partial Q}{\partial x} = q_l \tag{5.19}$$

where A = cross-sectional area of the flow,
          Q = water discharge, and
          q_l = lateral inflow per unit length.

Conservation of momentum:

$$\frac{\partial Q}{\partial t} + \frac{\partial}{\partial x}\left(\beta \frac{Q^2}{A}\right) + gA\frac{\partial \eta}{\partial x} + gA\left(S_f - S_0\right) = 0 \tag{5.20}$$

where S_f = friction slope,
          S_0 = bed slope, and
          β = momentum correction coefficient $(\beta \approx 1)$.

Equations (5.19) and (5.20) are known as the de Saint Venant equations. They assume that all the main variables are uniform across the cross-section, that the bed slope is small, and that all curvature effects are neglected. For a full discussion about these equations, including alternative forms, and for a detailed derivation, see Montes (1998).

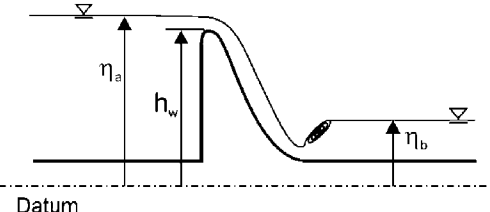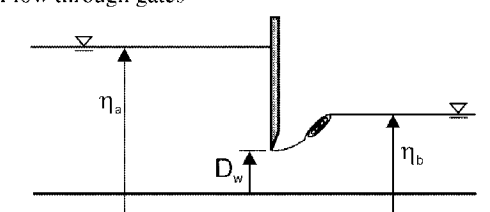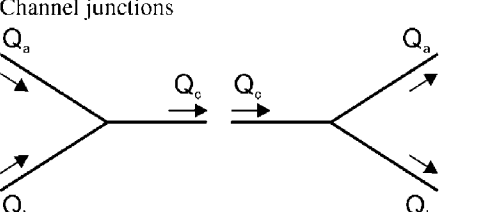The friction slope is assumed to be a function of the flow, such that
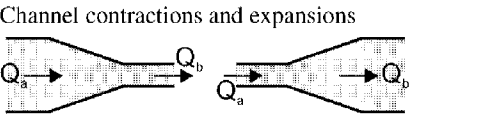
$$S_f = \frac{Q|Q|}{K^2}$$

(5.21)

where K = conveyance.

The conveyance is calculated using a resistance function, such as Manning's or Chézy's.

Special internal boundary conditions need to be considered in cases where flow is not well represented by the one-dimensional flow equations. Such situations may be encountered in flow over weirs or through gates. Some examples are presented in Table 5.1.

Table 5.1. Governing equations for one-dimensional flow for a number of special type of internal boundary conditions (h_a, h_b, and h_c denote the hydraulic head at points a, b, and c, respectively)

Flow type	Boundary conditions
Flow over weirs 	$Q_a = Q_b = f(\eta_a, h_w, \text{weir type and size})$
Flow through gates 	$Q_a = Q_b = f(\eta_a, \eta_b, D_w, \text{gate type, size, opening})$
Channel junctions 	$Q_c = Q_a + Q_b$ $h_c + \dfrac{V_c^2}{2g} + h_l = h_a + \dfrac{V_a^2}{2g}$ $h_c + \dfrac{V_c^2}{2g} + h_l = h_b + \dfrac{V_b^2}{2g}$ where h_l is an energy loss coefficient
Channel contractions and expansions 	$Q_a = Q_b$ $h_b + \dfrac{V_b^2}{2g} + h_l = h_a + \dfrac{V_a^2}{2g}$

Usually ignored by most models is the fact that the physical coordinate x is not the same as the local coordinate that follows (it is tangent to) the streamline direction, s: x is a distance in an unchanging coordinate system, while s is the true distance traveled by the water. In fact, the equations above are correct only if $dx = ds$ (i.e., if the ratio of channel length (s) to the downstream distance (x) remains equal to 1). That is not the case for most riverflows, especially in the case of large increases in discharge over highly sinuous paths. As the flow rates increase and the stages rise, the main body of water tends to assume different paths, especially in channels with compound cross-sections. In those circumstances, DeLong (1989) has shown that the appropriate metric coefficient relating the true channel distance to the reference length, defined by

$$M_a = \frac{1}{A} \int_A \frac{dx}{ds} dA \tag{5.22}$$

needs to be added to Equation (5.19). This coefficient represents an area-weighted sinuosity. Similarly, a flow-weighted sinuosity coefficient, defined by

$$M_q = \frac{1}{Q} \int_Q \frac{dx}{ds} dQ \tag{5.23}$$

needs to be incorporated into Equation (5.20). In Equation (5.23), dQ represents the increment in discharge corresponding to the incremental area dA. The reader is referred to DeLong (1989) for more details. However, it should be pointed out that momentum is a vector quantity; therefore, (unlike mass) its conservation cannot be enforced by a single scalar quantity describing the motion along a sinuous streamline.

5.2.4 Bed Evolution

In systems with boundaries that are subject to deposition and/or scour, it is necessary to model the movement of the sediment particles with the flow. Sediment transport modeling is a complex topic and is subject to much uncertainty. Sediment transport science has been covered in Chapters 3 and 4. In this section, some of the issues related to modeling these processes are presented.

Just as for the fluid flow, the mathematical model for sediment transport is usually based on conservation laws; i.e., conservation of suspended sediment load, bedload, and bed-material for each size fraction class. A number of additional auxiliary equations are needed, such as for the bed-material sorting (the process of exchange of sediment particles between the water stream and some conceptual model of a layered bed), bed resistance, sediment transport capacity, etc. Without being exhaustive, but keeping a good level of generality, the set of basic one-dimensional differential equations governing the transport of sediments can be written in the following manner:

Suspended-load transport:

$$\frac{\partial}{\partial t}\left(AC_j\right)+\frac{\partial}{\partial x}\left(QC_j\right)=\frac{\partial}{\partial x}\left(D_L A\frac{\partial C_j}{\partial x}\right)+\Phi_{s,j}$$

(5.24)

Bedload transport:

$$\frac{\partial G_j}{\partial t}+u_{bj}\frac{\partial G_j}{\partial x}=u_{bj}\Phi_{b,j}$$

(5.25)

Conservation of bed-material (sediment continuity):

$$\frac{\partial\left(\bar{C}A\right)}{\partial t}+(1-p)\frac{\partial A_s}{\partial t}+\frac{\partial Q_s}{\partial x}+C_L q_L+\sum_j\Phi_{s,j}+\sum_j\Phi_{b,j}=0$$

(5.26)

Bed-material sorting:

$$(1-p)\frac{\partial\left(\beta_j A_m\right)}{\partial t}+(1-p)\beta_j\Phi_0 H\{\Phi_0\}+(1-p)\beta_{0j}\Phi_0 H\{-\Phi_0\}+\Phi_{s,j}+\Phi_{b,j}=0$$

(5.27)

where A_m = cross-sectional area of the active layer,

A_s = bed-material area above some datum,

C_j = suspended-load concentration for size class j,

$\bar{C}$ = total suspended-load concentration,

C_L = sediment concentration of lateral flow,

D_L = dispersion coefficient in the longitudinal direction,

G_j = bedload transport rate of size fraction j,

p = porosity of bed sediments,

Q_s = sediment flow rate,

q_L = lateral flow rate per unit of length,

u_{bj} = average velocity of the bedload in size fraction j,

β_{0j} = fraction of the bed-material underlying the active layer belonging to size class j,

β_j = fraction of the bed-material in the active layer belonging to size class j,

$\Phi_{s,j}$ = net flux of suspended load from the active layer to the water stream (source/sink term), and

$\Phi_{b,j}$ = exchange of sediments in size class j between the active layer and the bedload transport layer (source/sink term).

Additionally, $H\{\Phi\}$ is the step function defined by

$$H\{\Phi\} = \begin{cases} 1 & \Phi \geq 0 \\ 0 & \Phi < 0 \end{cases} \tag{5.28}$$

The quantity Φ_0 is defined by

$$\Phi_0 = \frac{\partial A_s}{\partial t} - \frac{\partial A_m}{\partial t} \tag{5.29}$$

Note also that, in Equation (5.26),

$$\frac{\partial Q_s}{\partial x} = \sum_j \frac{\partial G_j}{\partial x} \tag{5.30}$$

Equivalent equations can be developed for multi-dimensional flows, which are similar to Equations (5.3) and (5.18), for three- and two-dimensional models, respectively.

The diffusion coefficient D_L in the suspended-load equation—Equation (5.24)—is the result of combining a laminar flow equation using Fick's law for the diffusion, with a turbulent flow term that uses the diffusion analogy to represent the turbulent correlations. Because D_L is heavily influenced by channel geometry and embodies the essentially three-dimensional nature of turbulence, it is very difficult to provide good theoretical estimates of its value. In practice, it may vary by orders of magnitude within the same river or watercourse. When no direct reliable measurements of this quantity exist, D_L is reduced to a numerical parameter and is determined by model calibration. A more complete treatment of this subject can be found in Fischer et al. (1979).

The source/sink term in the transport Equations (5.24) and (5.25) can be evaluated using non-equilibrium transport concepts. In rivers and streams, it is usually acceptable to assume that the bed-material load discharge is equal to the sediment transport capacity of the flow; i.e., the bed-material load is transported in an equilibrium mode. In other words, the exchange of sediment between the bed and the fractions in transport is instantaneous. However, there are circumstances in which the spatial-delay and/or time-delay effects are important. For example, reservoir sedimentation processes and the siltation of estuaries are essentially non-equilibrium processes. In the laboratory, it has been observed that it may take a significant distance for a clear water inflow to reach its saturation sediment concentration.

Residual transport capacity for the j-th size fraction is defined as being the difference between its transport capacity, C_j^*, and the actual transport rate, C_j. Armanini and Di Silvio (1988) assumed the source term in Equation (5.24) to be directly proportional to the residual transport capacity:

$$\Phi_{s,j} = \frac{Q}{\lambda_{s,j}}\left(\beta_j C_j^* - C_j\right)$$

(5.31)

where $\lambda_{s,j}$ = characteristic length for the suspended load.

Similarly, for the source/sink term of the bedload transport equation we can write

$$\Phi_{b,j} = \frac{Q}{\lambda_{b,j}}\left(\beta_j G_j^* - G_j\right)$$

(5.32)

where $\lambda_{b,j}$ = characteristic length for the bedload, and

G_j^*, G_j = the carrying capacity and the actual transport rate of the bedload, respectively.

More details are presented in Armanini and Di Silvio (1988) and references therein, including methods for computing the characteristic lengths $\lambda_{s,j}$ and $\lambda_{b,j}$.

Bell and Sutherland's (1983) work suggests that the bedload discharge G_j^* is related to the bedload capacity G_j by a loading law of the form

$$\frac{\partial G_j}{\partial x} = K\left(t\right)\left(G_j^* - G_j\right) + a_1 \frac{G_j}{G_j^*}\frac{\partial G_j^*}{\partial x} + a_2 \frac{G_j}{\beta_j}\frac{\partial \beta_j}{\partial x}$$

(5.33)

where $K\left(t\right)$ = a coefficient with units of [L^{-1}], and

a_1, a_2 = dimensionless coefficients.

There are other approaches—for example, based on particle fall velocities and near bed concentrations at reference levels—but regardless of the approach used, non-equilibrium transport should be considered and, if necessary, included in a general sediment transport model.

The velocity of the bedload in Equation (5.25) can be found using one of the expressions provided in the literature. See Bagnold (1963) or van Rijn (1984a), for example.

Equation (5.26) can be simplified without great loss of generality. Firstly, in most circumstances, the change in suspended sediment concentration in any given cross-section is much smaller than the change in river bed; i.e.,

$$\frac{\partial\left(\bar{C}A\right)}{\partial t} << \left(1 - p\right)\frac{\partial A_s}{\partial t}$$

(5.34)

Secondly, if the parameters in the sediment transport function for a cross-section can be assumed to remain constant during a time step, we can write

$$\frac{\partial Q_s}{\partial t} = 0 \quad \text{or} \quad \frac{\partial Q_s}{\partial x} = \frac{dQ_s}{dx} \tag{5.35}$$

This assumption is valid only if there is little variation of the cross-sectional geometry; i.e., no significant erosion and/or deposition occurs in a time step. This assumption allows the decoupling of water and sediment routing computations. In practice, this condition can be met by using a small enough time step.

Then, ignoring for now the source/sink terms, introducing Equations (5.34) and (5.35) into Equation (5.26) yields

$$(1-p)\frac{\partial A_s}{\partial t} + \frac{dQ_s}{dx} + C_L q_L = 0 \tag{5.36}$$

which is a form of the bed continuity equation widely used in numerical models.

Distribution of bed sediments during the erosion/deposition process is straightforward in two- and three-dimensional models, in which case the sediments are distributed uniformly across the computational cell. In one-dimensional models, however, special techniques must be used to represent the non-uniform cross-sectional variation of the deposited sediments. For example, in reservoirs and slow deposition in many rivers, sediment deposits are formed by filling the lowest parts of the channel first and by lifting the channel bed horizontally across the section, as depicted in Figure 5.3 (a).
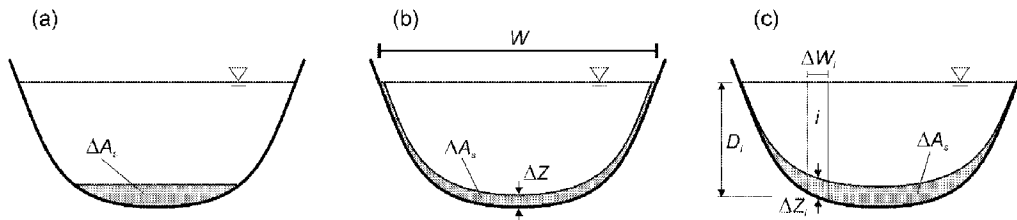
Figure 5.3. Sediment distribution methods of deposited and/or scoured sediments within a cross-section by a one-dimensional model. (a) horizontal distribution during deposition; (b) uniform distribution; and (c) cross-sectional distribution proportional to flow parameters.

The most common method used by one-dimensional models is by spreading the cross-sectional change, ΔA_s, with a constant thickness (measured along the vertical) across the wetted perimeter. The thickness ΔZ of the deposited/eroded materials is calculated from

$$\Delta Z = \frac{\Delta A_s}{W} \tag{5.37}$$

where W = channel top width.

This type of bed change is shown in Figure 5.3 (b). Other methods use selected flow parameters to compute the local bed variation. The cross-section is divided in slices of arbitrary width, ΔW_i, and the local bed variation ΔZ_i is computed for each of these slices. Common variables are the low depth D, the excess of bed shear stress $\tau - \tau_c$, and the conveyance K, yielding, respectively,

$$\Delta Z_i = \frac{D_i}{A} \Delta A_s \tag{5.38}$$

$$\Delta Z_i = \frac{\left(\tau_i - \tau_{ci}\right)^m}{\sum_i \left(\tau_i - \tau_{ci}\right)^m \Delta W_i} \Delta A_s \tag{5.39}$$

and

$$\Delta Z_i = \frac{K_i}{\sum_i K_i \Delta W_i} \Delta A_s \tag{5.40}$$

where m = an exponent,

   τ_c = the Shields critical bed shear stress,

and the subscripts i refer to each of the slices used to subdivide the cross-section (see Figure 5.3 (c)).

5.2.5 Auxiliary Equations

5.2.5.1 Flow Resistance

The sets of differential equations presented in the previous sections require an additional set of relationships to define the boundary conditions. For two- and three-dimensional models, relationships are needed to represent the effects of solid boundaries on the flow field. These relationships are important because sediment transport processes are dominant in the near-bed region; therefore, it is important to have accurate predictions of the flow parameters in that region.

Near the bed, the equation of motion for steady, uniform turbulent flow is given by (see Figure 5.4)

$$\tau_z \Delta x \Delta y = \rho g \left(D - z \right) \Delta x \Delta y \sin \theta \tag{5.41}$$
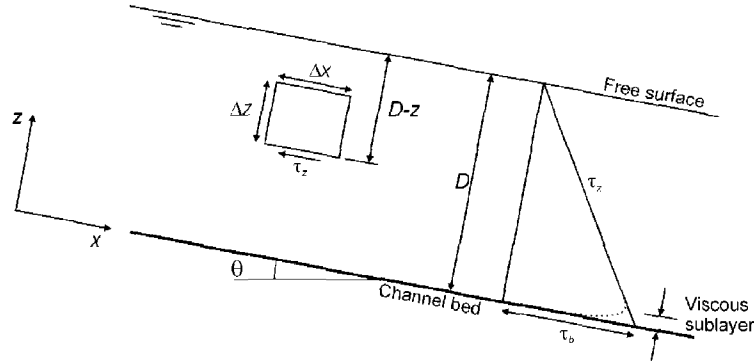
Figure 5.4. Vertical distribution of shear stress in uniform, turbulent, open channel flow.

Using $S_0 = \sin \theta$, at the bed ($z = 0$), Equation (5.41) becomes

$$\tau_b = \rho g D S_0 \tag{5.42}$$

where τ_b =   bed shear stress.

Note that, by definition,

$$\tau_b = \rho U_*^2 \tag{5.43}$$

therefore,

$$U_* = \sqrt{g D S_0} \tag{5.44}$$

where U_* =   the shear velocity.

The effects of the solid boundaries on the velocity distribution in turbulent flows are usually accounted for using an equivalent sand grain roughness, or Nikuradse roughness, k_s (Nikuradse, 1933). The bed roughness influences the near bed velocity profile due to the flow eddies generated by the roughness elements. These small eddies are quickly absorbed by the flow as they move away from the bed. A general form for the velocity distribution over the flow depth is given by

$$u = \frac{U_*}{\kappa} \log \left(\frac{z}{z_0} \right) \tag{5.45}$$

where κ =   the von Kármán's constant (≈ 0.41 in clear free surface flows).

5-17

The zero-velocity level z_0 ($u = 0$ at $z = z_0$) was found to depend on the flow regime; i.e., if the solid boundaries are smooth or rough. In hydraulically smooth flow, the roughness elements are much smaller than the viscous sublayer—the viscous sublayer is a layer where the viscous stresses dominate over the turbulent stresses (see Figure 5.4)—while in hydraulically rough flow, the viscous sublayer does not exist; therefore, the velocity profile is not dependent on fluid viscosity. There is a transition range between the two flow regimes, called hydraulically transitional flow, where the velocity profile is affected by both viscosity and bottom roughness. The different flow regimes and their corresponding velocity profiles are summarized in Table 5.2.

Table 5.2. Zero-velocity level equations for the various flow regimes, depending on wall roughness. ν is the fluid viscosity

Flow regime	$R_{e^*} \left(= \dfrac{U_* k_s}{\nu} \right)$	Zero-velocity level, z_0
Hydraulically smooth flow	$R_{e^*} \leq 5$	$0.11 \dfrac{\nu}{U_*}$
Hydraulically rough flow	$R_{e^*} \geq 70$	$0.033 k_s$
Hydraulically transitional flow	$5 < R_{e^*} < 70$	$0.11 \dfrac{\nu}{U_*} + 0.033 k_s$

Opposite to bed shear stress, wind stresses occur in the gas-liquid interface, or free surface, and are caused by the atmospheric circulation. A common semi-empirical relationship for the wind stresses is

$$\tau_s = \frac{C_f}{\rho_{air}} V^2 \tag{5.46}$$

where ρ_{air} = the density of air,
       V = the wind velocity measured at the 10 m level, and
       C_f = a drag coefficient and is of the order of 0.001.

The direction of the stresses is the same as of the wind.

In one-dimensional models, friction is used to compute the conveyance K, usually from an equation such as Manning's equation:

$$Q = KS_f^{1/2} = \frac{\delta}{n} AR^{2/3} S_f^{1/2} \tag{5.47}$$

where Q = flow discharge,
       A = flow area,
       R = hydraulic radius ($= A/P$),

P = wetted perimeter,
S_f = free surface slope,
n = Manning's roughness coefficient, and
δ = a parameter (= 1 in the metric system, = 1.49 in English units).

Note that Equation (5.47) is a steady state equation that, nonetheless, is used in unsteady hydraulic models. There are other formulae that use different friction factors, such as the Chézy roughness coefficient, C, and the Darcy-Weisbach coefficient f:

$$K = CAR^{1/2} = A\left(\frac{8gR}{f}\right)^{1/2}$$ (5.48)

Using Equations (5.47) and (5.48), it is easy to see that simple relationships exist between n, C, and f.

In one-dimensional flows, the roughness coefficient contains more than just skin friction losses. The overall resistance to the flow posed by channel meandering, vegetation types and density, cross-sectional changes in shape and size, irregularity of the cross-sections, etc., is included in the overall n for each channel reach. Estimating roughness is not a trivial task and requires considerable judgment. There are published flow resistance formulae that are more or less successful when applied to specific situations, but their lack of generality precludes their use in a numerical model for broad applications (see, for example, Klaassen et al. (1986) for more details). Some help exists in the form of tables, such as those that can be found in Chow (1959) and Henderson (1966). Barnes (1967) provides a photographic guide. The method by Cowan (1956) is summarized here. The basis of this method is the selection of a basic Manning's n value from a short set and to the application of modifiers according to the different characteristics of the channel. The method can be applied in steps, with the help of Table 5.3:

1. Select a basic n_0.
2. Add a modifier n_1 for roughness or degree of irregularity.
3. Add a modifier n_2 for variations in size and shape of the cross-section.
4. Add a modifier n_3 for obstructions (debris, stumps, exposed roots, logs,).
5. Add a modifier n_4 for vegetation.
6. Add a modifier n_5 for meandering.

The final value of the Manning's n is given by

$$n = n_0 + n_1 + n_2 + n_3 + n_4 + n_5$$ (5.49)

The hydraulic resistance characteristics of vegetation depend on a number of parameters, such as plant flexibility or stiffness, density of vegetation, plant leaf characteristics (area, shape, and density), etc. For example, rigid vegetation increases flow resistance because the water has to expend more work to go around the obstacles posed by the individual plant stems and stalks. On

the other hand, some types of highly flexible grass that bend easily with the flow have the effect of paving the bed, making it smoother and reducing its drag, and, therefore, decreasing flow resistance.

Table 5.3. Modifiers for basic Manning's n in the method by Cowan (1956), with modifications from Arcement and Schneider (1987)

Basic Manning's roughness values (n_0)			
Concrete	0.011-0.018	Gravel	0.028-0.035
Rock cut	0.025	Coarse gravel	0.026
Firm soil	0.020-0.032	Cobble	0.030-0.050
Coarse sand	0.026-0.035	Boulder	0.040-0.070
Fine gravel	0.024		

Modifier for degree of irregularity (n_1)			
Smooth	0.000	Moderate	0.006-0.010
Minor	0.001-0.005	Severe	0.011-0.020

Modifier for cross-sectional changes in size and shape (n_2)			
Gradual	0.000	Frequent	0.010-0.015
Occasional	0.005		

Modifier for the effect of obstructions (n_3)			
Negligible	0.000-0.004	Appreciable	0.020-0.030
Minor	0.005-0.019	Severe	0.060

Modifier for vegetation (n_4)			
Small	0.001-0.010	Very large	0.050-0.100
Medium	0.011-0.025	Extreme	0.100-0.200
Large	0.025-0.050		

Modifier for channel meandering (n_5)	
L_m/L_s	n_5
1.0-1.2 (minor)	0.0
1.2-1.5 (appreciable)	$0.15(n_0 + n_1 + n_2 + n_3 + n_4)$
> 1.5 (severe)	$0.30(n_0 + n_1 + n_2 + n_3 + n_4)$

L_m = meander length; L_s = length of straight reach

The effects caused by vegetation are complex, and there are no generally valid predictive models for their effects. Multi-dimensional modeling of turbulent dispersion using advanced turbulence models has been carried out—e.g., Shimizu and Tsujimoto (1994) and Naot et al. (1995) and (1996)—but its application to engineering models is difficult and requires significant computational effort. Simpler predictors for one-dimensional modeling have been developed by many authors, but they are usually based on limited amounts of data and are valid only for the region in which they were derived. Some of those expressions are presented in Table 5.4. Their use in any model should always be verified and supported with field measurements.

Table 5.4. Resistance relations for flow through vegetated channels

Author	Resistance equation	Notes
Gwinn and Ree (1980)	$n = \dfrac{1}{2.08 + 2.30\xi + 6\log(10.8VR)}$	R = hydraulic radius; ξ = a coefficient that depends on five retardance classes; the goodness-of-fit of the expression was not reported.
Kouwen and Li (1980)	$\dfrac{1}{\sqrt{f}} = a + \kappa \log\dfrac{R}{k_s}$; $k_s = 0.14 h_v \left[\dfrac{\left(\dfrac{MEI}{\tau}\right)^{0.25}}{h_v} \right]^{1.59}$	a = dimensionless coefficient that is a function of the cross-sectional shape; h_v = local height of the vegetation; M = stem density; E = stem modulus of elasticity; I = stem area's second moment of inertia; Temple (1987) has correlated MEI with the vegetation height h_v for a range of dormant and growing grasses.
Pitlo (1986)	$n = \dfrac{0.0343}{(1 - D_v) + 0.0016}$	D_v = vegetation density; i.e., fraction of channel cross-section occupied by the submerged vegetation; the goodness-of-fit was not reported; based on measurements in one channel.
HR Wallingford (1992)	$n = 0.0337 + 0.0239\dfrac{D_v}{VR}$	Based on measurements taken in the Candover Brook, Hampshire, United Kingdom.
Bakry et al. (1992)	$n = a_1 D_h^{b_1}$; $n = a_2 + b_2 \log(VR)$; $n = a_3 + b_3 D_v$	D_h = hydraulic depth ($= A/W$); a_1 = coefficient ranging between 0.0087 and 0.0634; b_1 = coefficient ranging between -0.404 and 2.566; a_2 = coefficient ranging between -0.067 and 3.798; b_2 = coefficient ranging between -0.089 and 0.001; a_3 = coefficient ranging between 0.032 and 0.049; b_3 = coefficient ranging between 0.0072 and 0.12; units are metric.

Somewhat similar to the flow through vegetated channels is the case of mountain rivers, where flow resistance is dominated by grain roughness in gravel beds, rather than by the vegetation effects. Flow resistance is high at low stage and submergence and tends to decrease with increasing submergence (submergence is defined as the ratio between the water depth D and the size of the roughness elements, typically d_{84}). Many flow resistance relationships have been

developed, but most suffer from a high content of empiricism and are site dependent. Errors on the order of 30% or higher are common. A summary of some of the most well-known relationships is presented in Table 5.5. These empirical formulae should be applied with care, within the range for which they were developed, and require careful verification and validation using field data.

Table 5.5. Resistance formulae for flow in mountain rivers

$$\sqrt{\frac{8}{f}} = A + B\log(X)$$

Author	A	B	X	Range of validity
Bray (1979)	0.701	6.68	$\dfrac{D}{d_{50}}$	$2.5 \le \dfrac{D}{d_{65}} \le 120$
Thompson and Campbel (1979)	5.66	$-0.566\dfrac{k_s}{R}$	$12\dfrac{R}{k_s}$	$\dfrac{D}{d_{84}} > 1.2$
Griffiths (1981)	2.15	5.60	$\dfrac{R}{d_{50}}$	$1 \le \dfrac{R}{d_{50}} \le 200$
Bathurst (1985)	4	5.62	$\dfrac{D}{d_{84}}$	$0.3 < \dfrac{R}{d_{84}} < 1$
Bray and Davar (1987)	3.1	5.7	$\dfrac{R}{d_{84}}$	$\dfrac{D}{d_{50}} > 1$

$$\sqrt{\frac{8}{f}} = AX^B$$

Author	A	B	X	Range of validity
Bray (1979)	5.03	0.268	$\dfrac{D}{d_{90}}$	$2.5 \le \dfrac{D}{d_{65}} \le 120$
Griffiths (1981)	3.54	0.287	$\dfrac{D}{d_{50}}$	$0.0085 < S_0 < 0.011$
Bray and Davar (1987)	5.4	0.25	$\dfrac{R}{d_{84}}$	$\dfrac{D}{d_{50}} > 1$
Bathurst (2002)	3.84 3.10	0.547 0.93	$\dfrac{D}{d_{84}}$	$\dfrac{D}{d_{84}} < 11; \quad 0.002 \le S_0 \le 0.040$

5.2.5.2 Sediment Transport

Sediment transport capacity—e.g., the bedload capacity G_j^* of Equation (5.32)—is computed using common sediment transport formulae, a subject that is covered in detail in Chapter 3 of this manual for non-cohesive sediments, and in Chapter 4 for cohesive sediments. Note, however, that most formulations are based on steady, uniform conditions. For unsteady transport under flood conditions, other approaches may have to be used—see Song and Graf (1995) and Bestawy (1997). Furthermore, in natural waterways, the presence of vegetation may require the use of different methods. Sediment transport in vegetated areas is an important topic due to increasing eco-hydraulics applications in water quality. For example, in grassed areas where the transported particles are usually very small and there is no bedload, the suspended-load transport equation, Equation (5.24), can be used, but with appropriately prescribed dispersion coefficients and sink terms. Deletic (2000) has developed expressions specifically for the trapping efficiency of grassed areas, from which the sink term can be readily calculated. Simões (2001) has successfully modeled the three-dimensional flow through sparse rigid vegetation, in which the dispersion coefficients were computed using rather simple turbulence closures.

Another factor contributing to the increased complexity of this subject is that there is no universal way to deal with sediment mixtures. There are almost as many approaches as there are authors. Furthermore, many of the methodologies are problem dependent and lack sufficient generality to be applicable (with reliability) to a wide range of problems. Here, some of the most common and useful methodologies are briefly presented, with the intent of underlining the importance of this subject.

By fractional transport capacity, we mean the technique to compute the transport rate of sediment mixtures with significant spread in particle sizes. It is important not only to compute the total transport capacity, but also the individual capacities for each of the particle size classes. There are essentially four ways to accomplish this task: (1) direct computation for each size fraction, (2) correction of bed shear stresses, (3) by fractioning the capacity of each size class, and (4) by using a distribution function.

The direct computation of each size fraction (e.g., Einstein, 1950) works by computing directly the sediment transport rate for each grain size present in the mixture, q_{sj} (the lower case denotes the quantity per unit width). Then, the total transport rate per unit width is computed from

$$q_s = \sum_j q_{sj} \qquad (5.50)$$

Einstein (1950) was the first to recognize the effect of the presence of the larger particle sizes on the transport rate of the smaller sizes. He introduced a hiding factor to account for that effect, an approach that is now used by many, sometimes in modified and/or simplified manner.

The correction of bed shear stress approach works by introducing a correction factor to the computation of the shear stress acting upon the different particle sizes present in the bed. Thus,

transport rate predictors for uniform bed-material are extended for sediment mixtures. If τ_j^* is the dimensionless shear stress acting upon the j-th size class particles, then the transport rate per unit width for that class is

$$q_{sj} = f\left(\xi_j \tau_j^*\right) \quad \text{or} \quad q_{sj} = f\left(\tau_j^* - \xi_j' \tau_{cj}^*\right) \tag{5.51}$$

where ξ_j, ξ_j' = correction factors accounting for particle sheltering and exposure effects, and

τ_{cj}^* = dimensionless critical (Shields) shear stress for particles in size class j.

The total transport rate is computed from Equation (5.50). The first form of Equation (5.51) was introduced by Egiazaroff (1965) and has been used by many researchers since then.

The fractioning of the capacity of each size class works in the following way: first, the potential transport capacity for each size fraction j, C_j, is computed from uniform sediment formulae as if the size fraction was the only sediment present in the bed. Then, it is reduced to match the availability of that particular size class, i.e.,

$$C_{tj} = p_j C_j \tag{5.52}$$

where p_j = percentage of material belonging to size class j present in the bed, and
C_{tj} = actual fractional transport potential for the j-th size class.

The total transport potential, C_t, is given by

$$C_t = \sum_j C_{tj} \tag{5.53}$$

Equation (5.53) represents the most widely used form of fractional transport used in numerical modeling. It has many shortcomings (see Hsu and Holly, 1992), among which is the fact that it predicts zero transport capacity for fractions that are not present in the bed—for example, it predicts zero transport of any sand entering a reach whose bed is composed only of gravel, irrespective of the hydraulic conditions. To overcome this problem, instead of p_j, many models use $\varepsilon p_j + (1-\varepsilon) p_j^*$, where p_j^* is the percentage of the j-th size class present in transport (i.e., entering the reach), and ε is a weighting factor $(0 \le \varepsilon \le 1)$. For many circumstances, it was found that $\varepsilon = 0.7$ provides a good approximation; however, this value is not universal.

Finally, the last method uses a distribution function to compute the transport capacity for each individual size class. This is accomplished by first computing the total transport capacity using a bed-material load equation and then distributing it into fractional transport capacities by using a distribution function:

$$C_{ij} = F_j C_t \quad \text{with} \quad \sum_j F_j = 1 \tag{5.54}$$

The advantage of this method is the fact that the distribution function F_j does not have to resemble the size distribution of the bed-material and that it can include the sheltering and exposure effects by relating F_j to both the sediment properties and the hydraulic conditions. This approach is less used than the three previously described methods. One well-known application of this concept is the work by Karim and Kennedy (1982).

Intimately connected to selective transport is the concept of bed sorting. As a result of computing sediment transport by size fraction, particles of different sizes are transported at different rates. Depending on the hydraulic parameters, the incoming sediment distribution, and the bed composition, some particle sizes may be eroded, while others may be deposited or may be immovable. Consequently, several different processes may take place. For example, all the finer particles may be eroded, leaving a layer of coarser particles for which there is no carrying capacity. No more erosion may occur for those hydraulic conditions, and the bed is said to be armored. This armor layer prevents the scour of the underlying materials, and the sediment available for transport becomes limited to the amount of sediment entering the reach. Future hydraulic events, however, such as an increase of flow velocity, may increase the flow carrying capacity, causing the armor layer to break and restart the erosion processes in the reach. Many different processes may occur simultaneously within the same channel reach. These depend not only on the composition of the supplied sediment (i.e., the sediment entering the reach), but also on bed composition within that reach.

It is important to track bed composition during flood events. During high flows, armor layers are often ruptured, exposing the underlying material, which is finer and more susceptible to erosion. This may be particularly important in reaches just downstream from dams, where reduced sediment supply usually results in base level lowering until a certain equilibrium condition is reached—that is, until the bed becomes armored for the prevailing (regulated) hydraulic conditions. If the armor layer is removed, a new degradation process is initiated, which may lead to further erosion long after the flood takes place. Furthermore, a certain type of sediment transport seems to happen only during flood situations, such as the transport characterized by dunes of finer sediment moving over gravel beds with a mobile armor layer (paved beds). This type of transport has the effect of destabilizing the armor layer, even if the flow is too weak to break that armor under the normal (non-flood) hydraulic regime, resulting in potentially additional degradation that normally would not occur (Klaassen, 1990).

There are many different approaches to bed sorting. Some of the most common are, perhaps, the ones by Bennett and Nordin (1977) and Borah et al. (1982), but many other approaches are also used. Most of the existing bed sorting algorithms are highly case dependent and lack sufficient generality. Therefore, they have to be selected carefully. For a more detailed treatment of the subject, see, for example, Armanini (1995).

5.3 Numerical Solution Methods

In most cases, there are no known analytical solutions for the governing equations described in the previous sections, except for the simplest of geometric configurations and flow regimes. However, there is a vast body of numerical mathematics that can be used to find the solutions for an alternative, but approximate, numerical (discrete) statement to the continuous problem expressed by the governing partial differential equations and their corresponding boundary conditions. The resulting numerical description of the mathematical model at hand consists of a set of algebraic equations that can be programmed and solved in a computer: the numerical model.

This section will offer a brief description of some of the methods most commonly used to solve the fluid flow equations. The techniques of interest are those based on some type of gridded discretization of the problem at hand, in which the continuous variables for which the solution is sought are solved only at specific discrete locations of the physical domain. The algebraic equations that form the numerical model are functions of those discrete quantities.

For the same problem (i.e., the same set of differential governing equations and boundary conditions), it is possible to obtain very distinct sets of algebraic numerical equations, depending on the technique used to discretize the equations. This chapter will be concerned with three such techniques: finite differences, finite elements, and finite volumes. In practice, there are many other techniques available to numerically solve the fluid flow equations. On the other hand, it is possible to state certain finite difference and finite volume techniques as a subset of the finite element technique. We will not deal with these fine points here, but the interested reader is directed to standard textbooks in computational fluid dynamics, such as those by Ferziger and Peric (2002) and by Wesseling (2001), for example.

As mentioned above, the translation from continuous to discrete replaces one problem (the continuous formulation) by another (the discrete formulation). The latter should provide a solution that should converge to the solution of the former. In this context, convergence is a term that denotes a relationship between the numerical and the analytical solutions. Convergence should be obtained as the grid spacing (Δx in one-dimensional problems) and time step (Δt in unsteady problems) are refined; i.e., as $\Delta x, \Delta t \rightarrow 0$. Figure 5.5 depicts several types of solution behavior for the discrete problem equations, including instability and convergence to the wrong solution.

Convergence is ensured by Lax's theorem—which has been proven for linear problems only, but which is nonetheless at the foundation of computational fluid dynamics—which states that consistence and stability are sufficient to ensure the convergence of a numerical scheme. Consistence is a term applied to the algebraic equations: a numerical scheme is said to be consistent with the partial differential equation if its truncation error disappears in the limit when $\Delta x, \Delta t \rightarrow 0$. Stability is a term that applies to the numerical solution itself: a solution is stable if it remains bounded at all times during the computations.
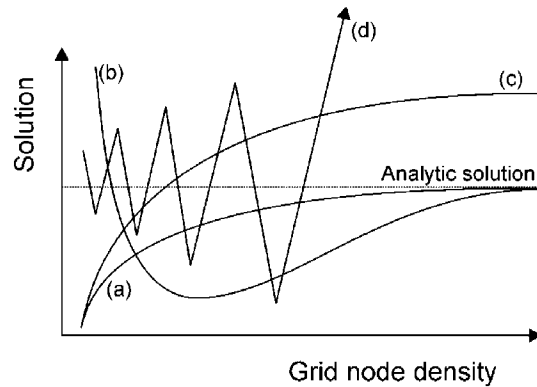
Figure 5.5. Different possible solution behaviors for numerical solution schemes: the solutions produced by schemes (a) and (b) converge to the analytical solution upon grid refinement; (c) converges to the wrong solution; and (d) does not converge at all.

5.3.1 Finite Difference Methods

Finite difference methods are probably the most simple and most common methods employed in fluid flow models, as well as in other disciplines requiring the numerical solution of partial differential equations. They are based on the approximation of the individual derivative terms in the equations by discrete differences, thus converting them into sets of simultaneous algebraic equations with the unknowns defined at discrete points over the entire domain of the problem. For example, the partial derivative of $u(x,y)$ at point (i,j) of the discretized domain in the x-direction can be written as

$$\frac{\partial u(x,y)}{\partial x} = \lim_{\Delta x \to 0} \frac{u(x+\Delta x,y)-u(x)}{\Delta x} \approx \frac{u_{i+1,j}-u_{ij}}{\Delta x_{ij}} \tag{5.55}$$

and similarly for the y-direction (see Figure 5.6).

Note that Equation (5.55) does not represent the only possible choice of discretization. For example, without loss of mathematical rigor, one could choose instead

$$\frac{\partial u}{\partial x} \approx \frac{u_{ij}-u_{i-1,j}}{\Delta x_{i-1,j}} \tag{5.56}$$

Equation (5.55) is called forward difference, and Equation (5.56) is called backward difference. One could define central differences, or even use multiple Δx to define differential operators that span many grid nodes. On the other hand, the grid can be quite complex. Curvilinear non-orthogonal grids are indeed used to describe complex flow domains, but the corresponding

differential operators are also more complicated than the ones shown above. For a more detailed overview of finite difference methods in computational fluid dynamics, the reader is directed to Tannehill et al. (1997).
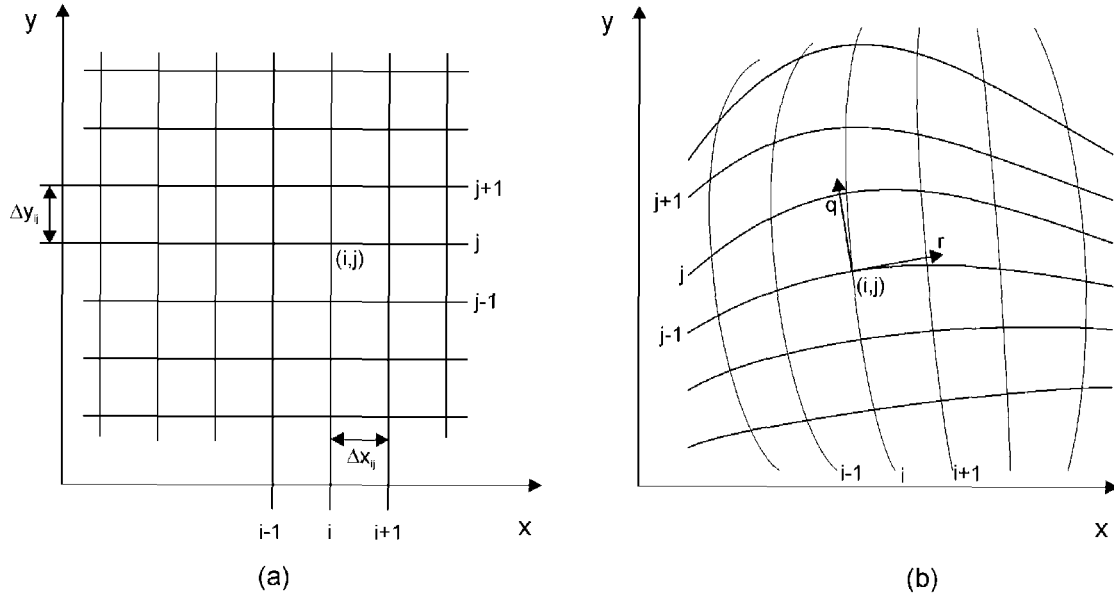

Figure 5.6. Typical mesh systems used in finite difference methods. (a) Cartesian orthogonal mesh; (b) curvilinear mesh (not necessarily orthogonal). The local coordinate system for point (i,j) in (b) is defined by the unit vectors q and r, which are tangent to the grid lines. The points where the variables are defined are located at the intersection of the grid lines.

In one-dimensional free surface flow, the most popular scheme to solve the de Saint Venant equations is the Preissman scheme (Preissman, 1961). For an extensive coverage of the method, the reader is directed to Cunge et al. (1980). Here, only a brief description is presented.

The Preissman scheme is a four-point scheme (also called box scheme), as shown schematically in Figure 5.7. If $f(x,t)$ is any of the flow variables of interest (e.g., water depth and discharge), then

$$\frac{\partial f}{\partial t} \approx \left(1-\psi\right)\frac{f_j^{n+1} - f_j^{n}}{\Delta t} + \psi\frac{f_{j+1}^{n+1} - f_{j+1}^{n}}{\Delta t} \tag{5.57}$$

$$\frac{\partial f}{\partial x} \approx \left(1-\theta\right)\frac{f_{j+1}^{n} - f_j^{n}}{\Delta x} + \theta\frac{f_{j+1}^{n+1} - f_j^{n+1}}{\Delta x} \tag{5.58}$$

and

$$f = (1-\psi)(1-\theta) f_j^n + \psi(1-\theta) f_{j+1}^n + \theta(1-\psi) f_j^{n+1} + \psi\theta f_{j+1}^{n+1} \tag{5.59}$$

where θ, ψ =   weighting coefficients.

Direct application of the Preissman scheme to the de Saint Venant equations, Equations (5.19) and (5.20), results in a non-linear system of algebraic equations. To avoid having to deal with the numerical difficulties normally associated with non-linear systems, in practice the system is linearized by using a Taylor series expansion of the system coefficients and then by rewriting it in terms of the variations of the unknowns rather than solving for the unknowns themselves directly. In other words, if the original system is expressed in terms of the free surface η and the discharge Q as the dependent variables, after the Taylor series expansion the algebraic system of equations is rewritten in terms of $\Delta\eta_j$ and ΔQ_j, where $\Delta\eta_j$ and ΔQ_j represent the variation of η_j and Q_j in a time step Δt and for each discretization point j. The system can then be solved using traditional iterative (such as the Newton iteration method) or direct methods (such as the double-sweep method).
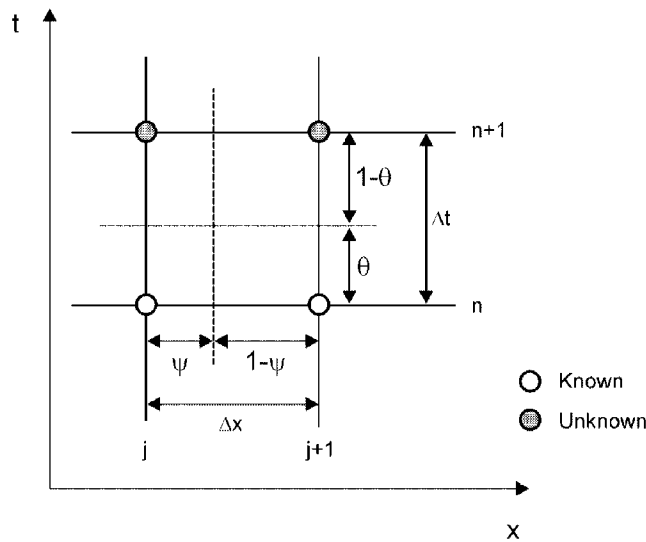

Figure 5.7. The four-point Preissman finite difference operator.

The weighting coefficients are used to control the numerical error and stability of the scheme. $\psi = \theta = \frac{1}{2}$ produces a scheme whose truncation errors are of order Δt^2 and Δx^2. The scheme is stable and non-dissipative (i.e., it does not smear the solution). Increasing θ introduces truncation errors that cause dissipation. Using $\theta = 1$ yields the largest numerical dissipation, which produces poor results in unsteady problems but provides the fastest convergence (useful for steady-state problems). In practice, it has been found that $\theta = 0.67$ is a good value for most problems. If $\theta < \frac{1}{2}$, the Preissman scheme is always unstable.

5.3.2 Finite Element Methods

Finite element methods have been used successfully for fluid flow problems since the 1960's. They are particularly useful to solve problems with complex geometries, as they do not require the structured grid system needed in finite difference techniques. In an unstructured grid, the computational nodes do not need to be defined in an ordered manner, as opposed to structured grids where each node is identified by an (i,j) pair (or (i,j,k) trio in three-dimensional models), such as those shown in Figure 5.6. An example of unstructured grid is shown in Figure 5.8.
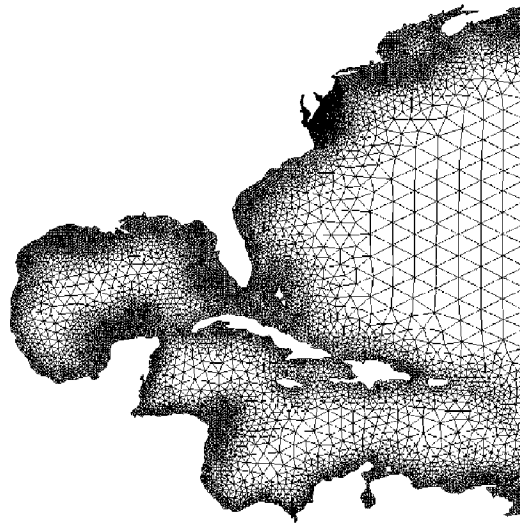

Figure 5.8. Finite element mesh for part of the American Atlantic coast, as generated by the two-dimensional automatic finite element grid generator software, CCALMR, Oregon Health and Science University. Note that the darker areas represent a very high density of triangles that cannot be resolved at the scale used in this figure.

There are two main approaches for the formulation of finite element methods: variational methods and weighted residual methods. In variational methods, the variational principle for the governing equation is minimized. In general fluid mechanics problems, exact forms of the variational principles for the governing non-linear equations are difficult to find (unlike in the linear equations encountered in solid mechanics); therefore, weighted residual methods are much more popular. Residual methods are based on minimizing some sort of error, or residual, of the governing equations. Let Ξ be the residual of the differential equation (for example, $\Xi = \Delta^2 \psi$). Mathematically, minimization of Ξ to zero can be achieved by orthogonally projecting Ξ on a subspace of weighting functions, W_f; i.e., by taking the inner product of the residual and the weighting functions:

$$\left(\Xi, W_f\right) = \int_0^1 W_f \Xi \, dx = 0, \quad 0 < x < 1 \tag{5.60}$$

This process provides a mathematical framework to derive algebraic equations for any differential equation.

In finite element methods, the mathematical domain is divided into non-overlapping polyhedral subdomains (the elements) and Equation (5.60) is enforced in each subdomain, taking into consideration the boundary conditions. Within each element, the dependent variables are approximated by interpolating functions, Φ_a. The form assumed by Φ_a is determined by the type of element used. Some of the most commonly used elements for fluid mechanics applications are presented in Figure 5.9.
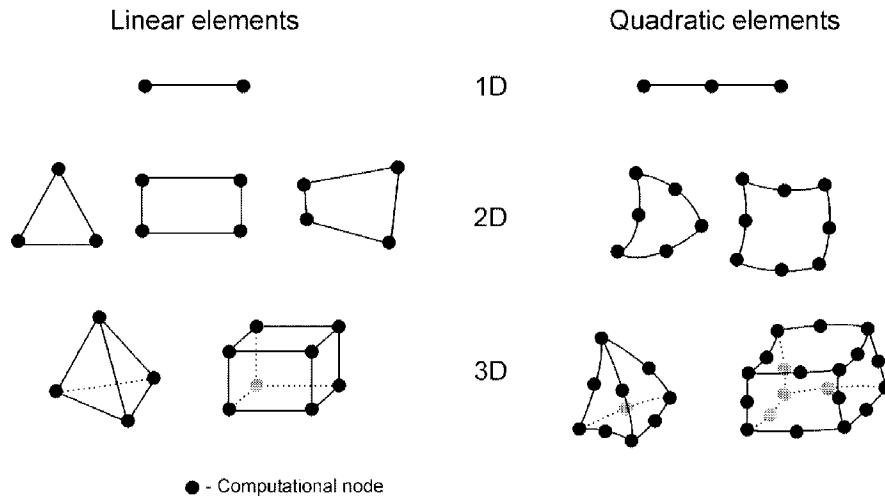

Figure 5.9. Some of the more common finite elements used in fluid flow modeling.

Note that the interpolating functions Φ_a can be used in lieu of the weighting functions W_f in Equation (5.60). In this case, the scheme is known as the Galerkin method. There are many other variations of the theme; i.e., in which Φ_a and W_f take different forms, and where Equation (5.60) also gets modified. Some of those methods commonly employed in computational fluid dynamics are the generalized Galerkin, the Taylor-Galerkin, and the Petrov-Galerkin methods. It is not in the scope of this text to produce detailed derivations of the methods. The interested reader should refer to Chung (2002) for a more comprehensive coverage of this subject.

5.3.3 Finite Volume Methods

Finite volume methods use conservation laws; i.e., the integral forms of the governing equations. The domain of computation is subdivided into an arbitrary number of control volumes, and the equations are discretized by accounting for the several fluxes crossing the control volume boundaries. There are two main types of techniques to define the shape and position of the control volumes with respect to the discrete grid points where the dependent variables are calculated: the node-centered scheme and the cell-centered scheme. Both schemes are

schematically pictured in Figure 5.10. The node-centered scheme places the grid nodes at the centroids of the control volume, making the control volumes "identical" to the grid cells. In cell-centered schemes, the control volume is formed by connecting adjacent grid nodes.
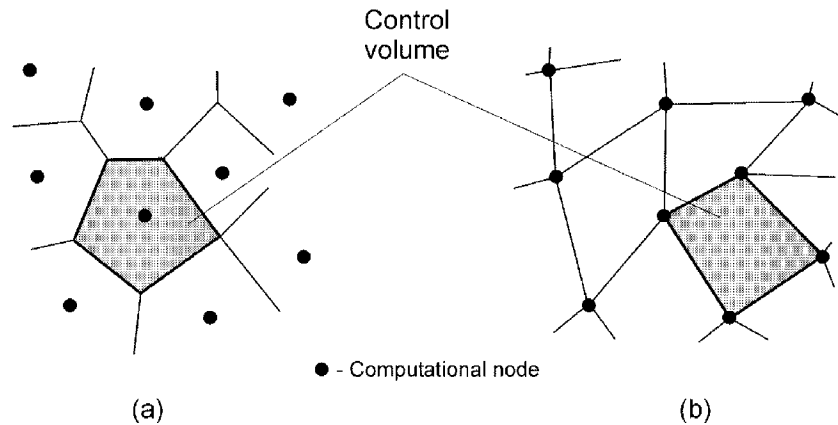

Figure 5.10. Representation of the control volumes formed by node-centered (a) and cell-centered (b) formulations used in finite volume discretizations.

The main advantage of finite volume methods is that the spatial discretization is done directly in the physical space, without the need to make any transformations between coordinate systems. It is a very flexible method that can be implemented in both structured and unstructured grid systems. Because the method is based directly on physical conservation principles, mass, momentum, and energy are automatically conserved by the numerical scheme.

Under certain conditions, the finite volume method is equivalent to the finite difference method or to particular forms of lower order finite element methods. The user is directed to Chung (2002) for more details on finite volume methods and their relationship with finite difference and finite element methods.

5.3.4 Other Discretization Methods

There are many other numerical discretization techniques that, for certain specific applications, offer significant advantages over the methods presented in the previous sections. It is outside of the scope of this chapter to cover them all, but a very brief overview will be presented of some selected methods. One such method is the spectral element method (SEM), used first by Patera (1984). The method is a particular type of the method of weighted residuals, sometimes also used with the Galerkin formulation, in which special "spectral" functions are used, usually Chebychev, Legendre, or Laguerre polynomials. These functions provide a physically more realistic description of flow phenomena than those used in conventional finite element methods, therefore leading to solutions with higher accuracy. In practice, however, their application is limited to simple geometries and simple boundary conditions.

The SEM tries to combine the advantages of the finite element method—especially its flexibility—with the greater accuracy of spectral schemes (e.g., Canuto et al., 1996). Its advantage lies in its non-diffusive approximation of the convection terms. Apart from its limited gamut of applications, its principal disadvantage is the much higher numerical effort required in comparison to the more traditional discretization methods.

Least squares methods have been used by many with the finite element formulation (e.g., Fix and Gunzburger, 1978). In this method, there is no need to do the integration by parts normally required in the standard Galerkin method. Instead, the inner products of the governing equations are minimized with respect to the nodal values of the variables. After the process is completed, higher order derivatives remain, requiring higher order trial functions than those used in the standard finite element methods.

A method based on boundary integral equations is the boundary element method (Brebbia, 1978). The solutions are obtained using the boundaries of a region, and interpolation functions coupled with the solutions of the governing equations are used to describe the interior of the domain. The equations are solved for nodes on the boundary alone. The values of the solution in the domain are calculated on the basis of the boundary information and the interpolation functions. The method has the advantage of requiring fewer equations to compute the solution, but the governing equations must be linear (or must first be linearized using a Kirchhoff transformation).

Some discretization methods use clusters of points for the spatial discretization in a gridless manner, rather than using points organized in connected grids in a conventional manner—see, for example, Batina (1993). In a gridless discretization, there are no coordinate transformations, nor is there the need to compute face areas or volumes. A least squares method is used to compute all the necessary gradients of the flow using a determined number of neighboring points surrounding each node. The points can be chosen along a certain direction to improve accuracy (e.g., in the characteristic directions). The differential form of the governing equations is used in a Cartesian coordinate system. The clusters of points may be denser in certain regions and sparser on others in order to better capture the flow gradients, in this respect having the flexibility of unstructured grid formulations. In spite of solving the conservation form of the flow equations, however, it is not yet clear that the gridless method can ensure conservation of mass, momentum, and energy.

Although the most common methods use Eulerian coordinates, there are instances in which a Lagrangian coordinate approach may be more appropriate. In Eulerian coordinate methods, the computational nodes, where the variables are calculated, are fixed in space, as opposed to Lagrangian coordinate methods, where the nodes are allowed to move with the fluid particles. Moreover, in many cases it is more advantageous to couple both Eulerian and Lagrangian methods, a method known as coupled Eulerian-Lagrangian (CEL)—Noh (1964). In CEL methods, the computational domain is separated in subsections, or subdomains, and the lines that define the boundary between each subdomain are approximated by time-dependent Lagrangian lines. In this framework, each subdomain is discretized by a time-independent Eulerian grid system which has its boundary prescribed by Lagrangian calculations. For each time step, first the Lagrangian computations are performed, then the Eulerian computations, then a further step

that couples both computations. This last step determines which part of the Eulerian mesh is active and the pressures acting upon the Lagrangian boundaries. CEL methods have been applied in flows with moving boundaries, such as the interface that separates two distinct fluids in multiphase flows.

Many other methods that were not described in this section have been developed, such as the particle-in-cell method, Montecarlo methods, smooth particle hydrodynamics (used by astrophysicists in the analysis of dust clouds and exploding stars), and others whose application to computation fluid dynamics has been in fields other than those of river engineering. The interested reader can find descriptions of these methods in the relevant literature or in some of the textbooks in the references to this chapter.

5.4 Modeling Morphologic Evolution

In the category of morphologic evolution, we include models capable of computing not only bed changes, but also channel width changes. In the previous section, only fixed-width models were considered. Fixed-width models should be applied only to cases in which the prototype channel's width adjustments are not significant.

The causes behind river width adjustments are varied and involve many time scales and a wide range of fluvial processes and geotechnical mechanisms, making its modeling a challenge. In some instances, bank erosion is caused by large variations in discharge, especially by floods. In others, bank saturation and dewatering is the main mechanism of concern: as the river rises, the banks soften and get heavier due to saturation; when the river level falls, the supporting hydrostatic forces are removed, resulting in instability and collapse (this mechanism sometimes causes a wave of bank failure that proceeds rapidly upstream, a phenomenon known as explosive channel widening). Yet in other cases, bank retreat is less related to flow stage and intensity, but more to precipitation and ground-water events that generate erosion through sapping or piping. Non-fluvial processes that may cause bank erosion include freezing, precipitation, snowmelt, and vegetation. Human activity and trampling and grazing by livestock are also part of this latter category. Some of the processes and resulting failure mechanisms are represented in Figure 5.11. As a consequence of this gamut of different phenomena, it is important to identify the dominant erosion processes and failure mechanisms in the prototype and to include them in any conceptual or mathematical model of the same, which sometimes is a very difficult task to accomplish.

A variety of approaches are used in analyzing and predicting river width changes. One such approach involves the use of regime theory. Regime theory attempts to predict the form of equilibrium channels (e.g., width and depth) using basic hydraulic quantities (the flow discharge and sediment load)—Lacey (1920). In the past, such approaches were mostly empirical, resulting in equations that were not dimensionally homogeneous and whose range of validity was limited to the basins and data used in their derivation. Recently, Julien and Wargadalam (1995) attempted to provide a semi-theoretical basis to this approach by using the basic governing principles of open channel flow to derive a new set of relationships for equilibrium channels.

However, while regime equations are widely used by engineers, their use in modeling is very limited because they are unable to predict the rates of change of the main cross-sectional geometric parameters.

The most common approach used in models of bank erosion is based on mechanistic principles. The mechanistic approach uses geotechnical concepts for modeling bank mechanics. The bank retreat and advance processes are modeled as a result of fluvial erosion of the bank materials, as well as a result of near-bed degradation and/or increase in bank steepness and consequent geotechnical failure. The main controlling mechanism determining bank stability is related to the conditions at the base of the bank.

Mechanistic models can become very complex because each different failure mechanism (e.g., planar, rotational, and cantilever in Figure 5.11 (a)-(c)) requires a separate analysis. Furthermore, there are additional complexities due to the essentially three-dimensional nature of the flow near the toe of the banks, turbulence effects, roughness variability, variations in bed particle size, presence of cohesive sediment materials (there is a vast difference in the failure mechanics between cohesive and non-cohesive materials due to significant differences in their soil mechanics), vertical stratification and longitudinal variability of the bank materials, cross-sectional variation of the sediment transport rate, etc. Due to the limited scope of this monograph, a detailed exposition of these phenomena will not be included here. Instead, a summary of the most important failure types are presented next. The reader can find further details in ASCE (1998a) and (1998b) and in the references therein.
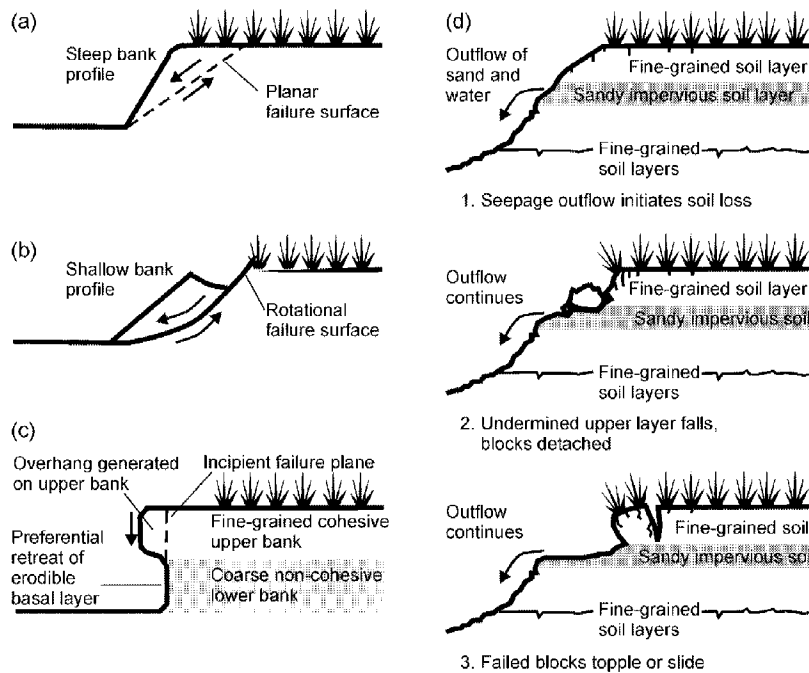

Figure 5.11. Dominant bank failure mechanisms due to geotechnical failure. (Adapted, with modifications, from Hagerty, 1991.)

5-35

The different types of bank failure are represented in Figure 5.12. The first type is the rotational slip, which may be defined as base, toe, or slope failure according to the point at which the failure arc intercepts the channel bed—see Figure 5.12 (a). This type of failure is easily analyzed using traditional geotechnical methods; e.g., Fredlund (1987).

Plane slip failure, Figure 5.12 (b), occurs mainly in very steep eroding riverbanks, often at the outer margin of meander bends and along severely incised channels. The approaches used to deal with this type of failure are based on the balance of forces acting normal to and along the failure (slip) plane of the potential failing block. The analysis leads to an equation that relates the critical height for mass failure, H_c, to a number of geotechnical parameters:

$$H_c = \frac{4c\left(\sin\theta\cos\phi\right)}{\gamma\left(1-\cos(\theta-\phi)\right)} \tag{5.61}$$

where c =   cohesion,
        γ =   bank material unit weight,
        ϕ =   friction angle, and
        θ =   angle of bank slope, Figure 5.12(b).

Toppling failure results from tension cracks that develop downward from the ground surface, thus limiting the width of the potential failure block, as shown in Figure 5.12 (c). They develop parallel to the bank behind steep banks and are due to the tensile stress in the soil. The potential depth of tension cracking H_c is in the order of 10 ft.
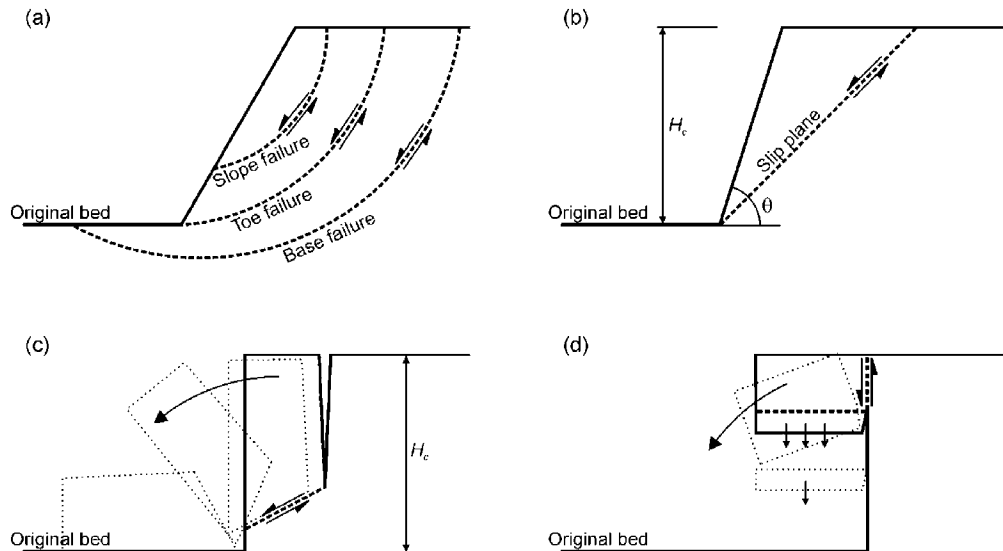

Figure 5.12. Types of bank failure usually employed in river widening models. (a) rotational slip failures, (b) plane slip failure, (c) toppling failure, and (d) cantilever failure.

Overhanging banks, Figure 5.12 (d), result from the erosion of an erodible layer below that of a layer more resistant to eroding, in a stratified bank. They may fail by tensile, beam, or shear (not shown) collapse, and they occur when the weight of the cantilever block exceeds the soil strength. This type of failure often occurs in areas with riparian and flood plain vegetation, where the plant roots contribute to reinforce the strength of the cantilever blocks.

As a result of the failure described above, mass is delivered to the toe of the bank slope, and its removal also needs to be properly modeled. This removal depends mostly on the rate of entrainment of this matter by the flow, as well as the capacity of the flow to transport the sediments downstream. Vastly different rates of removal may happen in practice, such as impeded removal (the bank failures supply debris at a higher rate than the flow can remove them), unimpeded removal (the debris delivery processes are balanced by ones removing them; therefore, no changes in basal slope or angle develop), and excess basal capacity (basal scour capability vastly exceeds the debris delivery rate). The basal matter removal rates have a vast importance in bank stability. For example, impeded removal results in basal accumulation, decreasing bank angle and height, and increasing stability, while excess basal capacity results in channel bed lowering, higher bank heights, and steeper angles, therefore decreasing stability. Basal debris behavior (whether the debris crumbles into non-cohesive individual particles, or whether cohesive effects dictate particle size, mass, or no erosion rates) and local hydraulics need to be accurately modeled in order to properly represent mass wasting removal from the toe.

The final approach to modeling width changes considered here is based on extremal hypothesis or theories. The fixed-width, one-dimensional models use the water depth D, the flow velocity V, and slope, S_f, as independent variables. The three independent equations that must be satisfied are the conservation of water,

$$Q = WDV \tag{5.62}$$

where W = the channel width;

a flow resistance equation (Chézy's equation is used for convenience),

$$V = C\left(\frac{WD}{P}S_f\right)^{1/2} \tag{5.63}$$

where C = Chézy's roughness coefficient, and
         P = the wetted perimeter;

and a sediment transport equation,

$$Q_s = f\left(D,W,V,S_f,d,\text{etc.}\right) \tag{5.64}$$

where Q_s = sediment transport capacity, and
         d = sediment particle size.

A fourth independent relationship must, however, be used if the channel width is to be considered as another independent variable. The fourth relationship is obtained by minimizing or maximizing some quantity, such as minimizing the rate of dissipation of energy.

The existing variable-width models in this category are based on the minimum energy dissipation rate theory developed by Song and Yang (1979a, 1979b, 1980) and Yang and Song (1979, 1986) and this general theory's special case, the minimum stream power theory, used by Chang and Hill (1976, 1977) and Chang (1979). The minimum energy dissipation rate theory states that when a closed and dissipative system reaches its state of dynamic equilibrium, its energy dissipation rate must be at its minimum value:

$$\varphi = \varphi_w + \varphi_s = \text{a minimum} \tag{5.65}$$

where φ = total rate of energy dissipation,

φ_w = rate of energy dissipation due to water movement, and

φ_s = rate of energy dissipation due to sediment movement.

The minimum value must be consistent with the constraints applied to the system. If the system is not at its dynamic equilibrium condition, its energy dissipation rate is not at its minimum value, but the system will adjust itself in a manner that will reduce its energy dissipation rate to a minimum value and regain equilibrium. Because of changing flow and sediment conditions, a natural river is seldom in its true equilibrium condition. However, a natural river will adjust its channel geometry, slope, pattern, roughness, etc., to minimize its energy dissipation rate subject to the water discharge and sediment load supplied from upstream.

For an alluvial channel or a river where the energy dissipation rate for transporting water is much higher than that required to transport sediment; i.e., $\varphi_w \gg \varphi_s$, the theory of minimum energy dissipation rate can be replaced by a simplified theory of minimum stream power (Yang, 1992). For this case, a river will minimize its stream power, γQS, per unit of channel length subject to hydrologic, hydraulic, sediment, geometric, geologic, and manmade constraints (γ is the specific weight of water).

Note that modeling of morphologic changes does also include the modeling of bank deposition. In many systems, especially those involving the development of channel meandering, bank erosion and deposition are phenomena that are simultaneously present. For example, within the same cross-section, one bank may be retreating while the opposite bank may be advancing, as shown in Figure 5.13.

Just as in many other areas of application, the complexity and variety of geomorphic factors involved in river width adjustment phenomena require a careful and methodical approach to their modeling, with large support of field observations and prototype data. ASCE (1998b) proposed an eight-step approach to deal with these issues. In spite of being specific to bank evolution modeling, its basic principles are applicable to other areas of interest in hydraulic modeling; therefore, it is briefly presented here. A schematic view of the entire process is presented in Figure 5.14.
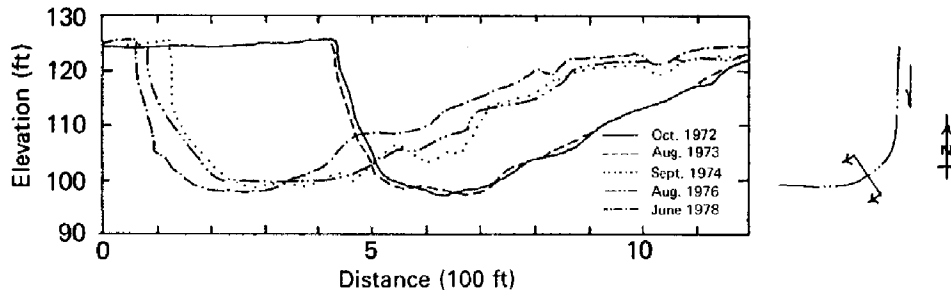
Figure 5.13. Development of mile 190.8 of the Sacramento River, 1972 through 1978, showing erosion in the left bank and deposition in the right bank, resulting in lateral bend migration (USACE, 1981).
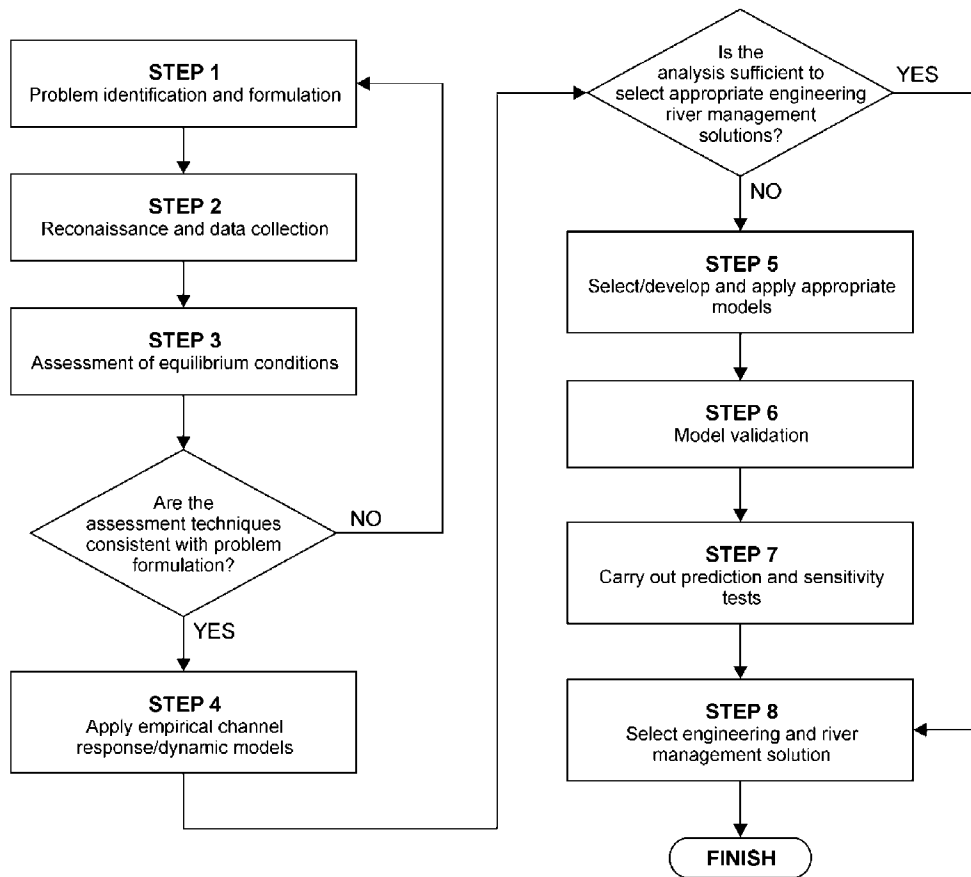

Figure 5.14. Procedure for the identification, analysis, and modeling of river width adjustment problems, after ASCE (1998b), with modifications.

Step 1, problem identification and formulation, involves determining the factors at play, which may be associated with river engineering factors, social activities, and may relate to existing conditions or future activities. It establishes the level of analysis required and defines the appropriate level of response. It is followed by step 2, field reconnaissance and data collection, in order to identify the nature and extent of the width adjustment problem. In this stage, channel characteristics are identified, as well as bank conditions and materials, hydrologic conditions, vegetation, any engineering works, and any other parameters that are considered relevant for the case at hand. During this stage, there is an assessment of the existing data available and, if necessary, it is the time to design and mount an adequate data gathering program.

At this stage, ASCE (1998b) recommends a simple assessment of the equilibrium conditions using the techniques of regime theory (step 3). The results of this analysis are compared with existing conditions to provide an indication of the present morphological status of the prototype. This makes it possible to determine the impact of the proposed engineering works.

In step 4, simple empirical channel response models are applied. This step may help to interpret existing and proposed conditions and to identify the dominant processes and trends at play. The information gathered at this stage forms a framework for the more detailed modeling work that follows (if appropriate). In step 5, more advanced models are developed and used, if necessary, to provide the more detailed information. These models should be validated with existing prototype data (step 6) and applied to current conditions, and also to assess the impacts of the proposed engineering works (step 7). At this stage, a sensitivity analysis involving all the pertinent parameters should be carried out, with particular emphasis on the parameters that are difficult to determine or that have significant spatial and/or temporal variability. In step 8, all the information gathered in the previous steps is used to formulate and implement the appropriate plan of action.

5.5 Reservoir Sedimentation Modeling

The basic governing equations involved in reservoir sedimentation processes are the same as in other bodies of water and are presented in the above sections. Other factors, however, may increase their complexity. Some of those factors are represented in Figure 5.15. Additionally, limnological variables may play a significant role. For example, there is a relationship between phytoplankton development and reservoir hydrodynamics: increased amounts of phytoplankton result in shallower thermoclines, warmer surface layers, and corresponding differences in hydrodynamics. The impact of limnological processes in reservoir circulation is a field that is poorly studied and that will not be covered in this chapter. Interested readers may refer to the survey paper by Bourget and Fortin (1995) and references therein.

The circulation in reservoirs is generally multi-dimensional, non-uniform, and unsteady. It is influenced by the hydrologic conditions of the reservoir and its watershed, by climate, by physiography, by the morphology of the reservoir, and by dam operation, among other parameters. Some of the water movements are periodical (e.g. seiche), and some are permanent (caused by the inflows of the main river and tributaries). Density stratification is usually present,

due to the temperature, salinity, turbidity, and density of the reservoir waters. All these effects have a direct impact on the sedimentation processes in a reservoir, in its sediment trapping efficiency, and in the distribution of sediment deposits within the reservoir. As such, all the dominant physical processes must be included in a successful model. It is not the scope of this section to describe all of these complex processes with the detail they deserve. In this section, we will concentrate only on some of the most important aspects of reservoir hydraulics, sediment transport, and density currents.
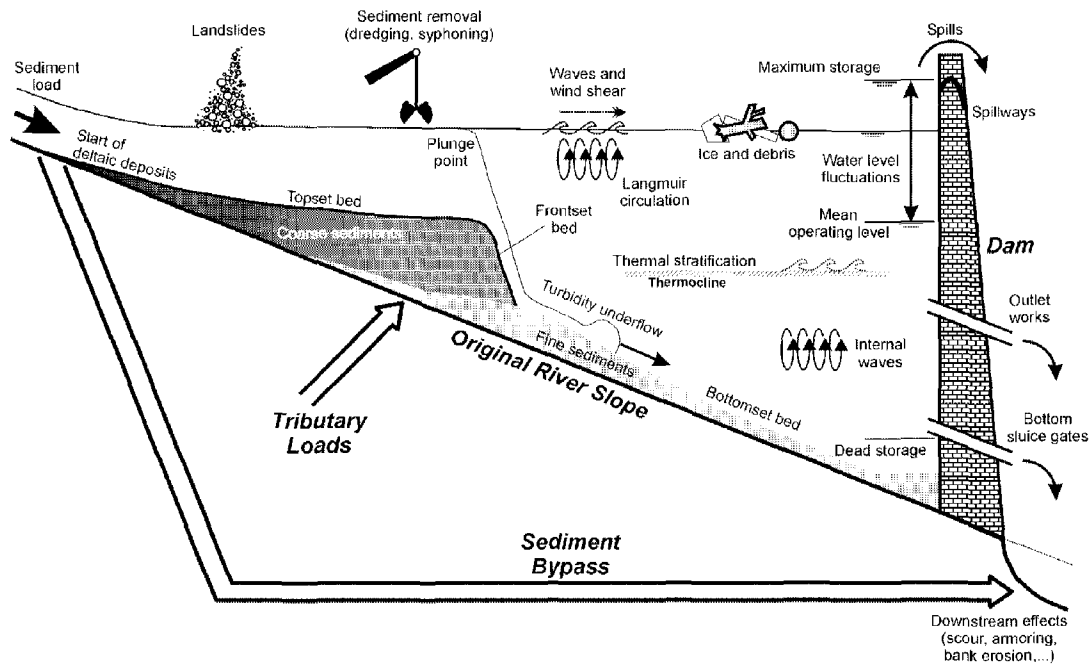

Figure 5.15. Schematic representation of the physical processes that may influence the sedimentation processes in a reservoir.

5.5.1 Reservoir Hydraulics

The equations governing fluid flow in reservoirs are the same as those governing the flow in rivers and other bodies of water, and they were presented in Section 5.2. Approximations to those equations are often made, depending on the dominant processes at play in the reservoir. Two- and one-dimensional models are widely used for engineering applications. One-dimensional models are appropriate in run-of-the-river reservoirs, where the flow is highly channelized and follows closely the thalweg, and where transverse mixing is well accomplished. On the other hand, when the reservoir pool is wide and without a single clear flow direction, multi-dimensional models must be used. Two different types of reservoirs where this might occur are shown in Figure 5.16. Tarbela Reservoir is a long and narrow reservoir, typical of

mountain regions, where the flow behaves virtually like a one-dimensional river. In this case, the reservoir is defined by the area of the river where the backwater effects from the dam determine a level-pool free surface elevation. San Luis Reservoir has the configuration of a shallow, wide lake that is typical of low and flat regions, where flow circulation is essentially two-dimensional.
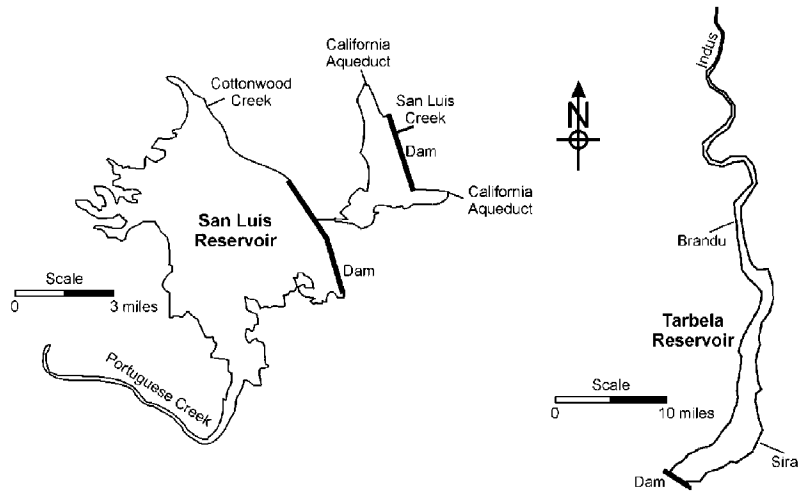

Figure 5.16. Pool contours for San Luis Reservoir, California, and for Tarbela Reservoir, Pakistan. Note the different scales in which the reservoirs are represented.

The type of mathematical model chosen for each particular application should reflect the physical characteristics of the reservoir. As an example, consider the de Saint Venant equation, Equation (5.20), rewritten using the velocity V and the depth of flow D as the dependent variables:

$$\underbrace{\underbrace{\frac{\partial(DV)}{\partial t}}_{\text{local}} + \underbrace{\frac{\partial(DV^2)}{\partial x}}_{\text{convective}}}_{\text{inertial force}} + \underbrace{\frac{\partial}{\partial x}\left(\frac{gD^2}{2}\right)}_{\text{pressure gradient}} + \underbrace{gDS_f}_{\text{friction}} - \underbrace{gDS_0}_{\text{weight}} = 0 \tag{5.66}$$

The terms corresponding to the different forces acting on the control volume water column are shown in Equation (5.66). These forces are the dynamic mechanisms governing wave motion. Moreover, usually only some of these forces are significant and the others may be neglected. As a consequence, different types of wave modeling can be used (it may be helpful to follow this discussion using Table 5.6). Inertial or small gravity waves are waves dominated by inertial and pressure forces. Waves in which friction, gravity, and pressure forces dominate—where the inertial terms are negligible—are called diffusion waves. When only gravity and friction forces are present, the waves are called kinematic waves. When all forces in Equation (5.66) are important, then we talk of dynamic waves. Dynamic waves are the most general type of waves in open channel flow, and they are said to be steady when the local acceleration term—first term in Equation (5.66)—can be neglected.

Table 5.6. Shallow water wave types and the dominating forces that characterize them. The column tables represent, in order from left to right, the terms in Equation (5.66), and a cross mark (x) indicates that the corresponding term is important.

Wave type	Dominant forces				
	Local inertial	Convective inertial	Pressure	Friction	Gravity
Inertial waves	x	x	x		
Diffusion waves			x	x	x
Kinematic waves				x	x
Steady dynamic waves		x	x	x	x
Dynamic waves	x	x	x	x	x

For flood-wave modeling, Singh and Li (1993) developed a method to determine which type of flood-wave model is important in reservoirs. For the kinematic wave model to be important, the following inequality must be verified:

$$T \geq a \frac{D_0}{V_0 S_0}$$

(5.67)

where
a = a constant (= 138 if Manning's n is used, = 171 if Chézy's coefficient is used),
D_0 = mean flow depth of reservoir before arrival of the flood (in m),
V_0 = mean flow velocity in reservoir before arrival of the flood (m/s),
S_0 = bed slope, and
T = wave period (in s).

For the diffusion model, they indicate that

$$T \geq \frac{40}{S_0 \sqrt{g/D_0}}$$

(5.68)

and for inertial wave model,

$$T \leq \frac{0.01}{S_0 \sqrt{g/D_0}}$$

(5.69)

5.5.2 Sediment Transport in Reservoirs

Most studies of sedimentation in reservoirs are concerned with the silting processes; i.e., the amount of sediments trapped in the reservoir and their distribution within the reservoir. Regardless of whether the reservoir's purpose is flood protection or water supply, the rate of loss of its capacity is of interest because it determines the reservoir's useful life. The movement of the sediments within the reservoir is also important, due to the presence of contaminants that affect the quality of the reservoir's waters. There are several widely used empirical methods to determine the trapping efficiency and the distribution of sediments in reservoirs that will not be considered here. For detailed presentations of those methods, the reader is referred to Bureau of Reclamation (1987). Here, it suffices to point out that the movement of sediments in reservoirs is governed by the same flow and sediment transport equations presented in earlier sections. Next, we briefly present some specific aspects of interest in reservoir sedimentation, of which we exclude sediment density currents, to be presented in the following section.

The movement, deposition, and erosion of sediments in reservoirs in most models are treated similarly as the same processes in rivers or other quiescent bodies of water. There is little distinction between sedimentation formulae for river and channels, and for reservoirs. However, there are noteworthy differences between the two. For example, sediment deposits in reservoirs generally contain much finer materials (both in particle diameter and in relative percentages) than are found in their tributaries. Fine sediments that are usually considered wash load and, therefore, do not need to be modeled in river systems, find their way into reservoirs, where they are trapped. Consequently, silts and cohesive fines are often dominant in reservoirs. Cohesive sediments are considered in Chapter 4 of this manual and will be not pursued further here.

Most sediment transport equations were derived in very idealized conditions for uniform channel flow, and few were developed specifically for reservoirs. Because most equations are highly dependent on the data that were used to determine the values of their coefficients, it seems important to use equations that may have included reservoir data in their derivation or, better yet, that were derived specifically for reservoirs. Unfortunately, not many exist, and the authors know only of three, which are summarized next.

For reservoirs in South Africa, Rooseboom (1975) found that an equation based on unit stream power theory describes well the carrying capacity of flow through reservoirs. He proposed the following equation:

$$\log C_t = \alpha + \beta \log\left(V_m S_f\right) \tag{5.70}$$

where C_t = total sediment concentration, and
         V_m = mean flow velocity.

The product $V_m S_f$, which is called the average unit stream power, can be expressed in terms of Chézy's equation, yielding

$$V_m S_f = \frac{PQ^3}{C^2 A^4}$$ (5.71)

where Q = flow discharge,
       P = wetted perimeter,
       A = flow area, and
       C = Chézy roughness coefficient.

The values of the constants α and β were determined using field measurements in reservoirs and were found to be $\alpha = 5.30$ and $\beta = 0.283$. With these parameters, Equation (5.70) can be written as

$$C_t = 2 \times 10^5 \left(V_m S_f \right)^{0.283}$$ (5.72)

where $V_m S_f$ is calculated in m/s and C_t is in mg/l.

Westrich and Juraschek (1985) developed a sediment transport equation for silt-sized material in reservoirs:

$$C_v = \frac{0.0018 \tau_b V}{(s-1) \rho g D \omega_s}$$ (5.73)

where C_v = sediment capacity concentration (by volume),
       τ_b = bed shear stress,
       s = specific gravity of silt,
       ρ = fluid density,
       g = acceleration due to gravity,
       D = water depth, and
       ω_s = settling velocity of the sediment particles.

Equation (5.73) was derived in the laboratory with particles having a settling velocity ranging from 0.6 to 9 mm/s. Note that the predicted transport capacities obtained from Equation (5.73) do not depend on bed-material composition, but only on the material in suspension. This equation also has the advantage of having been derived for silt sizes, while most sediment transport equations were derived for sand and gravel sizes (see Chapter 3). Atkinson (1992) expanded Equation (5.73) to include suspended sediment mixtures, including the effects that the presence of each size particle has on the fall velocity of the other size particles.

The Tsinghua University's equation (International Research and Training Center on Erosion and Sedimentation, 1985) is an empirical equation especially derived for calculating the transport capacity of flushing flows in reservoirs:

$$Q_s = \Omega \frac{Q^{1.6} S_0^{1.2}}{W^{0.6}}$$

(5.74)

where Q_s = sediment discharge (metric tons/s),
       Q = water discharge (m³/s),
       S_0 = bed slope,
       W = channel width (m), and
       Ω = a factor that depends on sediment type.

The recommended values for Ω are presented in Table 5.7. The Tsinghua University's equation was derived from data of flushing reservoirs in China. The scatter of the data used is considerable, albeit not unusually high. Furthermore, the practice in China is to flush the reservoirs annually; therefore, little consolidation takes place between flushing events. In these conditions, the importance of reservoir operations is reduced. Extrapolation to reservoirs in other parts of the world should be done with caution.

Table 5.7. Values of the factor Ω in Tsinghua University's equation

Value of Ω	Type of sediments
1600	Loess sediments
650	Other sediments with median size finer than 0.1 mm
300	Sediments with median size larger than 0.1 mm
180	For flushing with a low discharge

During reservoir flushing operations, sediments are removed by hydraulic incision of the reservoir deposits. The thus formed channels have side slopes that vary across a wide range of values. Observed values are as low as 1.4° for poorly consolidated material, and as high as 90° in highly consolidated sediments. Because the effectiveness of the flushing operations depends on the size of the channels formed during the drawdown, it is important to have accurate predictions of the channel's side slopes.

In reservoirs, the side slopes of the channels formed during flushing depend on sediment properties, degree of consolidation, depth of deposits, and range of water fluctuations during flushing. Although the techniques described in Section 5.4 could be applied in this situation, specific techniques for reservoirs developed by Atkinson (1996) will be presented here.

Atkinson (1996) used observations of side slopes in several reservoirs from all over the world in his work. He also used theoretical concepts and laboratory observations of estuarine muds. He proposed two prediction methods. In the first method, he adopted earlier work by Migniot (1981) and used reservoir data to find an expression for the angle α at which the slope is just stable:

$$\tan \alpha = 6.30 \rho_d^{4.7}$$

(5.75)

where ρ_d = dry density of sediments, in metric ton/m³.

5-46

A second method was developed using a numerical model, in which the results were presented in graphical format, as shown in Figure 5.17. Both methods were tested using observations in several reservoirs. As shown in Figure 5.18, there are discrepancies between computed and observed values, with Equation (5.75) overpredicting the measurements by an order of magnitude, while the method of Figure 5.17 seems to underpredict them by the same order of magnitude. Care should be exercised when using any of these methods in reservoir sedimentation models.
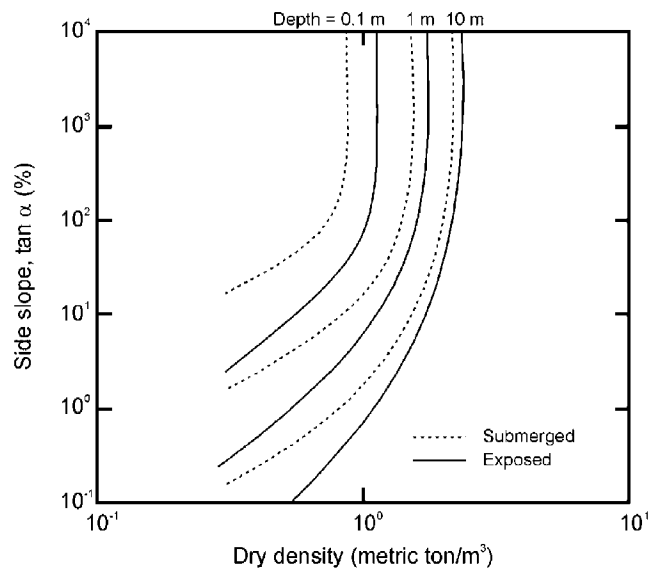

Figure 5.17. Side slope prediction at the limit of stability (Atkinson, 1996).

5.5.3 Turbid Underflows

Density currents are flows of fluids with different densities and occur normally in the stratified environments of lakes and reservoirs. They are gravity-driven flows caused primarily by the difference in the densities $\Delta\rho$ of the fluids involved. In a reservoir, they occur mainly because of the differences in density between the impounded and the inflowing waters. Density currents can be caused by differences in temperature ($\Delta\rho \approx 2$ kg/m^3), salinity ($\Delta\rho \approx 20$ kg/m^3), turbidity ($\Delta\rho \approx 20$ to 200 kg/m^3), or a combination of any of these factors. Turbidity currents are density currents caused primarily by the presence of turbidity (they transport granular material), and they occur as underflows; i.e., they plunge under the lower density waters of the impoundment. Turbid density currents are important because they can significantly influence the distribution of sediments within a reservoir. If they reach the dam, they can be vented, allowing the removal of sediments without significant drawdown of the pool level. This section concerns the modeling of turbidity currents and their impacts on reservoir bathymetry. A more general treatment of density currents can be found in Turner (1973).
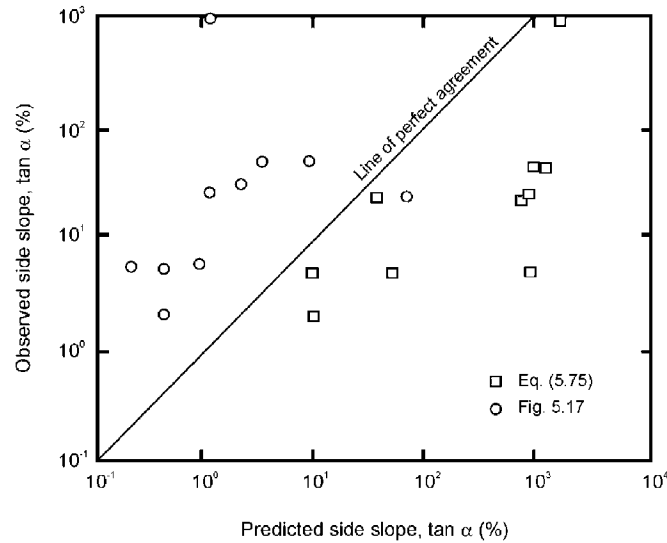
Figure 5.18. Comparison between the side slope prediction methods of Atkinson (1996).

5.5.3.1 Plunge Point

As the sediment transporting inflow waters enter the impounded waters, they plunge beneath the clear waters and travel downstream along the submerged thalweg. The point where the turbid inflowing water plunges beneath the ambient water is called the plunge point, or plunge line. The location of the plunge point is determined by the balance between stream momentum, the pressure gradient across the turbid-clear water interface, and the resisting shear forces. It is also influenced by morphologic factors, such as bed slope, bed roughness, and cross-sectional shape and area. In practice, the plunge point can be estimated from the densimetric Froude number F_p, defined as

$$F_p = \frac{V}{\sqrt{\varepsilon_i g D_p}} \tag{5.76}$$

where
V = inflow velocity,
ε_i = relative density difference, $= (\rho_i - \rho_r)/\rho_r$,
ρ_i = density of the inflow water,
ρ_r = density of the receiving (ambient) water,
g = acceleration due to gravity, and
D_p = depth at the plunge point.

F_p has been observed to vary in the range between 0.2 and 0.8, and some of the values are presented in Table 5.8. Furthermore, Equation (5.76) is usually manipulated assuming a certain cross-sectional geometry, so that D_p can be found explicitly. A number of different authors assume different cross-sectional geometries, resulting in different expressions for the plunge depth equation. Some of the most common ones are presented in Table 5.9.

Table 5.8.—Values of the densimetric Froude number at the plunge point, after Morris and Fan (1998)

	Source of data	F_p
Laboratory data	Turbid water, 3-19 g/l	0.78
	Turbid water, 10-30 g/l	0.55-0.75
	Turbid water, 100-300 g/l	0.2-0.4
	Saline water	0.3-0.8
	Cold water	0.67
Field data	Liujiaxia Reservoir, Tao River	0.78
	Guanting Reservoir	0.5-0.78

In Table 5.9, the method of Akiyama and Stefan (1981) is the only one using the initial mixing coefficient, γ, which is defined as the ratio of entrained flow to the incoming flow:

$$\gamma = \frac{Q_{b0} - Q_i}{Q_i}$$

(5.77)

where Q_{b0} = flow rate immediately downstream of the plunge point.

Note that if γ is known, Equation (5.77) can be used to compute Q_{b0}:

$$Q_{b0} = (1 + \gamma) Q_i$$

(5.78)

The empirical coefficient γ represents the initial mixing that occurs when the plunging turbidity current is subjected to the entrainment of the clear ambient water. The density of the inflow is correspondently decreased:

$$\rho_{b0} = \frac{\gamma \rho_r + \rho_i}{1 + \gamma}$$

(5.79)

where ρ_{b0} = density after entrainment at the plunge point.

Table 5.9. Formulations of the plunge depth D_p, according to several authors, with corresponding densimetric Froude numbers, F_p, where applicable

Authors	h_p	Notes
Savage and Brimberg (1975)	$D_p = \left(\dfrac{q_i^2}{g\varepsilon_i F_p^2}\right)^{1/3}$ $F_p^2 = \dfrac{2.05}{(1+\alpha)}\left(\dfrac{S_0}{f_b}\right)^{0.487}$	q_i is the inflow discharge per unit width, f_b is the bed friction coefficient, and α is the ratio of interfacial friction to bed friction.
Hebbert et al. (1979)	$D_p = \dfrac{1}{2\zeta}\left(\dfrac{2Q_i^2}{F_p^2 g\varepsilon_i (\tan\phi)^2}\right)^{1/5}$ $F_p^2 = \dfrac{\sin S_0 \tan\phi}{C_d}\left(1 - 0.85\sqrt{C_d}\sin S_0\right)$	Assumes triangular cross-section defined by the half-angle ϕ at the thalweg, for which $\zeta = 0.97$. Q_i is the inflow rate. C_d is a drag coefficient.
Jain (1981)	$D_p = 0.814\left(\dfrac{\alpha}{1+\alpha}\right)^{0.126}\left(\dfrac{f_t}{S_0}\right)^{0.325}\left(\dfrac{q_i^2}{g\varepsilon_i}\right)^{1/3}$	f_t is the total friction coefficient (i.e., interfacial plus bed friction).
Akiyama and Stefan (1981)	$D_p = 1.1(1+\gamma)\left(\dfrac{f_t q_i^2}{g\varepsilon_i S_0}\right)^{1/3}$	γ is the initial mixing coefficient.
Ford and Johnson (1983)	$D_p = \left(\dfrac{1}{F_p^2}\right)^{1/3}\left(\dfrac{Q_i^2}{W^2 g\varepsilon_i}\right)^{1/3}$	If F_p is known, D_p can be found iteratively by assuming a width W and calculating the depth.
Akiyama and Stefan (1985)	$D_p = \left(\dfrac{q_i^2}{g\varepsilon_i F_p^2}\right)^{1/3}$	Valid for channel slopes in the range $0.017 < S_0 < 0.124$.
Morris and Fan (1998)	$D_p = (g\varepsilon_i)^{-1/3}\left(\dfrac{Q_i}{F_p W}\right)^{2/3}$	Assumes a rectangular cross-section of width W.

From physical reasoning, it is expected that the mixing ratio will increase as the convective forces become dominant over the buoyant forces. Jirka and Watanabe (1980) represented this effect using an empirical relationship,

$$\gamma = 1.2F_p + 0.2 \tag{5.80}$$

which was derived for cooling ponds where $F_p \geq 0.167$. Unfortunately, the current knowledge about inflow mixing is incomplete. For example, there is the indication that for some reservoirs γ is independent of F_p. A more detailed discussion about this subject is given in Ford and Johnson (1983).

The stability of the density flows downstream from the plunge point is governed by the parameter θ (Rouse, 1950):

$$\theta = \frac{v_g \varepsilon_i}{V^3} = \frac{1}{F_d^2} \frac{1}{R_e} \qquad (5.81)$$

where F_d = the densimetric Froude number and R_e is the Reynolds number, defined as

$$R_e = \frac{VD}{v} \quad \text{and} \quad F_d = \frac{V}{\sqrt{g\varepsilon_i D}} \qquad (5.82)$$

According to Rouse (1950), underflows are stable if $R_e F_d^{3/2} < 440$. Other criteria were given by Ippen and Harleman (1952) and by Keulegan (1949). The former applies to laminar flows and requires $\theta > 1/R_e$ for stability, while the latter indicates that stability requires $\theta < 0.127$ for laminar flows and $\theta < 0.178$ for turbulent flows.

5.5.3.2 Governing Equations

The governing equations for turbid underflows are based on the same conservation principles described in Section 5.2; namely, the conservation of mass, Equation (5.2), and conservation of momentum, Equations (5.1). To illustrate the use of those equations in the modeling of turbidity currents, this section will present the basic governing equations for the case of the steady-state flow in a vertical, two-dimensional plane under a stagnant fluid of density ρ_r. In this case $v = 0$; therefore, the continuity equation—Equation (5.2)—becomes

$$\frac{\partial u}{\partial x} + \frac{\partial w}{\partial z} = 0 \qquad (5.83)$$

Integrating Equation (5.83) over the depth, from 0 to D, and taking into consideration that the horizontal velocity u is zero at the fluid's interface and the vertical velocity w is zero at the bed, one obtains

$$\frac{\partial}{\partial x}(DU) = -w_h \qquad (5.84)$$

where U is the depth-averaged longitudinal velocity, defined by Equation (5.10), and w_h is the vertical velocity at the fluids interface. Figure 5.19 provides a sketch showing the symbols used for turbidity underflows. w_h is defined as the velocity of entrainment of the ambient fluid into the turbid current and is generally assumed to be proportional to the velocity U of the current:

$$-w_h = E_w U \qquad (5.85)$$

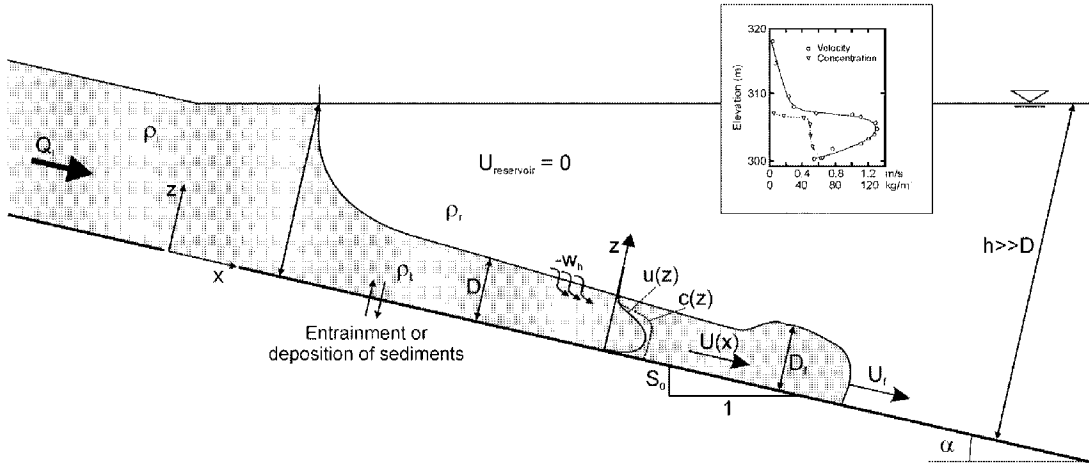where E_w = entrainment coefficient of the ambient fluid.

Figure 5.19. Sketch showing the symbols used to describe turbidity underflows. The inset shows typical velocity and concentration profiles in reservoirs, as measured by Fan (1991).

Conservation of longitudinal momentum (along the x axis) can be taken directly from Equation (5.1) for $i = 1$ and, with the assumptions discussed above, written for the turbid underflow as

$$\frac{\partial u^2}{\partial x} + \frac{\partial uw}{\partial z} = -\frac{1}{\rho_t} \frac{\partial}{\partial x}\left(p_t + \rho_t gz\cos\alpha\right) + \frac{1}{\rho_t}\frac{\partial \tau_{zx}}{\partial z} \qquad (5.86)$$

The pressure due to the above clear water is assumed to be hydrostatic, and within the turbid flow itself, p_t is decomposed in part due to the ambient fluid, p_a, and in part due to the presence of sediments, p_s $(= p_t - p_a)$. Using this approximation, and after integrating along the vertical, Equation (5.86) becomes

$$\frac{\partial\left(DU^2\right)}{\partial x} = -\frac{1}{2}g\varepsilon_t\cos\alpha\frac{\partial\left(C_s D^2\right)}{\partial x} + g\varepsilon_t C_s D\sin\alpha - U_*^2 \qquad (5.87)$$

The full derivation can be found in more detail in Parker et al. (1987), for example. In Equation (5.87), ε_t is the relative density difference, $= (\rho_t - \rho_r)/\rho_r$, U_* is the shear velocity, and C_s is the depth-integrated value of the concentration in the turbid flow, defined as

$$C_s = \frac{1}{D}\int_0^D c(z)dz \qquad (5.88)$$

Finally, the equation for the conservation of the solid particles can be obtained in a similar way from Equation (5.3) with the same type of simplifying assumptions. Expressing the turbulent Reynolds flux of sediments using a diffusion analogy; i.e., using

$$-\frac{\partial\left(\overline{c'w'}\right)}{\partial z} = D_z \frac{\partial^2 c}{\partial z^2}$$ (5.89)

we can write

$$\frac{\partial(uc)}{\partial x} + \frac{\partial(wc)}{\partial z} = \omega_s \cos\alpha \frac{\partial c}{\partial z} + D_z \frac{\partial^2 c}{\partial z^2}$$ (5.90)

where ω_s = sediments fall velocity.

Integrating Equation (5.90) over the depth yields

$$\frac{\partial(DUC)}{\partial x} = \omega_s \left(E_s - c_0\right)$$ (5.91)

In deriving Equation (5.91), the entrainment coefficient E_s proposed by Parker et al. (1987) was used to represent the erosion of bed sediments. The term $\omega_s c_0$ represents the deposition of sediments on the bed, where c_0 is the sediment concentration at the bed.

Equations (5.84), (5.87), and (5.91) represent conservation of fluid mass, momentum, and sediment mass, and constitute the set of governing equations for modeling steady, one-dimensional, turbid underflows. The partial derivatives $(\partial/\partial x)$ in those equations can be replaced by total derivatives (d/dx).

Finally, it is noteworthy to point out that alternative forms of the governing equations are useful in certain circumstances. They express the profiles of the interface between the turbid water and the clear water above using the depth D and the Richardson number R_i, defined as

$$R_i = \frac{g\varepsilon_i DC_s \cos\alpha}{U^2}$$ (5.92)

They are:

$$\frac{dD}{dx} = \frac{1}{1-R_i}\left[\frac{1}{2}(4-R_i)E_w + \frac{1}{2}R_i\frac{\omega_s}{UC_s}\left(E_s - c_0\right) - R_i\tan\alpha + \left(\frac{U_*}{U}\right)^2\right]$$ (5.93)

$$\frac{dR_i}{dx} = \frac{3R_i}{D(1-R_i)}\left[\frac{1}{2}(2+R_i)\left(E_w + \frac{1}{3}\frac{\omega_s}{UC_s}\left(E_s - c_0\right)\right) - R_i\tan\alpha + \left(\frac{U_*}{U}\right)^2\right]$$ (5.94)

5.5.3.3 Additional Relationships

The governing equations presented in the previous section work with three unknowns: D, U, and C_s. However, relationships for the parameters E_s, E_w, ω_s, U_*, and c_0 are needed. Empirical relationships for these parameters have been developed by several authors. In this section, a brief presentation of some of the most commonly used parameters is made.

Determination of flow resistance is a topic that still needs research. In many cases, the traveling velocity of the turbidity currents is constant, and the currents can be well approximated by uniform flow. The shear velocity, which is defined by Equation (5.43), can be expressed in terms of a friction coefficient, f_t, using a Darcy-Weisbach type of equation:

$$f_t = \frac{\tau_b}{\rho U^2 / 8} = 8\left(\frac{U_*}{U}\right)^2 \tag{5.95}$$

The total friction coefficient f_t is the sum of the bed friction acting on the wetted perimeter, f, and the friction acting upon the clear-turbid liquid interface. Under the conditions of uniform, conservative underflow, the velocity can be estimated by a Chézy or Darcy-Weisbach type of equation:

$$U = C\sqrt{g\varepsilon_t D S_0} = \sqrt{\frac{8}{f_t}}\sqrt{g\varepsilon_t D S_0} \tag{5.96}$$

C ranges between 280 and 560 cm$^{1/2}$/s. A frequently used relationship for f_t is given by (Harleman, 1961)

$$f_t = (1+\alpha)f \tag{5.97}$$

where f =   friction factor taken from the Moody diagram for pipe flow, and
         α =   factor representing the shear distribution at the interface as a function of bed shear (= 0.43).

Parker et al. (1987) wrote

$$U_*^2 = c_D U^2 \tag{5.98}$$

in which the value of the friction coefficient c_D ranges from 10^{-3} to 10^{-1} for Reynolds numbers—see Equation (5.82)—between 4×10^2 and 2×10^6. From Equation (5.95), it is clear that $c_D = f_t/8$.

Procedures to compute the values of the fall velocity ω_s can be found in any standard textbook about sediment transport, some of which are presented in Chapter 3. The value of the reference

concentration c_0 is evaluated close to the bed, at a height of $0.05h$, and can be expressed as a function of the grain size as

$$c_0 = r_0 C_s \qquad (5.99)$$

where the shape factor r_0 is a function of grain size. Parker et al. (1987) found $r_0 \approx 2$, remaining more or less constant in the range $1 < U_* / \omega_s < 50$ for uniform sediments. For non-uniform sediments

$$r_{0i} = 1.64 + 0.40 \delta_i^{1.64} \qquad (5.100)$$

where δ_i = normalized grain size, $= d_i/d_{50}$,

and Equation (5.99) becomes

$$c_{0i} = r_{0i} C_{si} \qquad (5.101)$$

The entrainment coefficient for the bed sediments, E_s, can be computed after Garcia and Parker (1991):

$$E_s = \frac{a Z_u^5}{1 + \frac{a}{0.3} Z_u^5} \qquad (5.102)$$

where a = a numerical constant ($= 1.3 \times 10^{-7}$), and
Z_u = a similarity variable defined by

$$Z_u = \begin{cases} 0.586 \dfrac{U_*}{\omega_s} R_{ep}^{1.23} & \text{if} \quad 1.0 \le R_{ep} \le 3.5 \\[2ex] \dfrac{U_*}{\omega_s} R_{ep}^{0.60} & \text{if} \quad R_{ep} > 3.5 \end{cases} \qquad (5.103)$$

with the particle Reynolds number R_{ep} defined by

$$R_{ep} = \frac{\sqrt{g \varepsilon_i d^3}}{\nu} \qquad (5.104)$$

where d = mean diameter of the sediment particles.

The coefficient for the entrainment of the ambient fluid, E_w, can also be prescribed by an empirical relationship given by Parker et al. (1987):

$$E_w = \frac{0.075}{\sqrt{1 + 718 R_i^{2.4}}}$$
(5.105)

where the bulk Richardson number R_i is defined by Equation (5.92). The scatter of the experimental data is rather high. Alternatively, a simpler relationship proposed by Egashira and Ashida (1980) can be used:

$$E_w = 0.0015 R_i^{-1}$$
(5.106)

Many relationships have been proposed to determine the velocity of the advancement of the turbid underflow, U_f. An analysis based on the difference in pressure across the front of the advancing flow, assuming that $\rho_r \approx \rho_t$, yields (Turner, 1973)

$$U_f = \sqrt{2 \varepsilon_t D}$$
(5.107)

A simple relationship for small slopes is (e.g. Turner, 1973)

$$U_f = 0.75 \sqrt{\varepsilon_t D_f}$$
(5.108)

with D_f defined in Figure 5.19, an equation that has been well verified by others was developed by Britter and Linden (1980):

$$\frac{U_f}{\sqrt[3]{\varepsilon_t q_i}} = 1.5 \pm 0.2$$
(5.109)

where q_i = inflow discharge.

To conclude this section, the venting of the turbidity currents that reach the dam will be considered. The venting of the sediment-laden flows is done by low level outlet gates, but it is necessary to have adequate information to avoid discharging clear water instead of the desired turbid fluid. This information includes not only the timing of arrival and concentration of the currents, but also the position of the interface between the clear reservoir water and the turbid underflow. The results presented next follow the discussion in Section 14.7.5 of Morris and Fan (1998).

The limiting height for the aspiration of a density current, based on experiments with saline water, is given by the following expressions:

$$\frac{\varepsilon_t g h_a^3}{q^2} = 0.43 \text{ for slots}$$
(5.110)

$$\frac{\varepsilon_i g h_a^5}{Q} = 0.154 \text{ for orifices} \tag{5.111}$$

where h_a = aspiration height (defined in Figure 5.20),
        Q = total discharge through orifice, and
        q = discharge per unit width for slotted gates.

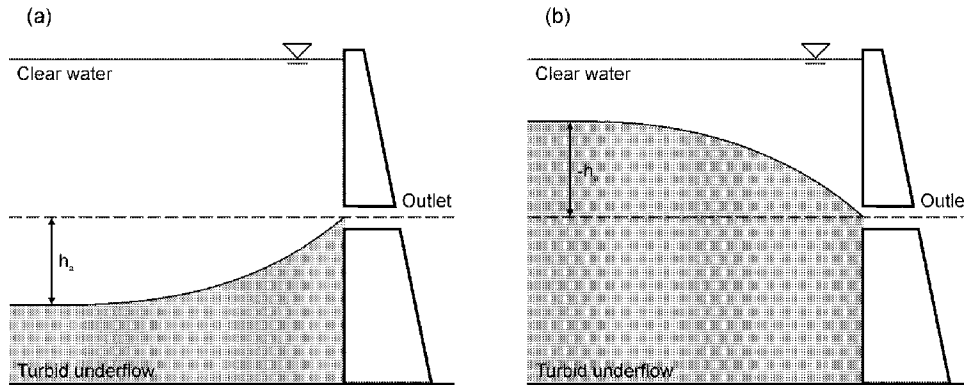(a)   (b)

Figure 5.20. Venting of turbid underflows by the dam's bottom outlets showing (a) the limit height for aspiration of the turbidity current from below an outlet that is too high, and (b) the limit height for aspiration of clear water from above an outlet that is below the turbid-clear water interface. (Adapted from Morris and Fan (1998), with modifications.)

More recent research produced the relationships of Table 5.10. Observations from releases in the Sanmexia Reservoir during 1961 and 1962 produced the following orifice equation:

$$h_a = \Gamma \left(\frac{Q^2}{\varepsilon_i g} \right)^{1/5} \tag{5.112}$$

where Γ = 0.9 for the lower aspiration limit, Figure 5.20 (a), in 1961,
         = 1.1 for the lower aspiration limit in 1962, and
         = -0.4 for the clear water aspiration limit, Figure 5.20 (b), in both years.

Table 5.10. Expressions for the limiting heights for venting density underflows from bottom outlets

	Slot	Orifice
Limiting depth for aspiration of turbid water from below, Figure 5.20 (a)	$\left(\dfrac{\varepsilon_i g h_a^3}{q^2} \right)^{1/3} = 0.75$	$\left(\dfrac{\varepsilon_i g h_a^5}{Q^2} \right)^{1/5} = 0.8$
Limiting height for aspiration of clear water from above, Figure 5.20 (b)	$\left(\dfrac{\varepsilon_i g (h_a)^5}{q^2} \right)^{1/3} = -0.75$	$\left(\dfrac{\varepsilon_i g (h_a)^5}{Q^2} \right)^{1/5} = -1.2$

5.5.4 Difference Between Reservoirs and Other Bodies of Water

The previous subsections were devoted to presenting some of the most important processes directly involved with sedimentation modeling in reservoirs. However, these basic processes are virtually identical to those governing other bodies of pooled water, such as retention basins, ponds, pools, and lakes. Nonetheless, these are often distinguished as different types of water bodies. Due to the importance of lake circulation, which stems from ecological and water quality concerns, we will briefly address some of the most important differences between lakes and reservoirs as they may relate to modeling (see also Table 5.11).

Table 5.11. Principal differences between lakes and reservoirs (Marzolf, 2003)

	Lakes	Reservoirs
Ratio of surface to watershed area	Smaller, ~10	Larger, >500
Retention time	Longer	Shorter
Depth	Deeper	Shallower
Inflows	None to several	One dominant
Outflows	None to one	One
Transparency	Clear	Variable

The differences between lake and reservoir circulation and sedimentation result from the differences between specific combinations of the general forcing mechanisms that dominate the particular behavior of each water body. A major difference between the circulation of the two results from dam operation and the position of the dam outlets. Deep sluice gates remove water that is much different in nature than the water removed via the usually shallower lake outlets. In some dams, gates at different levels are operated, in turn, to selectively remove warmer or colder water from the reservoir—a requirement of downstream river management practices that has direct impacts on its ecology. Some gates are specifically designed to vent density currents. Some reservoirs are emptied periodically. As a result, the reservoir levels have much greater variation than those of lakes, as does the position of the thermocline, the latter having a major impact on reservoir limnology.

Recent studies indicate significant limnological differences between lakes and reservoirs. Straškraba (1998) shows a significant difference between the retention times of phosphorus for lakes and reservoirs (Figure 5.21). Retention of phosphorus results from the direct sedimentation of the phosphorus-carrying particles present in the inflowing river water, as well as from the sedimentation of particles formed within the water body itself—mostly by phytoplankton. This difference, which is due to sedimentation, indicates significant differences in the sedimentation processes between lakes and reservoirs, including their respective diffusion and resuspension processes. Due to the complex cycling of phosphorus, which is affected by chemical and biological processes by phytoplankton, zooplankton, and fish, other significant limnological differences may be expected.
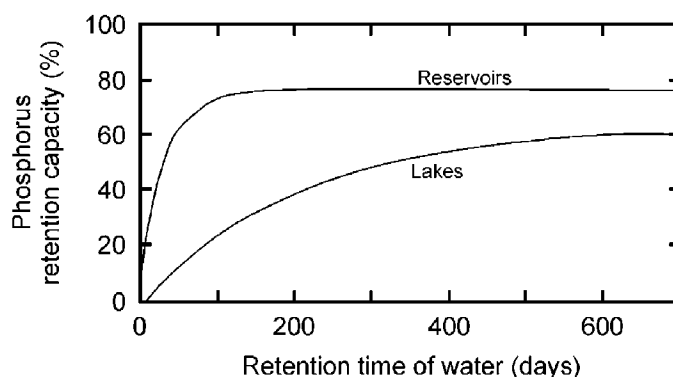
Figure 5.21. Phosphorus retention capacity in lakes and reservoirs, adopted with modification from Straškraba (1998). The retention capacity is given as a percentage of the lake/reservoir output as related to the loads, due to their respective inflows.

Another important feedback mechanism described by Straškraba relates phytoplankton development and hydrodynamics. Increase in phytoplankton results in decreased light penetration, decreased depth of the seasonal thermocline, and increased temperature of the uppermost water strata. This increase in temperature contributes to increased phytoplankton growth, therefore causing a positive feedback phenomenon. Of course, the depth of the thermocline and the temperature of the uppermost layer have a substantial and direct impact on the circulation of the water body. This feedback can be reproduced in a model only if physical and biological parameters are both included, which is not done in most hydrodynamic models. Other complex relations between limnology and hydrodynamics can be drawn. Here, it suffices to say that a model may have to include these effects if accurate computations of the circulation and sedimentation of reservoirs, lakes, and other bodies of water are sought. The particular type of interaction depends on the specific dominating processes at play, which may differ significantly between each water body. It is the responsibility of the modeler to identify and implement such processes, and multidisciplinary research in this topic is still vastly needed.

5.6 Data Requirements

In general, the basic data requirements for loose boundary hydraulic models can be grouped in three broad categories: geometric data, hydraulic data, and sediment data. These data establish the boundary conditions necessary to solve the governing equations and are an integral part of a model. The term "model" thus refers to the ensemble of the set of governing equations, their numeric solution technique, their implementation in a computer program, and the data that defines the prototype. In practice, data collection is more often the responsibility of the user of the computer program that implements the numerical part of the model, or of someone else that then conveys that data to the user. However, data collection and preparation are no less important than the computer model itself, and often play the dominant role in determining the accuracy and applicability of the final numerical solutions generated by the computer.

The geometry data defines the topography of the reach to be simulated; i.e., the channel bed, banks, and flood plains. In two- and three-dimensional models, the data is most often presented as a set of points given by its x, y, and z coordinates. The data is then interpolated to the locations of the grid nodes used in the discretization of the problem. Interpolation may be done using standard triangulation techniques, or with more sophisticated techniques, such as kriging. In river channels, special techniques are often used that, in the interpolation process, emphasize the contribution of the data points along the flow streamlines, as they have the potential of better capturing the longitudinal characteristics of the riverbed (i.e., the meandering of the thalweg).

In one-dimensional models, the geometry is usually defined by cross-sections. Each cross-section is a line representing a particular section of the modeled reach and is given by a set of points, each defined by a lateral distance and a bed elevation above a common datum. This line provides the information about the section shape and the locations of the subchannels, and should be taken between locations well above the highest stage levels. It should also be taken perpendicularly to the flow streamlines. Additionally, the distance between the cross-sections needs to be given, and this distance must be collected along the flow streamlines. Under bankfull conditions, this distance can be taken along the channel's thalweg, but this may vary under flooding conditions.

There are techniques that provide specific guidelines on how to collect cross-section data in the field. For example, some of the criteria recommended by Samuels (1990) are as follows:

- Select all sites of key interest;
- Select cross-sections adjacent to major structures and control points;
- Select cross-sections representative of the river geometry;
- As a first estimate, select cross-sections $20W$ apart, where W is the cross-section's top width;
- Select sections a maximum of $0.2D/S_w$ apart, where D is the water depth and S_w is the free surface slope;
- For unsteady flow modeling, select sections a maximum of $L/30$ apart, where L is the length scale of the physically important wave (flood or tide);
- Select sections a minimum of $10^{INT(\log Z)-\varepsilon}/(\delta S - S_w)$ apart, where ε is the machine precision, Z is the water surface elevation, $INT()$ is the function that represents the integer part of its argument, and δS is the relative error in the slope;
- The ratio of the areas between two adjacent cross-sections should lie between 2/3 and 3/2.

Hydraulic data encompasses the necessary upstream and downstream flow conditions, as well as friction factors and local head losses. Subcritical flows require the flow discharge at the upstream boundary and the stage at the downstream end, while supercritical flows require both the discharge and the stage at the upstream boundary (the analysis leading to this result can be found in any hydraulics textbook, such as Henderson, 1966). In two- and three-dimensional flows, this is equivalent to prescribing flow velocity field at the upstream boundary, and a stage at the downstream boundary. Because usually only the upstream discharge is known, a vector velocity field must be synthesized, which is usually done by distributing the discharge proportionally to

the conveyance along each node of the computational boundary, and then fitting a logarithmic profile along the vertical direction. Thus, any number of hydrographs can be discretized on an arbitrarily complex computational domain.

The stage can be defined in a number of ways. Stage-discharge rating curves, an elevation hydrograph, or a water-surface-slope hydrograph are common ways to achieve that purpose. More complex conditions may be defined in the case in which the downstream boundary is a dam. In such cases, the reservoir operational scheme may be used. When the dam outlet works are used, relationships for the gates and spillways may have to be employed. These relationships are a function of the head at the dam, and more complex iterative schemes need to be used. In tidal regions, special relationships may be necessary.

In some models, especially if steady-state solutions are sought, special downstream boundary conditions are employed. These boundary conditions, generally known as non-reflective boundary conditions, prevent wave forms generated by spurious numerical solutions from being reflected back into the computational domain, as would happen in the case of a clamped down, free surface elevation. The use of these techniques allows the spurious waves to flow out of the computational domain and may significantly increase numerical convergence rates. A description of such techniques can be found in Keller and Givoli (1989).

Friction factors play an important role in determining stages and flow velocities, and they must be given in the form of numerical values associated with particular regions of the bed, or in the form of relationships that allow their representation as a function of other parameters—usually using hydraulic and/or sediment quantities. Local energy loss coefficients must also be given, such as those due to channel bends, natural or manmade obstacles to the flow, bridge piers and abutments, etc. Once again, these may be prescribed or may be calculated, and they commonly require iterative procedures.

Sediment data encompasses all the necessary information for sediment transport computations. The sediment inflow hydrograph must be given at the inflow boundaries. For two- and three-dimensional models, it is also necessary to specify the sediment concentration distribution along those boundaries, as well as the separation between bedload and suspended load. The sediment particle-size distributions are also needed. Bed size distributions need also to be determined for each computational grid node (or for each cross-section, in the case of one-dimensional models). Additionally, especially in the case of scour computations and bank widening, it is also necessary to provide the underlying bed-material size distribution. Water temperature variations must also be prescribed or modeled because they have an indirect impact on sediment transport via the sediment particles' fall velocities.

In practice, it is difficult to determine a priori some of the hydraulic parameters necessary for a successful simulation. For that reason, usually there is a model calibration stage in which stage and discharge observations along the study reach are used to adjust the values of those parameters, such as bed roughness, discharge coefficients, or other parameters particular to the model employed. Similarly, there should be a calibration stage for the sediment transport

calculations. Observations of the sediment outflow quantities, of variations in channel width and bed elevation, and of changes in sediment particle-size distributions can be used to properly adjust model parameters.

5.7 One-Dimensional Model Comparison

Most sediment routing models for long-term simulation of long reaches of a river are one-dimensional models. Only one-dimensional models are considered in the following comparisons. There are many sediment transport models, and each model has its strengths and weaknesses. Comprehensive reviews of the capabilities and performance of these models are provided in reports by the National Research Council (1983), and Fan (1988), among others. Fifteen U.S. Federal agencies participated in a Federal Interagency Stream Restoration Working Group (1998) to produce a handbook on *Stream Corridor Restoration Principles, Processes, and Practices*. They selected the following eight models for comparison: CHARIMA (Holly et al., 1990), FLUVIAL-12 (Chang, 1990), HEC-6 (USACE, 1993), TAS-2 (McAnally and Thomas, 1985) MEANDER (Johannesson and Parker, 1985), USGS (Nelson and Smith, 1989), D-O-T (Darby and Thorne, 1996, and Osman and Thorne, 1988), and GSTARS (Molinas and Yang, 1986). Table 5.12 summarizes the comparisons of these eight models. Because the U.S. Bureau of Reclamation has now replaced GSTARS with GSTARS 2.1 and GSTARS3 (Yang and Simões, 2000 and 2002), the newer versions of GSTARS are included in Table 5.12. HEC-6, TABS-2, USGS, and GSTARS 2.1 and GSTARS3 are Federal models in the public domain; CHARIMA, FLUVIAL-12, MEANDER, and D-O-T are academic or privately owned models. GSTARS3 comprises reservoir sedimentation modeling, while GSTARS 2.1 emphasizes river sedimentation.

5.8 Example: The GSTARS Models

In this section, the basic principles and their implementation in the GSTARS 2.1 and GSTARS3 models are presented as an example of alluvial river models. GSTARS3 is a recent extension of GSTARS 2.1 to reservoir sedimentation. The following presentation will concentrate on presenting GSTARS3. Examples of application of both models will be given in Section 5.8.6 below. The Generalized Sediment Transport model for Alluvial River Simulation, version 3 (GSTARS3, Yang and Simões, 2002) is a publicly and freely available model developed by the U.S. Bureau of Reclamation. Unlike many of the other one-dimensional alluvial river modeling computer programs, GSTARS3 has the goal to simulate the flow conditions in a semi-two-dimensional manner and the change of channel geometry in a semi-three-dimensional manner. By using stream tubes within an essentially one-dimensional backwater model, this can be accomplished without the intensive data and computational requirements of the more sophisticated, truly two- and three-dimensional models.

Table 5.12. Comparison of sediment transport models (Y = yes; N = no)

Model	CHAR IMA	Fluvial-12	HEC-6	TABS-2	Mean-der	USGS	D-O-T	GSTARS 2.1/ GSTARS3
Discretization and formulation:								
Unsteady flow | stepped hydrograph	Y|Y	Y|Y	N|Y	Y|Y	N|Y	Y|Y	N|Y	N|Y
One-dimensional | quasi two-dimensional	Y|N	Y|Y	Y|N	N|N	N|N	N	Y|Y	Y|Y
Two-dimensional | depth-average flow	N	N	N	Y|Y	Y|Y	Y|Y	N	N|Y
Deformable bed | banks	Y|N	Y|Y	Y|N	Y|N	Y|N	Y|N	Y|Y	Y|Y
Graded sediment load	Y	Y	Y	Y	Y	N	Y	Y
Non-uniform grid	Y	Y	Y	Y	Y	Y	Y	Y
Variable time stepping	Y	N	Y	N	N	N	N	Y
Numerical solution scheme:								
Standard step method	N	Y	Y	N	N	N	Y	Y
Finite difference	Y	N	Y	N	Y	Y	Y	Y
Finite element	N	N	N	Y	N	N	N	N
Modeling capabilities:								
Upstream water and sediment hydrographs	Y	Y	Y	Y	Y	Y	Y	Y
Downstream stage specification	Y	Y	Y	Y	Y	N	Y	Y
Flood plain sedimentation	N	N	N	Y	N	N	N	N
Suspended | total sediment transport	Y|N	Y|N	N|Y	Y|N	N|N	N|Y	N|Y	N|Y
Bedload transport	Y	Y	Y	N	Y	N	N	Y
Cohesive sediments	N	N	Y	Y	N	Y	N	Y
Bed armoring	Y	Y	Y	N	N	N	Y	Y
Hydraulic sorting of substrate material	Y	Y	Y	N	N	N	Y	Y
Fluvial erosion of streambanks	N	Y	N	N	N	N	Y	Y
Bank mass failure under gravity	N	N	N	N	N	N	Y	N
Straight | irregular non-prismatic reaches	Y|N	Y|N	Y|N	Y|Y	N|N	N|N	Y|Y	Y|Y
Branched | looped channel network	Y|Y	Y|N	Y|N	Y|Y	N|N	N|N	N|N	N|N
Channel beds	N	Y	N	Y	Y	N	Y	Y
Meandering belts	N	N	N	N	N	Y	N	N
Rivers	Y	Y	Y	Y	Y	Y	Y	Y
Bridge crossings	N	N	N	Y	N	N	N	N
Reservoirs	N	Y	Y	N	N	N	N	Y
User support:								
Model documentation	Y	Y	Y	Y	Y	Y	Y	Y
User guide | hot-line support	N|N	Y|N	Y|Y	Y|N	N|N	Y|N	N|N	Y|N

GSTARS3 was developed due to the need for a generalized water and sediment-routing computer model that could be used to solve complex river engineering problems for which limited data and resources were available. In order to be successful, such a model should have a number of capabilities, such as being able to compute hydraulic parameters for open channels with fixed as well as movable boundaries; having the capability of computing water surface profiles in the subcritical, supercritical, and mixed flow regimes (i.e., in combinations of subcritical and supercritical flows and through hydraulic jumps without interruption); being able to simulate and predict the hydraulic and sediment variations, in both the longitudinal and transverse directions; being capable of simulating and predicting the change of alluvial channel profile and cross-sectional geometry, regardless of whether the channel width is variable or fixed; and it should incorporate site-specific conditions, such as channel side stability and erosion limits.

GSTARS3 consists of four major parts. The first part is the use of both the energy and the momentum equations for the backwater computations. This feature allows the program to compute the water surface profiles through combinations of subcritical and supercritical flows. In these computations, GSTARS3 can handle irregular cross-sections, regardless of whether single channel or multiple channels separated by small islands or sand bars.

The second part is the use of the stream tube concept, which is used in water and sediment routing computations. Hydraulic parameters and sediment routing are computed for each stream tube, thereby providing a transversal variation in the cross-section in a semi-two-dimensional manner. The scour or deposition computed in each stream tube gives the variation of channel geometry in the vertical (or lateral) direction. Bed sorting and armoring in each stream tube follow the method proposed by Bennett and Nordin (1977), and the rate of sediment transport can be computed using any of the several transport functions implemented in the code (see below for more details).

The third part is the use of the theory of minimum energy dissipation rate in its simplified version of minimum total stream power to compute channel width and depth adjustments (see Section 5.4). The use of this theory allows the channel width to be treated as an unknown variable. Treating the channel width as an unknown variable is the most unique capability of GSTARS3. Whether a channel width or depth is adjusted at a given cross-section and at a given time step depends on which condition results in less total stream power.

The fourth part is the inclusion of channel bank side stability criteria based on the angle of repose of bank materials and sediment continuity.

5.8.1 Streamlines and Stream Tubes

The basic concept and theory regarding streamlines, stream tubes, and stream functions can be found in most basic textbooks of fluid mechanics. In this section, only some of the basic concepts are given, as they are applicable to GSTARS3 computations.

By definition, a streamline is a conceptual line to which the velocity vector of the fluid is tangent at each and every point, at each instant in time. Stream tubes are conceptual tubes whose walls are defined by streamlines. The discharge of water is constant along a stream tube because no fluid can cross the stream tube boundaries. Therefore, the variation of the velocity along a stream tube is inversely proportional to the stream tube area. Figure 5.22 illustrates the basic concept of stream tubes used in GSTARS3.
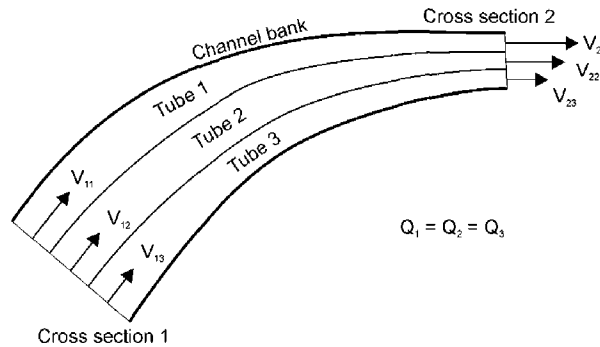
Figure 5.22. Top view of a hypothetical river reach illustrating the use of equal conveyance stream tubes in GSTARS3.

For steady and incompressible fluids, the total head, H_t, along a stream tube of an ideal fluid is constant:

$$\frac{F_p}{\gamma} + \frac{V^2}{2g} + D = H_t = \text{Constant} \qquad (5.113)$$

where
F_p = pressure acting on the cross-section,
γ = unit weight of water,
g = acceleration due to gravity,
D = hydraulic head, and
V = flow velocity.

In GSTARS3, however, H_t is reduced along the direction of the flow, due to friction and other local losses.

5.8.2 Backwater Computations

The basic concepts and backwater computational procedures can be found in most open-channel hydraulics textbooks (e.g., Henderson, 1966). For quasi-steady flows, discharge hydrographs are approximated by bursts of constant discharge. During each constant discharge burst, steady-state equations are used for the backwater computations. GSTARS3 solves the energy equation based on the standard-step method:

$$z_{b1} + D_1 + \alpha_1 \frac{V_1^2}{2g} = z_{b2} + D_2 + \alpha_2 \frac{V_2^2}{2g} + H_t \tag{5.114}$$

where α = velocity distribution coefficient,
         D = flow depth,
         z_b = bed elevation above datum, and
         H_t = total energy loss between sections 1 and 2.

The subscripts 1 and 2 denote two adjacent sections. The standard-step method for water surface profile computations is a trial-and-error iterative procedure to balance Equation (5.114). GSTARS3 uses the fixed-point iteration method described by Henderson (1966) for making estimated guesses to shorten the trial-and-error procedure. A more detailed description of this procedure can be found in Molinas and Yang (1985).

The energy equation is applied if there is no change of flow regime throughout the study reach. If there are changes in flow regime; i.e., if the flow changes from subcritical to supercritical or vice versa, the momentum equation is used:

$$\frac{Q\gamma}{g}(\beta_2 V_2 - \beta_1 V_1) = F_{p1} - F_{p2} + W \sin\phi - F_f \tag{5.115}$$

where β = momentum correction coefficient,
         F_p = pressure acting on a given cross-section,
         W = weight of water enclosed between sections 1 and 2,
         ϕ = angle of inclination of the channel, and
         F_f = total external friction force acting along the channel boundary.

The appropriate use of the two equations allows carrying backwater computations for subcritical, supercritical, or any combination of both flow conditions, even when hydraulic jumps are involved. Details of these computations were presented by Molinas and Yang (1985).

GSTARS3 uses the stream tube concept to accomplish a semi-two-dimensional approximation of the region being modeled. This allows the program to consider not only longitudinal, but also lateral variations of the hydraulics and sediment activity at each cross-section of the study. The water surface profiles are computed first. The channel is then divided into a selected number of stream tubes with the following characteristics: the total discharge carried by the channel is distributed equally among the stream tubes; stream tubes are bounded by channel boundaries and by imaginary vertical walls; the discharge along a stream tube is constant; and there is no exchange of water or sediments through stream tube boundaries (except due to stream curvature effects, discussed later in section 5.8.3.

Due to the nature of the backwater computations, the water surface elevation is assumed to be horizontal across each cross-section. The lateral locations of the stream tubes are computed at

each time step from the channel conveyance; i.e., stream tube boundaries are set to provide equal conveyance stream tubes. Stream tube locations are computed for each time step; therefore, they are allowed to vary with time. Sediment routing is carried out independently for each stream tube and for each time step. Bed-material composition is computed for each tube at the beginning of the time step, and bed sorting and armoring computations are also carried out separately for each stream tube. In GSTARS3, lateral variations of bed-material composition are accounted for, and this variation is included in the computations of the bed-material composition and sorting for each stream tube.

GSTARS3 is not a truly two-dimensional program; therefore, it cannot simulate areas with recirculating flows or eddies. Other limitations include the inability to simulate secondary flows, reverse flows, water surface variations in the transverse direction, and hydrograph attenuation that result from the use of the simplified governing equations described in this chapter.

5.8.3 Sediment Routing

Sediment routing is done separately for each stream tube using Equation (5.36). The change in the volume of bed sediment due to deposition or scour, ΔA_s, is approximated as

$$\Delta A_s = \left(aW_{i-1} + bW_i + cW_{i+1} \right) \Delta z_{bi} \tag{5.116}$$

where W_i =   top width of cross-section i for the stream tube at hand,

Δz_{bi} =   change in bed elevation (positive for aggradation, negative for scour), and

a,b,c =   constants that must satisfy $a+b+c=1$.

There are many possible choices for the values of a, b, and c. For example, $a = c = 0$ and $b = 1$ is a frequently used combination that is equivalent to assuming that the top width at station i represents the top width for the entire reach. If $b = c = 0.5$ and $a = 0$, emphasis is given to the downstream end of the reach. In practice, it is observed that giving emphasis to the downstream end of the reach may improve the stability of the calculations.

Using Equation (5.116), the partial derivative terms of Equation (5.36) are approximated as follows:

$$\frac{\partial A_s}{\partial t} \approx \frac{\left(aW_{i-1} + bW_i + cW_{i+1} \right) \Delta z_{bi}}{\Delta t} \tag{5.117}$$

$$\frac{dQ_s}{dt} \approx \frac{Q_{s,i} - Q_{s,i-1}}{\frac{1}{2}\left(\Delta x_i + \Delta x_{i-1} \right)} \tag{5.118}$$

$$\Delta z_{bi,j} = \frac{\Delta t}{\left(1-p_i\right)} \frac{q_L\left(\Delta x_i + \Delta x_{i-1}\right) + 2\left(Q_{s,i-1,j} - Q_{s,i,j}\right)}{\left(aW_{i-1} + bW_i + cW_{i+1}\right)\left(\Delta x_i + \Delta x_{i-1}\right)}$$ (5.119)

where j = size fraction index,
  p_i = porosity of sediment in a unit bed layer at cross-section i,
  q_L = lateral sediment discharge per unit channel length, and
  $Q_{s,i,j}$ = computed volumetric sediment discharge for size j at cross-section i.

The total bed elevation change for the stream tube at cross-section i, Δz_{bi}, is computed from

$$\Delta z_{bi} = \sum_j \Delta z_{bi,j}$$ (5.120)

The new channel cross-section at station i, to be used at the next time iteration, is determined by adding the bed elevation change to the old bed elevation. Figure 5.23 provides a definition of variables for sediment routing in a stream tube, and Figure 5.24 provides a simplified flow chart of the overall process followed in computing the changes in bed elevation.
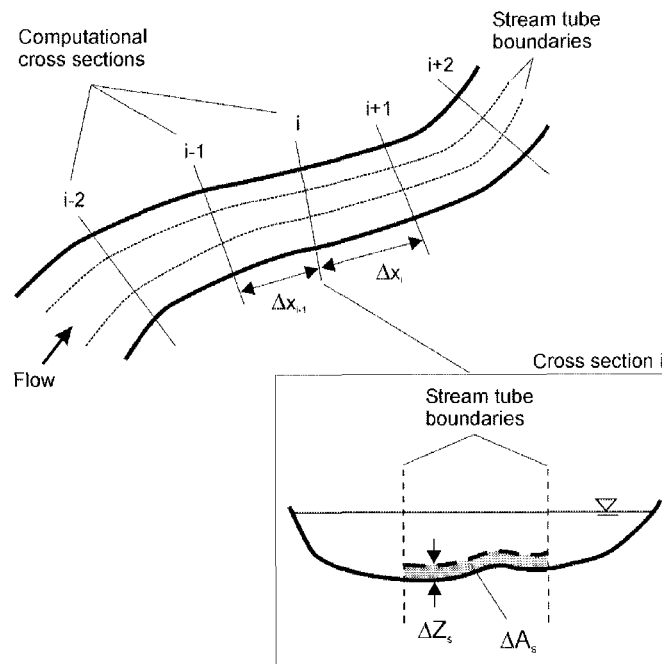

Figure 5.23. Definition of variables in the sediment routing equations, applied to one stream tube.
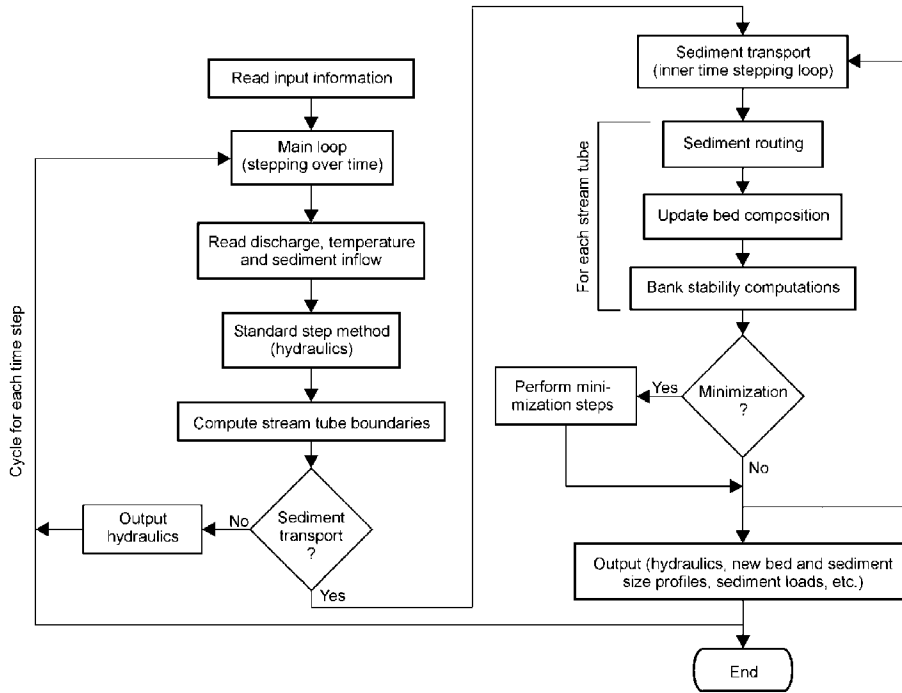
Figure 5.24. Simplified flow chart of program GSTARS3.

Accounting of bed composition is accomplished by the procedure proposed by Bennett and Nordin (1977). This method uses two or three conceptual layers (three layers for deposition and two layers for scour). The process is illustrated in Figure 5.25. The top layer, which contains the bed-material available for transport, is called the active layer. Beneath the active layer is the inactive layer, which is the layer used for storage. Below these two layers is the undisturbed bed, with the initial bed-material composition.
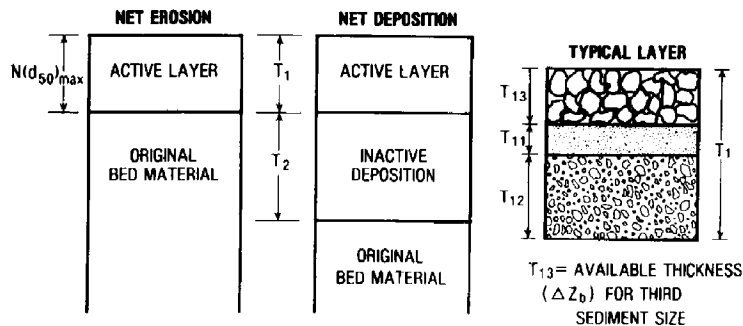
Figure 5.25. Bed composition accounting procedures (from Bennett and Nordin, 1977).

The active layer is the most important concept in this procedure. It contains all the sediment that is available for transport at each time step. The thickness of the active layer is defined by the user as proportional to the geometric mean of the largest size class containing at least 1 percent of the bed-material at that location. Active layer thickness is, therefore, closely related to the time step duration. Erosion of a particular size class of bed-material is limited by the amount of sediments of that size class present in the active layer. If the flow carrying capacity for a particular size class is greater than what is available for transport in the active layer, the term "availability limited" is used (Bennett and Nordin, 1977). On the other hand, if more material is available than that necessary to fulfill the carrying capacity computed by a particular sediment transport equation, the term "capacity limited" is used.

The inactive layer is used when net deposition occurs. The deposition thickness of each size fraction is added to the inactive layer, which, in turn, is added to the thickness of the active layer. The size composition and thickness of the inactive layer are computed first, after which a new active layer is recomputed and the channel bed elevation updated.

The procedures described above are carried out separately along each stream tube. Since the locations of stream tube boundaries change with changing flow conditions and channel geometry, those processes had to be adapted for use in GSTARS3. Bed-material is accounted for at the end of each time step for each stream tube. Bed-material composition is stored at each point used to describe the geometry for all the cross-sections. The values of the active and inactive layer thickness are also stored at those points. At the beginning of the next time step, after the new locations of the stream tube boundaries are determined, these values are used to compute the new layer thicknesses and bed composition for each stream tube.

Sediment transport capacities can be calculated from one of the 15 transport formulae programmed in GSTARS3, plus methods for the erosion and deposition of silt and clay, including high concentration of fines and flocculation and hindered settling. Sediment transport is computed by size fraction. The fractional transport method represented by Equations (5.52) and (5.53) is used. The hydraulic parameters used to compute the sediment carrying capacities in each reach (and stream tube) are computed as weighted averages from the hydraulic parameters from nearby stations. For each station i, the representative values of the area (A_{Ri}), depth (D_{Ri}), velocity (V_{Ri}), and friction slope (S_{Ri}) are computed as follows:

$$A_{Ri} = aA_{i-1} + bA_i + cA_{i+1} \tag{5.121}$$

$$D_{Ri} = aD_{i-1} + bD_i + cD_{i+1} \tag{5.122}$$

$$V_{Ri} = aV_{i-1} + bV_i + cV_{i+1} \tag{5.123}$$

$$S_{Ri} = aS_{i-1} + bS_i + cS_{i+1} \tag{5.124}$$

The weighting parameters a, b, and c can be chosen in any combination that satisfies $a + b + c = 0$. For example, in rivers whose properties change more rapidly from section to section, a scheme incorporating information from the upstream and downstream reaches may be more appropriate. The values of $a = c = 0.25$ and $b = 0.5$ may be adopted in those circumstances. By changing a, b, and c appropriately, the user can use the parameters that favor stability or that favor sensitivity. Usually, more sensitive schemes are less stable, and vice-versa.

Non-equilibrium sediment transport is taken into account using the method developed by Han (1980). In this method, which is based on the analytical solution of the convection-diffusion equation, the non-equilibrium sediment transport rate for each particle size class j is computed from

$$C_i = C_i^* + \left(C_{i-1} - C_i^*\right)\exp\left\{-\frac{\chi w_s \Delta x}{q}\right\} + \left(C_{i-1}^* - C_i^*\right)\left(\frac{q}{\chi w_s \Delta x}\right)\left[1 - \exp\left\{-\frac{\chi w_s \Delta x}{q}\right\}\right] \quad (5.125)$$

where
$\quad C \quad = \quad$ actual sediment concentration,
$\quad C^* \quad = \quad$ sediment carrying capacity, computed from a standard formula,
$\quad q \quad = \quad$ flow discharge per unit width,
$\quad w_s \quad = \quad$ sediment fall velocity,
$\quad i \quad = \quad$ cross-section index (increasing from upstream to downstream), and
$\quad \chi \quad = \quad$ dimensionless recovery factor.

In Equation (5.125), the particle size class index was dropped for convenience. Han and He (1990) recommend for χ a value of 0.25 for deposition and 1.0 for entrainment.

GSTARS3 computes the exchange of sediment across stream tube boundaries in certain specific circumstances. The movement of a sediment particle will have a direction which, in general, is neither the direction of the flow nor the direction of the bed shear stress. For example, in a bend of a channel with a sloping bed (such as the one in Figure 5.26), the larger particles will tend to roll down the slope (gravitational forces dominate), while the smaller particles may move up the slope (lift forces due to secondary currents dominate)—see, for example, Ikeda et al. (1987). A non-zero transverse flux results in exchange of sediments across stream tube boundaries. This exchange does not violate the theoretical assumptions behind the use of stream tubes because the trajectories of the sediment particles are not the same as the trajectories of the fluid elements (streamlines). Therefore, although there is no exchange of water between stream tubes, sediment may cross stream tube boundaries, and the use of stream tubes is still theoretically justified.

GSTARS3 includes the effects of stream curvature that contribute to the radial (transverse) flux of sediments, q_r, near the bed. The two effects considered are transverse bed slope and secondary flows. The effects due to secondary flows are modeled following Kikkawa et al. (1976), in which the angle that the bed shear stress vector makes with the downstream direction, β, is given by

$$\beta = \frac{DV}{U_*A_rR}\left(-4.167 + 2.640\frac{U_*}{\kappa V}\right)$$ (5.126)

where V =   average velocity along the channel's centerline,

         U_* =   shear velocity along the centerline,

         D =   water depth,

         R =   radius of curvature of the channel,

         A_r =   an empirical coefficient (for rough boundaries $A_r = 8.5$), and

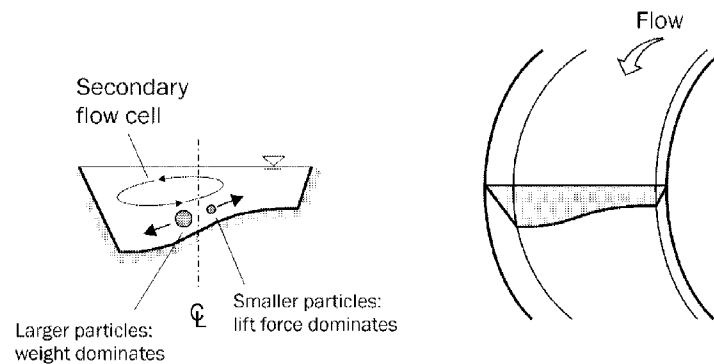 κ =   von Kàrmàn constant (= 0.41).

Figure 5.26. Bed sorting in bends, due to transverse bed slope and secondary currents.

In a bed with transverse slope, the gravity forces cause the direction of the sediment particles to be different from that of the water particles. Following Ikeda et al. (1987), the effects due to a transverse bed slope can be added to those due to curvature, such that

$$\frac{q_r}{q_s} = \tan\sigma = \tan\beta + \frac{1+\alpha\mu}{\lambda\mu}\sqrt{\frac{\tau_0^*}{\tau^*}}\tan\delta$$ (5.127)

where q_s =   unit sediment transport rate in the channel's longitudinal direction,

         σ =   angle between the direction of transport and the channel's downstream direction,

         τ_0^*, τ^* =   non-dimensional critical shear stress and bed shear stress, respectively,

         δ =   transverse bed slope,

         α =   rate of lift to drag coefficients on sediment particles (determined experimentally to be equal to 0.85),

         λ =   sheltering coefficient (= 0.59), and

         μ =   dynamic Coulomb friction factor (= 0.43).

The direction of sediment transport is calculated from Equation (5.127). The components of the sediment transport direction vector are given by

$$q_s = q_t \cos \sigma \qquad (5.128)$$

$$q_r = q_t \sin \sigma \qquad (5.129)$$

where q_t = sediment transport rate per unit width.

Equation (5.36) is then solved using $Q_s = q_s \Delta y$ and $C_L q_L = q_r$, where Δy = stream tube width. The above methods are applied only to sediment moving as bedload. GSTARS3 uses van Rijn's (1984b) method to determine if a particle of a given size is in suspension or moves as bedload.

5.8.4 Total Stream Power Minimization

The basic minimization procedures in GSTARS3 are based on the total stream power minimization theory—see Section 5.4. First, in order to apply the minimization procedure to channel reaches with gradually varied flows, γQS is integrated along the channel:

$$\varphi_T = \int \gamma QS dx \qquad (5.130)$$

where φ_T is defined as the total stream power. This expression is discretized following Chang (1982):

$$\varphi_T = \sum_{i=1}^{N-1} \gamma \left(\frac{Q_i S_i + Q_{i+1} S_{i+1}}{2} \right) \Delta x_i \qquad (5.131)$$

where N = number of cross-sections along the reach,
  Δx_i = distance between cross-section i and $i + 1$,
  Q_i = discharge and slope at station i, and
  S_i = slope at station i.

The direction for channel adjustments is chosen by minimizing the integral represented by Equation (5.131) for total stream power at different stations. This process is repeated for each time step: if alteration of the channel width results in lower total stream power than raising or lowering of the channel's bed, then channel adjustments progress in the lateral direction; otherwise, the adjustments are made in the vertical direction.

Figure 5.27 is used to illustrate the process described above. When erosion takes place, channel adjustments can proceed either by deepening or by widening the cross-section. Both channel widening and deepening can reduce the total stream power for the reach, but GSTARS3 selects

the adjustment that results in the minimum total stream power for the reach. If deposition is predicted by the sediment routing computations, then either the bed is raised or the cross-section is narrowed, but the choice must also result in a minimum of the total stream power for the reach. However, in each case, the amount of scour and/or deposition is limited by the predicted sediment load, and geological or manmade restrictions are also accommodated by the computational algorithms.

Quantitatively, the amount of channel adjustment during each time step is determined by the sediment continuity equation; i.e., Equation (5.119) for each stream tube. Channel widening or narrowing can take place only at the stream tubes adjacent to the banks. In this case, the hydraulic radius, R_h, replaces the top width, W, in Equation (5.119). For stream tubes that are not adjacent to the banks (i.e., interior tubes), bed adjustments can be made only in the vertical direction.
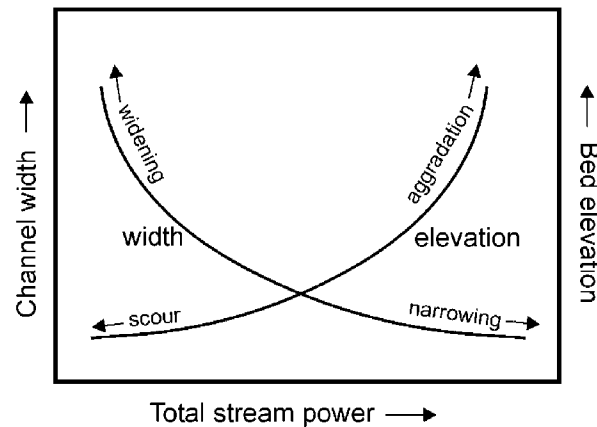

Figure 5.27. Total stream power variation as a function of changes in channel width and bed elevation, with constant discharge and downstream stage.

5.8.5 Channel Side Slope Adjustments

Channel geometry adjustment can take place in both lateral and vertical directions. For an interior stream tube, scour or deposition can take place only on the bed, and the computation of depth change shown in Equation (5.119) is straightforward. For an exterior stream tube, however, the change can take place on the bed or at the bank. As erosion progresses, the steepness of the bank slope tends to increase. The maximum allowable bank slope depends on the stability of bank materials. When erosion undermines the lower portion of the bank and the slope increases to a critical value, the bank may collapse to a stable slope. The bank slope should not be allowed to increase beyond a certain critical value. The critical angle may vary from case to case, depending on the type of soil and the existence of natural or artificial protection.

5-74

GSTARS3 checks the transverse bed slope for violation of a prescribed critical slope (i.e., the critical angle of repose of the bed-material). Each cross-section is scanned at the end of each time step to determine if any vertical or horizontal adjustments have caused the banks to become too steep. If any violations occur, the two points adjacent to the segment are adjusted vertically until the slope equals the user-provided critical slope. For the situation shown in Figure 5.28, the bank is adjusted from *abde* to *ab'd'e*, so that the calculated angle, θ, is equal to the critical angle, θ_c. The adjustments are governed by conservation of mass:

$$A_1 + A_2 = A_3 + A_4 \tag{5.132}$$

where A_1 =   area of triangle *abb'a*,
   A_2 =   area of triangle *bcb'b*,
   A_3 =   area of triangle *cd'dc*, and
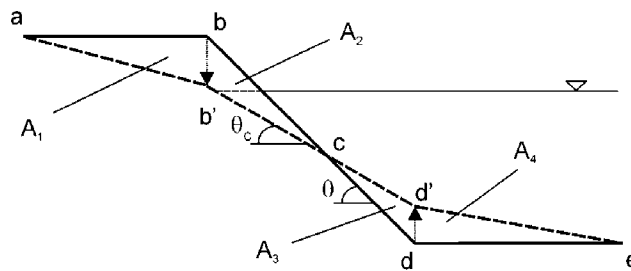 A_4 =   area of triangle *d'edd'*.

Figure 5.28. Representation of the bed adjustment to meet the angle of repose criteria.

5.8.6 Application Examples

To illustrate the application of the GSTARS models, three case studies applied to river and reservoir sedimentation problems are presented below. In the first application, the GSTARS 2.1 model is applied to predict river width changes. This case was taken from the GSTARS 2.1 User's Manual (Yang and Simões, 2000), where it appears as the third example problem in Appendix B. The data used is from a study conducted on Lake Mescalero Dam and Dike.

The Lake Mescalero Dam and Dike were constructed in 1974 and are located at the confluence of Ciewegita and Carrige Creeks on the Mescalero Apache Indian Reservation, about 2.5 miles southwest of Ruidoso, New Mexico. The data from the channel immediately downstream from the emergency spillway is used. The spillway is located in a bedrock cut in the sandstone and shale of the left abutment of the dam. The spillway consists of a 290-ft-long approach channel; a 103.8-ft-wide concrete weir; a 138-ft-long, concrete-lined discharge chute; a 15-ft-long flip bucket; and a concrete erosion cutoff wall located about 250 ft downstream from the flip bucket. The spillway crest rises 5.0 ft above the spillway approach channel floor and the discharge chute floor, to a crest elevation of 6905.0 ft.

The data for the flood of December 20, 1984 through December 31, 1984, was used. The water surface elevation of the reservoir was available for that period. Cross-sectional data were taken from a detailed topographic survey of the study area carried out on June 12, 1979. Figure 5.29 shows the layout of the channel below the spillway at that time. Also, cross-sectional channel geometry was available at two locations after the 1984 flood. These sections are used for comparison purposes.

The water surface elevation of the reservoir was available for the period of the flood. The discharge hydrograph was generated using the water levels and a standard weir equation, $Q = CLH^{3/2}$, with $C = 3.65$. The flood hydrograph is shown in Figure 5.29. The sediment data used was based on bed samples collected from several sites along the channel. Two typical size distributions are also shown in Figure 5.29. On the basis of the mean sediment size, a Manning's roughness coefficient of 0.06 was chosen for stage-discharge computations.
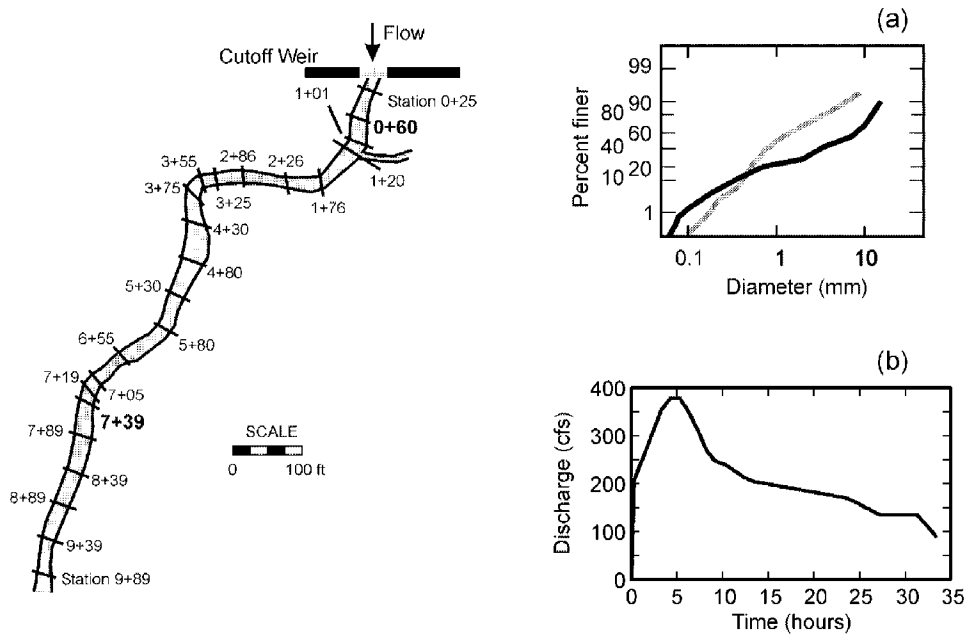

Figure 5.29. Layout of the cross-sections used in the simulation of scour downstream from Lake Mescalero's unprotected spillway. The cross-sections used to compare actual data with the simulations are highlighted. The figure also shows (a) typical particle size distributions found in the stream corridor and (b) the spillway hydrograph.

The cross-sections used in the comparisons are sections 0+60 and 7+39 (see Figure 5.29). Section 0+60 is located 60 ft downstream from the spillway, and section 7+30 is located 739 ft downstream from the spillway. Two runs were performed: one using stream power minimization to compute channel with changes and the other using only vertical scour (i.e., with fixed channel width). The comparison between the measured and the computed cross-sections is shown in Figure 5.30. Significant differences are observed when stream power calculations are activated,

especially for section 0+60. Both the shape of the cross-sections and their thalwegs were more accurately predicted when the stream power minimization computations were activated.
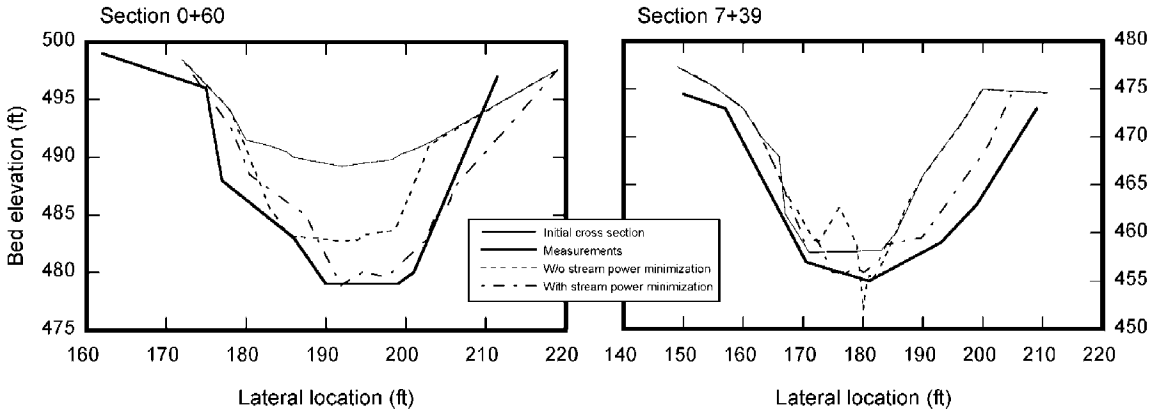

Figure 5.30. Comparison between measurements and simulation for two cross-sections of Lake Mescalero's spillway channel.

In the second example, GSTARS3 is used, and the experimental measurements of Swamee (1974) were chosen for the analysis. In Swamee's experiments, a small laboratory flume was used, to which a barrier was placed downstream to simulate a dam. Medium sand was used to study the deposition upstream of the barrier. The main characteristics of the experimental setup are as follows:

Channel width (cm)	20
Channel length (m)	32
Slope of bed	3.5×10^{-3}
Flow discharge (l/s)	2.0
Sediment d_{50} (mm)	0.4
Sediment discharge (l/s)	6.8×10^{-4}
Average temperature (°C)	12
Barrier height (cm)	9.0

In Swamee's experiments, an initial bed of sand (the same sand used for the input of sediment load) was used. Clear water at the prescribed discharge was fed to the channel for a sufficient amount of time to establish uniform flow conditions. The initial slope was determined after such an equilibrium was achieved. Then, a barrier was placed at the downstream end of the flume, thus raising the water surface at that end (profile of type M1). The barrier height was chosen to ensure that all the sediment in transport was trapped in its headwater reservoir. The sediment load was fed at the upstream end of the flume for a total run time of 70 hours.

An initial calibration was carried out to determine the main roughness characteristics of the channel. Note that Strickler's equation yields a Manning's n value of

$$n = \frac{d_{50}^{1/6}}{25.6} = 0.011 \tag{5.133}$$

where d_{50} is in ft.

If we use d_{90} in Equation (5.133), we obtain $n = 0.012$ ($d_{90} = 0.70$ mm). A sensitivity analysis was carried out using GSTARS3 and several n values. The results are shown in Figure 5.31. In practice, Swamee reported having observed bed forms (ripples and/or dunes) developing during the run. He was not specific about them; therefore, we could not use an adequate roughness estimator. However, he stated that the bed measurements were made by leveling the bed at the measuring stations, in segments with 0.5 m in length. Therefore, the measurements represented the average bed profile over that distance. That effect was well represented by the irregularity (waviness) shown by the bed and free surface elevation measurements. For the final runs, a n value of 0.020 was adopted.

Swamee measured the sediment load in transport and expressed it as a function of the bed shear stress:

$$q_{t*} = 100\tau_*^3 \tag{5.134}$$

where q_{t*} = non-dimensional unit-width sediment transport rate, and

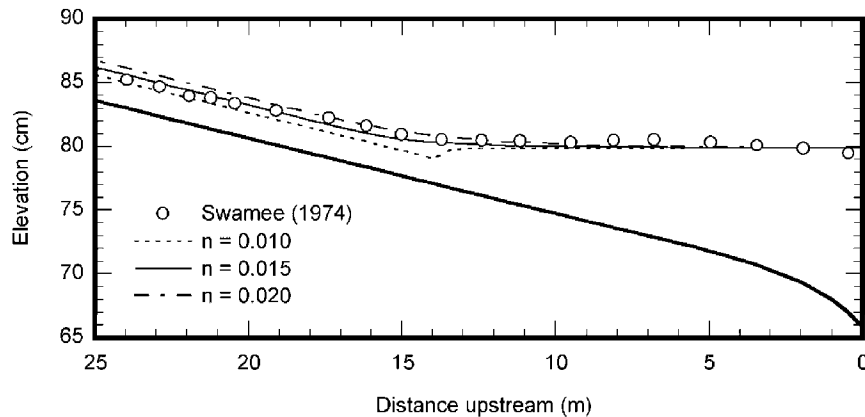 τ_* = non-dimensional bed shear stress.

Figure 5.31. Sensitivity runs for the equilibrium condition of run No. 1 of Swamee (1974). The bed of the channel is represented by the lower thick line.

They are defined as

$$q_{t*} = \frac{q_t}{U_* d} \tag{5.135}$$

and

$$\tau_* = \frac{\tau - \tau_c}{(\gamma_s - \gamma)d} \tag{5.136}$$

where q_t = total bedload per unit width (units of L^2T^{-1}),

U_* = shear velocity,

d = size of the sediment particles,

τ = bed shear stress,

τ_c = critical (Shields) bed shear stress, and

γ, γ_s = unit weight of water and sediment, respectively.

The values of the coefficient and exponent were determined by data fitting. Equation (5.134) was implemented in GSTARS3 and used in the present runs.

The GSTARS3 results are presented in Figure 5.32. Agreement between measurement and simulation is close overall. The small oscillations observed in the experimental data can be attributed to a number of different factors. They are not observed in the numerical model because of the uniform boundary conditions used (constant water and sediment discharge, uniform sediment size, channel with constant width, and water surface level without kinks). This reflects the stability of the computations, because under such uniform conditions only numerical oscillations could cause disturbances in the predicted bed profiles. It is clear that in the numerical experiments presented here, GSTARS3 can produce accurate, stable, and oscillation-free solutions.
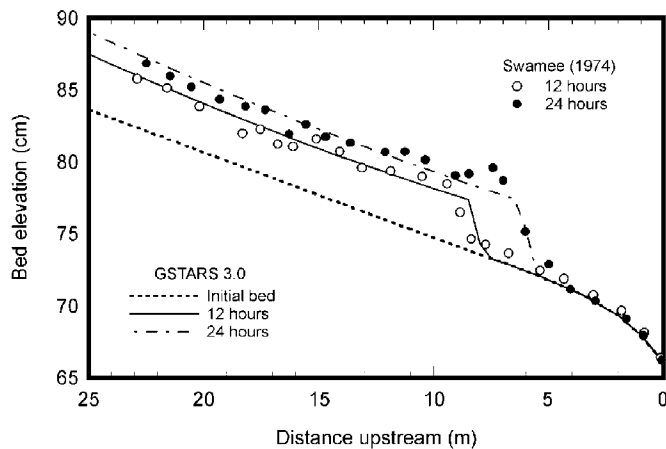

Figure 5.32. Comparison of experiments with simulations by GSTARS3 for two time instants: 12 and 24 hours after the start of the sediment loading.

Next, the GSTARS3 model is applied to Tarbela Dam. Tarbela Dam, in northern Pakistan along the Indus river, is the largest earth-filled dam in the world. The reservoir, with a capacity of 9.68×10^6 acre-feet, is a run-of-the-river type of reservoir with two major tributaries, the Siran and the Brandu. The reservoir's storage capacity has been continuously depleted since the dam was built in 1974, with an annual inflow rate of 240 million metric tons of sediment, mostly in the silt and clay range. This loss in capacity threatens irrigation water supply and hydropower production.

In this study, GSTARS3 is used to simulate 22 years of reservoir sedimentation (from 1974 through 1996) for a reach that spans 54.8 miles upstream from the dam. The hydrology of the system is given in Figure 5.33, together with the dam operation. The tributaries have a relatively small contribution when compared with the main stem discharge; therefore, they are not included in Figure 5.33 (but they were included in the computations).
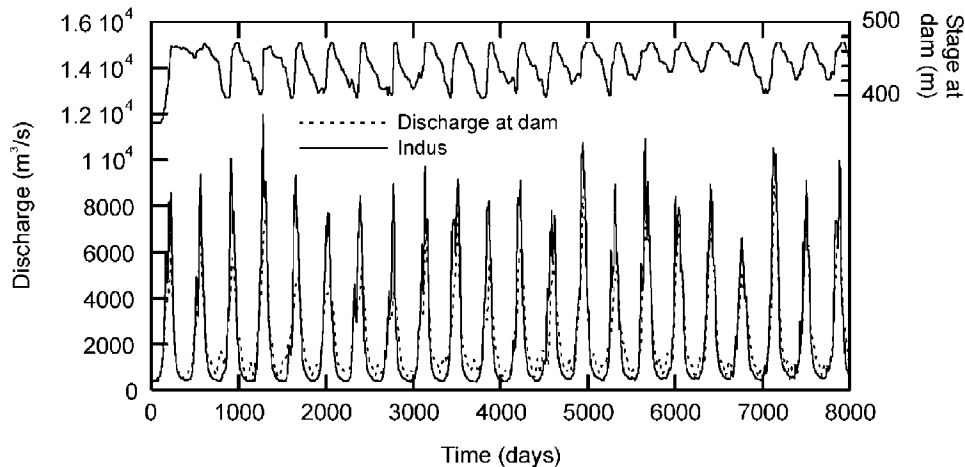

Figure 5.33. Hydrology and dam operation for Tarbela in the period of 1974 to 1996.

The Tarbela Reservoir bathymetry was discretized using existing surveyed cross-sections, which are marked in Figure 5.34. The GSTARS3 simulations were carried out using daily time steps for the hydraulic computations and 4.8 hours for sediment routing computations (8,040 time steps for hydraulics; 40,200 time steps for sediment). Yang's (1973) equation was extrapolated for the silt and clay range and was used in this simulation (the particle size distributions were in the range of 0.002 to 2.0 mm).

Computer runs on a PC-compatible desktop workstation running Microsoft Windows XP took less than 10 minutes. The simulation results for the thalweg are in good agreement with measurements, as shown in Figure 5.35. Two typical cross-sections are also shown in Figure 5.36. The quality of the simulation results produced by GSTARS3 shows that, at least for this case, it can be used for the long-term simulation of long rivers and river-like reservoirs.
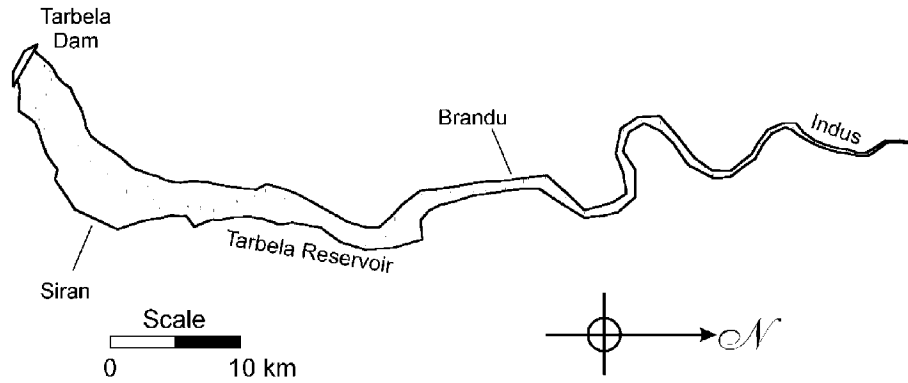
Figure 5.34. Tarbela Dam and Reservoir. The points (+) mark the locations of the cross-sections.
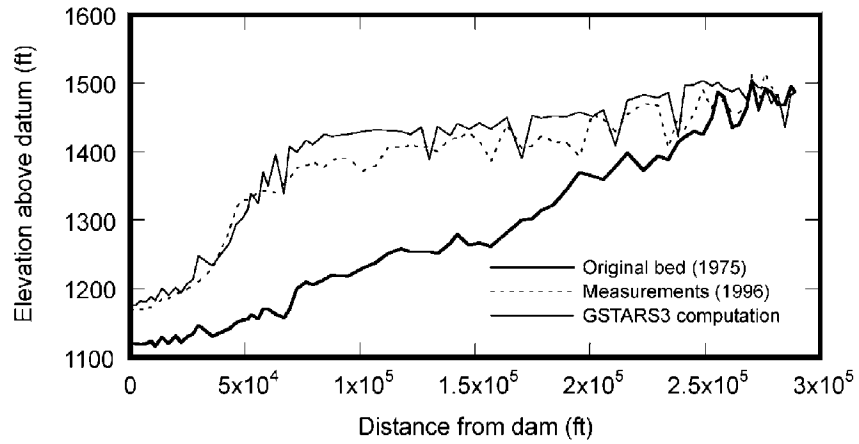

Figure 5.35. Results of the simulation of the Tarbela delta advancement over a period of 22 years.
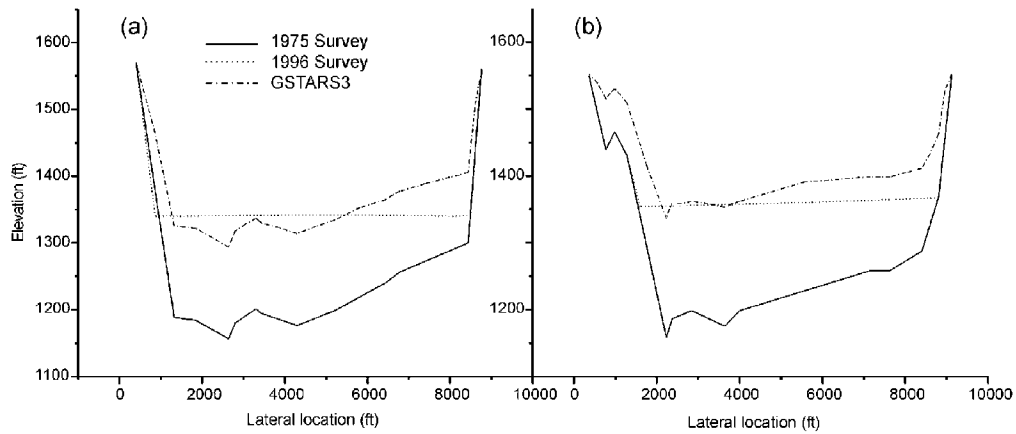

Figure 5.36. Cross-sections No. 24 and No. 30 in the simulation. Comparisons between the 1975 and 1996 survey data and GSTARS3 simulation.

5.9 Summary

Sediment transport computer models have been increasingly used as tools for solving practical engineering problems. These models are also used to improve our understanding of river morphological processes. This chapter provides a brief review of basic theoretical concepts used in developing models and some of the practical approaches used for solving engineering problems.

Generally speaking, river hydraulics and sediment transport in natural rivers are three dimensional. Truly two- or three-dimensional models may be needed for solving localized problems, using detailed, site-specific field data for testing and calibration. One-dimensional models are more suitable for long-term simulation of a long river reach, where the lateral variations of hydraulic and sediment conditions can be ignored. From a practical point of view, a semi-two-dimensional model may be adequate for solving many river engineering problems.

Due to the changing hydrologic conditions of a river, hydraulic conditions in a river are unsteady from a theoretical point of view. With the possible exception of routing during a flood near its peak, however, most river hydraulic conditions can be approximated by a semi-steady hydrograph using constant-discharge bursts of short durations.

There are many well-established numerical schemes for solving flow and sediment transport model governing equations. The one-dimensional, finite difference uncoupled method is the one most commonly used in practice. With the advent of more powerful and affordable computing platforms, increasing number of commercially available models, and more efficient and accurate data collection techniques, there is an increasing demand for the use of multi-dimensional models in river engineering problems.

The simulated results from sediment-transport computer models are sensitive to the selection of sediment-transport formulas in the model. The user of a model should have a good understanding of sediment transport theories and the limits of application of different sediment transport formulas.

It is assumed in most sediment-transport models that channel width is a constant and cannot be adjusted. This unrealistic assumption can lead to erroneous results when applied to an alluvial river. The GSTARS3 model is based on the stream tube concept and the minimum stream power theory. Both the energy and momentum equations are used for water surface profile computation. GSTARS3 incorporates the concepts of sediment routing by size fraction, formation and destruction of an armor layer, channel width adjustments, and channel side stability, among other things, to simulate site-specific conditions. A model similar to GSTARS3 should be adequate for solving many semi-two-dimensional, quasi-steady river engineering problems with a minimum amount of field data required for calibration and testing.

Due to the limited scope of a chapter such as this, many important topics were only briefly touched upon or not covered at all. For example, it was not the purpose of this chapter to cover the subject of open-channel flow, which is described with much more detail than would ever be

possible here in the classic works of Chow (1959) and Henderson (1966). Numerous textbooks cover a multitude of numerical solution methods, some of which are not even mentioned in this chapter but which play an important role in computational fluid dynamics. One such topic covers methods for the computation of flows with high gradients, such as those appearing in dam break flows; the interested reader can review this subject in Toro (2001). Mudflows and debris flows occur naturally and are important in many natural events, especially in regions with high gradient topography. Their rheology and modeling is complex and can be found in Coussot (1997) and Takahashi (1991), respectively. Flow turbulence is a field of active research and constant evolution. Turbulence in natural bodies of water is a topic covered in Nezu and Nakagawa (1993), and its modeling in hydraulics is covered in the monograph by Rodi (1993). The reader is advised to review the list of references at the end of this chapter for more in-depth coverage of many more topics, especially the textbooks, monographs, and survey papers, and the references therein.

5.10 References

Akiyama, J., and H. Stefan (1981). *Theory of Plunging Flow into a Reservoir*, St. Anthony Falls Hydraulic Laboratory Technical Memorandum I-97, University of Minnesota, Minneapolis, Minnesota.

Akiyama, J., and H. Stefan (1985). "Turbidity Current with Erosion and Deposition," *Journal of the Hydraulic Division of the ASCE*, vol. 111, no. HY12, pp. 1473-1496.

Arcement, G.J., and V.R. Schneider (1987). *Roughness Coefficients for Densely Vegetated Flood Plains*, U.S. Geological Survey Water–Resources Investigation Report 83–4247.

Armanini, A. (1995). "Non-uniform Sediment Transport: Dynamics of the Active Layer," *Journal of Hydraulic Research*, vol. 33, no. 5, pp. 611-622.

Armanini, A,. and G. Di Silvio (1988). "A One-dimensional Model for the Transport of a Sediment Mixture in Non-equilibrium Conditions," *Journal of Hydraulic Research*, vol. 26, no. 3, pp. 275-292.

ASCE (1998a). "River Width Adjustment. I: Processes and Mechanisms," *Journal of Hydraulic Engineering*, vol. 124, no. 9, pp. 881-902.

ASCE (1998b). "River Width Adjustment. II: Modeling," *Journal of Hydraulic Engineering*, vol. 124, no. 9, pp. 903-917.

Atkinson, E. (1992). *The Design of Sluices Settling Basins, a Numerical Modeling Approach*, Report OD 124, HR Wallingford Ltd., Wallingford, United Kingdom.

Atkinson, E. (1996). *The Feasibility of Flushing Sediment from Reservoirs*, Report OD 137, HR Wallingford Ltd., Wallingford, United Kingdom.

Bagnold, R.A. (1963). *The Nature of Saltation and of Bedload Transport in Water*, Proceedings of The Royal Society of London A332.

Bakri, M.F., T.K. Gates, and A.F. Khattab (1992). "Field-measured Hydraulic Resistance Characteristics in Vegetation-infested Canals," *Journal of Irrigation and Drainage Engineering*, vol. 118, no. 2, pp. 256-274.

Barnes, H.H. (1967). *Roughness Characteristics of Natural Channels*, U.S. Geological Survey Water-Supply Paper 1849.

Bathurst, J.C. (1985). "Flow Resistance Estimation in Mountain Rivers," *Journal of Hydraulic Engineering*, ASCE, vol. 111, no. 4, pp. 625-643.

Bathurst, J.C. (2002). "At-a-site Variation and Minimum Flow Resistance for Mountain Rivers," *Journal of Hydrology*, vol. 269, pp. 11-26.

Batina, J.T. (1993). "A Gridless Euler/Navier-Stokes Solution Algorithm for Complex Aircraft Configurations," AIAA Paper 93-0333.

Bell, R., and A. Sutherland (1983). "Nonequilibrium Bedload Transport by Steady Flows," *Journal of Hydraulic Engineering*, vol. 109, no. 3, pp. 351-367.

Bennett, J., and C. Nordin (1977). "Simulation of Sediment Transport and Armouring," *Hydrological Sciences Bulletin*, vol. 22, pp. 555-569.

Bestawy, A. (1997). *Bedload Transport and Bed Forms in Steady and Unsteady Flows*, Ph.D. dissertation, Catholic University of Leuven, Belgium.

Borah, D., C. Alonso, and S. Prasad (1982). "Routing Graded Sediments in Streams: Formulations," *Journal of the Hydraulic Division of the ASCE*, vol. 108, no. HY12, pp. 1486-1503.

Bourget, E., and M.J. Fortin (1995). "A Commentary on Current Approaches in the Aquatic Sciences," *Hydrobiologia*, vol. 300/301, pp. 1-16.

Bray, D.I. (1979). "Estimating Average Velocity in Gravel-bed Rivers," *Journal of the Hydraulic Division of the ASCE*, vol. 105, no. HY9, pp. 1103-1122.

Bray, D.I., and K.S. Davar (1987). "Resistance to Flow in Gravel-bed Rivers," *Canadian Journal of Civil Engineering*, vol. 14, no. 1, pp. 77-86.

Brebbia, C.A. (1978). *The Boundary Element Method for Engineers*, Pentech Press, London.

Britter, R.E., and P.F. Linden. (1980). "The Motion of the Front of a Gravity Current Traveling Down on an Incline," *Journal of Fluid Mechanics*, vol. 99, pp. 531-543.

Bureau of Reclamation (1987). *Design of Small Dams, 3rd edition,* Department of the Interior, Bureau of Reclamation, Denver, Colorado.

Canuto, C.M., A. Hussaini, and T. Zang. (1996). *Spectral Methods in Fluid Mechanics,* Springer Series in Computational Physics, Springer-Verlag, Berlin.

Chang, H.H. (1979). "Minimum Stream Power and River Channel Patterns," *Journal of Hydrology,* vol. 41, pp. 303-327.

Chang, H.H. (1982). "Mathematical Model for Erodible Channels," *Journal of the Hydraulic Division of the ASCE,* vol. 108, no. HY5, pp. 678-689.

Chang, H.H. (1990). Generalized Computer Program FLUVIAL-12, Mathematical Model for Erodible Channels, User's Manual.

Chang, H.H., and J. Hill (1976). "Computer Modeling of Erodible Flood Channels and Deltas," *Journal of the Hydraulic Division of the ASCE,* vol. 102, no. HY10, pp. 1461-1477.

Chang, H.H., and J. Hill (1977). "Minimum Stream Power for Rivers and Deltas," *Journal of the Hydraulic Division of the ASCE,* vol. 103, no. HY12, pp. 1375-1389.

Chow, V.T. (1959). *Open Channel Flow.* McGraw-Hill Publishing Company, New York.

Chung, T.J. (2002). *Computational Fluid Dynamics,* Cambridge University Press.

Coussot, P. (1997). *Mudflow Rheology and Dynamics,* IAHR Monograph, A.A. Balkema, Roterdam.

Cowan, W.L. (1956). "Estimating Hydraulic Roughness Coefficients," *Agricultural Engineering,* vol. 37 (July), pp. 473–475.

Cunge, J., F. Holly, and A. Verwey (1980). *Practical Aspects of Computational River Hydraulics,* Pitman, Marshfield, MA.

Darby, S.E., and C.R. Thorne (1996). "Development and Testing of Riverbank Stability," *Journal of Hydraulic Engineering,* vol. 122, no. 8, pp. 443-454.

Deletic, A. (2000). *Sediment Behaviour in Overland Flow Over Grassed Areas,* Ph.D. Thesis, University of Aberdeen, UK.

DeLong, L. (1989). "Mass Conservation: 1D Open Channel Flow Equations," *Journal of Hydraulic Engineering,* vol. 115, no. 2, pp. 263-269.

Egashira, S., and K. Ashida (1980). "Studies on the Structure of Density Stratified Flows," *Bulletin of the Disaster Prevention Research Institute,* vol. 29, Kyoto, Japan.

Egiazaroff, I. (1965). "Calculation of Nonuniform Sediment Concentrations," *Journal of the Hydraulic Division of the ASCE*, vol. 91, no. HY4, pp. 225-247.

Einstein, H. (1950). *The Bedload Function in Open Channel Flows*, Technical Bulletin no. 1026, U.S. Department of Agriculture, Soil Conservation Service.

Fan, J. (1991). *Density Currents in Reservoirs*, Workshop on Management of Reservoir Sedimentation, New Delhi, India.

Fan, S.S. (ed.) (1988). "Twelve Selected Computer Stream Sedimentation Models Developed in the United States," *Proceedings of the Interagency Symposium on Computer Stream Sedimentation Model, Denver, Colorado.* Published by the Federal Energy Regulatory Commission, Washington, DC.

Federal Interagency Stream Restoration Working Group (1998). *Stream Corridor Restoration Principles, Processes, and Practices.* (http://www.usda.gov/stream_restoration/)

Ferziger, J., and M. Peric (2002). *Computational Methods for Fluid Dynamics*, 2nd ed., Springer-Verlag.

Fischer, H., J. List, R. Koh, J. Imberger, and N. Brooks (1979). *Mixing in Inland and Coastal Waters*, Academic Press.

Fix, G., and M. Gunzburger (1978). "On the Least Squares Approximations to Indefinite Problems of the Mixed Type," *International Journal of Numerical Methods in Engineering*, vol. 12, pp. 453-469.

Ford, D., and M. Johnson (1983). *An Assessment of Reservoir Density Currents and Inflow Processes*, Technical Report E-83-7, U.S. Army Engineering Waterways Experiment Station, Vicksburg, Mississippi.

Fredlund, D.G. (1987). *Slope Stability Analysis Using PC-slope*. Geo-Slope Programming Ltd., Calgary, Alberta, Canada.

Garcia, M.H., and G. Parker (1991). "Entrainment of Bed Sediment into Suspension," *Journal of Hydraulic Engineering*, vol. 117, no. 4, pp. 414-435.

Griffiths, G.A. (1981). "Flow Resistance in Coarse Gravel Bed Rivers," *Journal of the Hydraulic Division of the ASCE*, vol. 107, no. HY7, pp. 899-918.

Gwinn, W.R., and W.O. Ree (1980). "Maintenance Effects on the Hydraulic Properties of a Vegetated-lined Channel," *Transactions of the ASAE*, vol. 23, no. 3, pp. 636-642.

Hagerty, D. (1991). "Piping/Sapping Erosion 1: Basic Considerations," *Journal of Hydraulic Engineering*, vol. 117, no. 8, pp. 997-998.

Han, Q. (1980). "A Study on the Nonequilibrium Transportation of Suspended Load." *Proceedings of the International Symposium on River Sedimentation*, Beijing, China, pp. 793-802. (In Chinese.)

Han, Q., and M. He (1990). "A Mathematical Model for Reservoir Sedimentation and Fluvial Processes," *International Journal of Sediment Research*, vol. 5, no. 2, International Research and Training Center on Erosion and Sedimentation, pp. 43-84.

Harleman, D. (1961). Stratified Flow. In *Handbook of Fluid Dynamics*. V. Streeter (ed.), McGraw-Hill, New York.

Hebbert, B., J. Imberger, I. Loh, and J. Petterson (1979). "Collie River Underflow into the Wellington Reservoir," *Journal of the Hydraulic Division of the ASCE*, vol. 105, no. HY5, pp. 533-545.

Henderson, F. (1966). *Open Channel Flow*, MacMillan Book Company, New York, NY.

Holly, M.F., J.C. Yang, P. Schwarz, J. Schaefer, S.H. Su, and R. Einhelling (1990). *CHARIMA - Numerical Simulation of Unsteady Water and Sediment Movement in Multiply Connected Networks of Mobile-bed Channels*, IIHR Research Report no. 343, Iowa Institute of Hydraulic Research, the University of Iowa, Iowa City, Iowa.

HR Wallingford (1992). *The Hydraulic Roughness of Vegetated Channels*, Report SR 305, HR Wallingford Ltd., Wallingford, United Kingdom.

Hsu, S., and F. Holly (1992). "Conceptual Bedload Transport Model and Verification for Sediment Mixtures," *Journal of Hydraulic Engineering*, vol. 118, no. 8, pp. 1135-1152.

Ikeda, S., M. Yamasaka, and M. Chiyoda (1987). "Bed Topography and Sorting in Bends," *Journal of Hydraulic Engineering*, vol. 113, no. 2, pp.190-206.

International Research and Training Center on Erosion and Sedimentation (1985). *Lecture Notes of the Training Course on Reservoir Sedimentation*, Sediment Research Laboratory of Tsinghua University, Beijing, China.

Ippen, A.T., and D.R.F. Harleman (1952). *Steady-state Characteristics of Sub-surface Flow*, Circular no. 521, U.S. National Bureau of Standards, pp. 79-93.

Jain, S.C. (1981). "Plunging Phenomena in Reservoirs," *Proceedings of the Symposium on Surface Water Impoundments*, H. Stefan (ed.), ASCE, pp. 1249-1257.

Jirka, G., and M. Watanabe (1980). "Thermal Structure of Cooling Ponds," *Journal of the Hydraulic Division of the ASCE*, vol. 106, no. HY5, pp. 701-715.

Johannesson, H., and G. Parker (1985). *Computer Simulated Migration of Meandering Rivers in Minnesota*, Project Report no. 242, St. Anthony Falls Hydraulic Laboratory, University of Minnesota.

Julien, P.Y., and J. Wargadalam (1995). "Alluvial Channel Geometry, Theory and Applications," *Journal of Hydraulic Engineering*, vol. 121, no. 4, pp. 312-325.

Karim, M., and J. Kennedy (1982). *Computer-based Predictors for Sediment Discharge and Friction Factor of Alluvial Streams*. IIHR Report no. 242, Iowa Institute of Hydraulic Research, University of Iowa, Iowa City, Iowa.

Keller, J.B., and D. Givoli (1989). "Exact Non-reflecting Boundary Conditions," *Journal of Computational Physics*, vol. 82, pp. 172-192.

Keulegan, G.H. (1949). "Interfacial Instability and Mixing in Stratified Fluids," *Journal of Research, NBS*, vol. 43, RP 2040.

Kikkawa, M., S. Ikeda, and A. Kitagawa (1976). "Flow and Bed Topography in Curved Open Channels," *Journal of the Hydraulic Division of the ASCE*, vol. 102, no. HY9, pp. 1327-1342.

Klaassen, G. (1990). *Sediment Transport in Armoured Rivers During Floods*, Report prepared for the Rijkswaterstaat, Delft Hydraulics, Holland.

Klaassen, G., H.J. Ogink, L.C. van Rijn (1986). *DHL-research on Bedforms, Resistance to Flow and Sediment Transport*, Delft Hydraulics Communication no. 362, July 1986.

Kouwen, N., and R.M. Li (1980). "Biomechanics of Vegetative Channel Linings," *Journal of the Hydraulic Division of the ASCE*, vol. 106, no. 6, pp. 713-728.

Lacey, G. (1920). "Stable Channels in Alluvium," *Proceedings of the Institute of Civil Engineers*, vol. 229, pp. 259-292.

Marzolf, R. (2003). Personal communication.

McAnally, W.H., and W.A. Thomas (1985). *User's Manual for the Generalized Computer Program System, Open-channel Flow and Sedimentation, TABS-2, Main Text*. U.S. Army Corps of Engineers, Waterways Experiment Station, Vicksburg, Mississippi.

Migniot, C. (1981). *Erosion and Sedimentation in Sea and River*. La Pratique des Sols et des Foundations, editions Le Moniteur, France.

Molinas, A., and C.T. Yang (1985). "Generalized Water Surface Profile Computations," *Journal of the Hydraulic Division of the ASCE*, vol. 111, no. HY3, pp.381-397.

Molinas, A., and C.T. Yang (1986). *Computer Program User's Manual for GSTARS (Generalized Stream Tube model for Alluvial River Simulation)*, U.S. Bureau of Reclamation, Engineering and Research Center, Denver, Colorado, USA.

Montes, S. (1998). *Hydraulics of Open Channel Flow*, ASCE Press.

Morris, G.L., and J. Fan (1998). *Reservoir Sedimentation Handbook*. McGraw-Hill Publishing Company, New York.

Naot, D., I. Nezu, and H. Nakagawa (1995). "Periodic Behaviour of Partly Vegetated Open Channel," *HYDRA 2000*, vol. 1, Thomas Telford, London, pp.141-146.

Naot, D., I. Nezu, and H. Nakagawa (1996). "Hydrodynamic Behavior of Partly Vegetated Open Channels," *Journal of Hydraulic Engineering*, vol. 122, no. 11, pp.625-633.

National Research Council. (1983). *An Evaluation of Flood-level Prediction Using Alluvial River Models*, National Academy Press, Washington, DC.

Nelson, J.M., and J.D. Smith (1989). "Evolution and Stability of Erodible Channel Beds," in *River Meandering*, S. Ikeda and G. Parker (eds.), Water Resources Monograph 12, American Geophysical Union, Washington, DC.

Nezu, I., and H. Nakagawa (1993). *Turbulence in Open Channel Flows*, IAHR Monograph, A.A. Balkema, Roterdam.

Nikuradse, J. (1933). *Strömungsgesetze in Rauhen Rohren*, Forschung Arb. Ing. Wesen no. 361, Germany. (In German.)

Noh, W.F. (1964). "CEL: a Time-dependent, Two-space-dimensional, Coupled Eulerian-Lagrangian Code," In *Methods in Computational Physic*, F.H. Harlow (ed.), Academic Press, New York.

Osman, A.M., and C.R. Thorne (1988). "Riverbank Stability Analysis; I : Theory," *Journal of Hydraulic Engineering*, vol. 114, no. 2, pp.134-150.

Parker, G., M. Garcia, Y. Fukushima, and W. Yu (1987). "Experiments on Turbidity Currents Over an Erodible Bed," *Journal of Hydraulic Research*, vol. 25, no. 1, pp.123-147.

Patera, A. (1984). "A Spectral Method for Fluid Dynamics, Laminar Flow in a Channel Expansion," *Journal of Computational Physics*, vol. 54, pp.468-488.

Pinder, G., and W. Gray (1977). Finite Element Simulation in Surface and Subsurface Hydrology, Academic Press.

Pitlo, R.H. (1986). "Towards a Larger Capacity of Vegetated Channels," *Proceedings of the EWRS/AAB 7ᵗʰ Symposium On Aquatic Weeds*, pp.245-250.

Preissman, A. (1961). "Propagation des Intumescences Dans les Cannaux et Rivièrs," *1ˢᵗ Congress of the French Association for Computation*, Grenoble, France, pp.433-442.

Rastogi, A., and W. Rodi (1978). "Calculation of General Three-dimensional Turbulent Boundary Layers," *AIAA Journal*, vol. 16, pp.151-159.

Rodi, W. (1993). *Turbulence Models and Their Application in Hydraulics*, IAHR Monograph, A.A. Balkema, Roterdam.

Rooseboom, A. (1975). *A Sediment-production Map for South Africa*, Report 61, Department of Water Affairs, Pretoria, South Africa.

Rouse, H. (1950). *Elementary Mechanics of Fluids*. John Wiley and Sons, Inc., New York.

Samuels, P.G. (1990). "Cross-section Location in 1-D Models," *International Conference on River Hydraulics*, W. White (ed.), John Wiley & Sons, pp.339–350.

Savage, S., and J. Brimberg (1975). "Analysis of Plunging Phenomena in Water Reservoirs," *Journal of Hydraulic Research*, vol. 13, no. 2, pp.187-204.

Shimizu, Y., H. Yamaguchi, and T. Itakura (1991). "Three-dimensional Computation of Flow and Bed Deformation," *Journal of Hydraulic Engineering*, vol. 116, no. 9, pp.1090-1108.

Shimizu, Y., and T. Tsujimoto (1994). "Numerical Analysis of Turbulent Open-channel Flow Over a Vegetation Layer Using a k-ε Turbulence Model," *Journal of Hydroscience and Hydraulic Engineering*, vol. 11, no. 2, pp.57-67.

Simões, F.J.M. (1995). *Modeling Turbulent Flow and Mixing in Compound Channels*, Ph.D. dissertation, the University of Mississippi, University, Mississippi.

Simões, F.J.M. (2001). "Three-dimensional Modeling of Flow Through Sparse Vegetation," *Proceedings of the 7th Federal Interagency Sedimentation Conference*, Reno, Nevada, March 25-29, pp.2001.

Singh, V.P., and J. Li (1993). "Identification of Reservoir Flood-wave Models," *Journal of Hydraulic Research*, vol. 31, no. 6, pp.811-824.

Song, T., and W. Graf (1995). "Bedload Transport in Unsteady Open-channel Flow," in *Rapport Annuel*, Laboratoire de Recherches Hydrauliques, Ecole Polytechnique Federal, Lausanne, Switzerland.

Song, C.C.S., and C.T. Yang (1979a). "Theory of Minimum Rate of Energy Dissipation," *Journal of the Hydraulic Division of the ASCE*, vol. 105, no. HY7, pp.769-784.

Song, C.C.S., and C.T. Yang (1979b). "Velocity Profiles and Minimum Stream Power," *Journal of the Hydraulic Division of the ASCE*, vol. 105, no. HY8, pp.981-998.

Song, C.C.S., and C.T. Yang (1980). "Minimum Stream Power: Theory," *Journal of the Hydraulic Division of the ASCE*, vol. 106, no. HY9, pp.1477-1487.

Straškraba, M. (1998). "Coupling of Hydrobiology and Hydrodynamics: Lakes and Reservoirs," in *Physical Processes in Lakes and Oceans*, J. Imberger (ed.), American Geophysical Union, pp.623-644.

Swamee, P. (1974). *Analytic and Experimental Investigation of Streambed Variation Upstream of a Dam*, Ph.D. Thesis, Dept. of Civil Engineering, University of Roorkee, India.

Takahashi, T. (1991). *Debris Flow*, IAHR Monograph, A.A. Balkema, Roterdam.

Tannehill, J., D. Anderson, and R. Pletcher (1997). *Computational Fluid Mechanics and Heat Transfer*, 2nd ed., Taylor and Francis.

Temple, D.M. (1987). "Closure of 'Velocity Distribution Coefficients for Grass-lined Channels,'" *Journal of Hydraulic Engineering*, vol. 113, no. 9, pp.1224-1226.

Tennekes, H., and J. Lumley (1972). *A First Course in Turbulence*, MIT Press, Cambridge, Massachusetts.

Thompson, S.M., and P.L. Campbel (1979). "Hydraulics of a Large Channel Paved With Boulders," *Journal of Hydraulic Research*, vol. 17, no. 4, pp.341-354.

Toro, E.F. (2001). *Shock-capturing Methods for Free-surface Shallow Flows*, John Wiley and Sons, Ltd., New York.

Turner, J.S. (1973). *Buoyancy Effects in Fluids*, Cambridge University Press, Cambridge, United Kingdom.

USACE (1981). Sacramento River and Tributaries Bank Protection and Erosion Control Investigation, California, U.S. Army Corps of Engineers, Sacramento District.

USACE (1993). *HEC-6 Scour and Deposition in Rivers and Reservoirs User's Manual*, U.S. Army Corps of Engineers, Hydrologic Engineering Center, Davis, California.

van Rijn, L.C. (1984a). "Sediment Transport, Part I: Bedload Transport," *Journal of Hydraulic Engineering*, vol. 110, no. 10, pp.1431-1456.

van Rijn, L.C. (1984b). "Sediment Transport, Part III: Bed Forms and Alluvial Roughness," *Journal of Hydraulic Engineering, ASCE*, vol. 110, no. 12, pp.1733-1754.

Vreugdenhil, C. (1994). *Numerical Methods for Shallow-water Flow*. Kluwer Academic Publishers.

Warsi, Z. (1993). Fluid *Dynamics: Theoretical and Computational Approaches*, CRC Press, Boca Raton, Florida.

Wesseling, P. (2001). Principles of Computational Fluid Dynamics, Springer-Verlag.

Westrich, B., and M. Juraschek (1985). "Flow Transport Capacity for Suspended Sediment," *21st Congress of the IAHR*, vol. 3, Melbourne, Australia, 19-23 Aug. 1985, pp.590-594.

White, F. (1991). *Viscous Fluid Flow*, 2nd ed., McGraw-Hill Publishing Company, New York.

Yang, C.T. (1973). "Incipient Motion and Sediment Transport," *Journal of the Hydraulics Division of the ASCE*, vol. 99, no. HY10, pp.1679-1704.

Yang, C.T. (1992). "Force, Energy, Entropy, and Energy Dissipation Rate," in *Entropy and Energy Dissipation in Water Resources*, V.P. Sing and M. Fiorentino (eds.), Kluwer Academic Publisher, Netherlands, pp.63-89.

Yang, C.T., and C.C.S. Song (1979). "Theory of Minimum Rate of Energy Dissipation," *Journal of the Hydraulic Division of the ASCE*, vol. 105, no. HY7, pp.769-784.

Yang, C.T., and C.C.S. Song (1986). *Theory of Minimum Energy and Energy Dissipation Rate*. Encyclopedia of Fluid Mechanics, vol. 1, Chap. 11, Gulf Publishing Company, N. Cheremisinoff (ed.), pp.353-399.

Yang, C.T., and F.J.M. Simões (2000). *User's Manual for GSTARS 2.1 (Generalized Sediment Transport model for Alluvial River Simulation version 2.1)*, Technical Service Center, U.S. Bureau of Reclamation, Denver, Colorado.

Yang, C.T., and F.J.M Simões (2002). *User's Manual for GSTARS3 (Generalized Sediment Transport model for Alluvial River Simulation version 3.0)*, Technical Service Center, U.S. Bureau of Reclamation, Denver, Colorado.